

Eduards Skuķis

**VIBRĀCIJAS KORELĀCIJAS TEHNIKA CILINDRISKO
KONSTRUKCIJU NESTSPĒJAS NOVĒRTĒŠANĀ**

Promocijas darbs

**VIBRATION CORRELATION TECHNIQUE FOR
CYLINDRICAL STRUCTURAL SAFETY ASSESSMENT**

Doctoral Thesis



RĪGAS TEHNISKĀ UNIVERSITĀTE

Būvniecības inženierzinātņu fakultāte

Materiālu un konstrukciju institūts

RIGA TECHNICAL UNIVERSITY

Faculty of Civil Engineering

Institute of Materials and Structures

Eduards Skuķis

Doktora studiju programmas “Būvniecība” doktorants

Būvniecības inženierzinātņu programmas doktorants

**VIBRĀCIJAS KORELĀCIJAS TEHNIKA
CILINDRISKO KONSTRUKCIJU NESTSPĒJAS
NOVĒRTĒŠANĀ**

Promocijas darbs

**VIBRATION CORRELATION TECHNIQUE FOR
CYLINDRICAL STRUCTURAL SAFETY
ASSESSMENT**

Doctoral Thesis

Zinātniskais vadītājs

Dr. sc. ing.

KASPARS KALNIŅŠ

Scientific supervisor

Dr. sc. ing.

KASPARS KALNIŅŠ

Rīga 2023 / Riga 2023

Skukis, E. Vibrācijas korelācijas tehnika cilindrisko konstrukciju nestspējas novērtēšanā. Promocijas darba. Rīga: RTU, 2023. 118 lpp.

Skukis, E. Vibration Correlation Technique for Cylindrical Structural Safety Assessment. The Doctoral Thesis. Riga: RTU Press, 2023. 118 p.

Iespiests saskaņā ar promocijas padomes “RTU P-06” 2023. gada 16. septembra lēmumu, protokols Nr. L-5.

Published in accordance with the decision of the Promotion Council “RTU P-06” of 16 September 2022, Minutes No. L-5.

DOCTORAL THESIS PROPOSED TO RIGA TECHNICAL UNIVERSITY FOR THE PROMOTION TO THE SCIENTIFIC DEGREE OF DOCTOR OF SCIENCE

To be granted the scientific degree of Doctor of Science (Ph. D.), the present Doctoral Thesis has been submitted for the defence at the open meeting of RTU Promotion Council on 17 March 2023 at 14.15 at the Faculty of Civil Engineering of Riga Technical University, 6A Ķīpsālas Street, Room 342

OFFICIAL REVIEWERS

Professor Dr. sc. ing. Dmitrijs Serdjuks
Riga Technical University

Professor Dr. sc. ing. Haim Abramovich
Technion – Israel Institute of Technology, Israel

Professor Dr. sc. ing. Chiara Bisagni
Delft University of Technology, Netherlands

DECLARATION OF ACADEMIC INTEGRITY

I hereby declare that the Doctoral Thesis submitted for the review to Riga Technical University for the promotion to the scientific degree of Doctor of Science (Ph. D.) is my own. I confirm that this Doctoral Thesis had not been submitted to any other university for the promotion to a scientific degree.

Eduards Skuķis (signature)

Date:

The Doctoral Thesis has been prepared as a thematically united collection of scientific publications. It combines seven scientific publications and a summary. Publications are written in English and available at Scopus database. The total number of pages is 118.

1. CONTENTS

Chapter 1: Overview	5
1.1. Introduction	5
1.2. Rationale.....	6
1.3. The research Goals	7
1.4. Main statement	7
1.5. Scientific novelty	7
1.6. Tasks	8
1.7. Structure.....	8
1.8. Publications and approbation.....	8
Chapter 2: Methodology.....	10
2.1. Experimental data collection.....	10
2.1.1. Shell Buckling Experiments.....	10
2.1.2. The Experimental Modal Analysis.....	13
2.1.3. Vibration Spectra and Modes.....	16
2.2. Data analysis	20
2.3. The sequence of vibration correlation technique	25
Chapter 3: Main Results	27
Chapter 4: Final remarks	30
4.1 Main conclusions	31
4.2 Critical recommendations.....	31
4.3 Further outlook	32
Acknowledgment	33
Bibliography.....	34
Annex I: Article: Skukis E., Kalnins K., Chate, “ <i>Preliminary assessment of correlation between vibrations and buckling load of stainless steel cylinders</i> ”, "Shell Structures: Theory and Applications", SSTA 2013	37
Annex II: Article: Kalnins K., Arbelo M.A., Ozolins O., Skukis E.,..., Degenhardt R, “ <i>Experimental non-destructive test for estimation of buckling load on unstiffened cylindrical shells using vibration correlation technique</i> ”, Shock and Vibration, 2015	42
Annex III: Article: Arbelo M.A., Kalnins K., Ozolins O., Skukis E.,..., Degenhardt R. “ <i>Experimental and numerical estimation of buckling load on unstiffened cylindrical shells using a vibration correlation technique</i> ”, Thin-Walled Structures, 2015.....	52
Annex IV: Article: Skukis E., Ozolins O., Kalnins K., Arbelo M.A “ <i>Experimental test for estimation of buckling load on unstiffened cylindrical shells by vibration correlation technique</i> ”, Procedia Engineering, 2017	60
Annex V: Article: Skukis E., Ozolins O.,..., Arbelo, M.A. “ <i>Applicability of the vibration correlation technique for estimation of the buckling load in axial compression of cylindrical isotropic shells with and without circular cutouts</i> ”, Shock and Vibration, 2017	69
Annex VI: Article: Franzoni F., Odermann F., Wilckens D., Skukis E.,..., Degenhardt, R “ <i>Assessing the axial buckling load of a pressurized orthotropic cylindrical shell through vibration correlation technique</i> ”, Thin-Walled Structures, 2019	85
Annex VII: Article: Skukis E., Jekabsons G., Andersons J., Ozolins O., Labans E., Kalnins, K “ <i>Robustness of empirical vibration correlation techniques for predicting the instability of unstiffened cylindrical composite shells in axial compression</i> ”, Polymers, 2020	100

CHAPTER 1: OVERVIEW

1.1. Introduction

Low mass plays a critical role in space missions. Depending on the area of application, it is on average between 10,000 to 20,000 EUR for each kilo of payload to be delivered to space. Therefore, structural mass reduction is a matter of a great effort. Carbon composites allow decreasing the mass of a structure down by 30 % while retaining the same load carrying capacity. All large space agencies, such as ESA for Europe, NASA for the USA or CNSA for China, as well as private providers, such as Space-X or Rocket lab, work on the application of carbon composites to reduce the transportation costs in future. There is intense competition in this field. The early design methods of the spatial single-curvature structures have been utilised for decades while enhancing work and recommendations for the design of more complex structures and complex use as reusable booster launch. Among restricting boundaries are design limit loads that are very sensitive to imperfections and defects, thus there is a clear driving factor for delivering a non-destructive actual limiting force prediction ensuring higher accuracy and reliability for associated risk assessment.

The aim of this Thesis is to investigate the prospects of the Vibration Correlation Technique method (VCT), which allows prediction of actual critical load levels from certain structures and configurations in a non-destructive manner on top of qualification experiments, thus contributing to a rising level of safety.

The principle of VCT method is based on the natural frequency and axial (coaxial) load correlation of a structure. It is based on physical phenomena where natural frequency decrease correlates with each increment of a load and corresponding structural stress level. Once the load reaches the state of buckling, the corresponding natural frequency tends to be equal to a zero for column type structures. While during trials, the natural frequency is measured at increasing load levels, an extrapolation of the predicted ultimate load may be calculated, without reaching the rupture of the structure. Thus, the VCT method may be utilised as an alternative critical load estimation approach ensuring additional safety of a structure considering uncertainties associated with physical specimen. However, in the case of defect-sensitive shells, as those used in space missions, the natural frequency-load interrelation may be highly complex and less robust. Empirical formulas have been developed for metallic-isotropic materials to approximate the correlation. Nevertheless, these formulas cannot be utilised for the design of anisotropic stiffened structures.

It should be noted that similarities in the philosophy of the VCT method can also be observed as natural phenomena. One of the most popular expressions that immediately comes to mind is the expression "the calm before the storm". Thus, before a strong hurricane, the sea becomes surprisingly calm for a while. Despite the intensifying wind, the surface of the water remains even and smooth and there is not the slightest fluctuation on it. Another example of a natural phenomenon that "silences" is volcanoes. If an active volcano nearby suddenly kicks up its activity with steam, smoke, and belowground rumblings, it obviously is erupting, however. Recently researchers have identified that even more dangerous sign is a sudden total silence.

A team led by researchers at Carnegie Institution of Science has been monitoring the seismic activity of more than 50 volcanic explosions in active volcanoes since 2009. At first, they were

looking for some pattern in the teeming geological activity before eruptions that could predict explosions. The pattern they found was a lack of activity just in the moment right before an eruption, volcanoes went suddenly and completely quiet and still.

Now that they know about this lull before the eruption, researchers hope to work the information into pre-eruption warnings. Unfortunately, the time provided would be short. Most eruptions had quiet periods of less than 30 minutes, and some had lulls lasting only a few minutes. The longest one measured 10 hours, but then it was also followed by the largest eruption that researchers had seen. This may be a hint for further VCT evolution.

1.2. Rationale

Over the years, the original NASA design recommendations have been used successfully in the design of numerous NASA space vehicles, including the Space Shuttle Solid Rocket Boosters (SRB) and External Tank (ET), as well as the Space Launch System (SLS). However, it has been shown over time that the Knock Down Factors (KDFs) and recommendations provided in the original NASA guideline can result in overly conservative buckling load predictions and designs when applied to these modern aerospace structures. This is primarily because the lower bound KDFs are comprised of test data from cylinders that were manufactured and tested using outdated processes and do not reflect the improvements observed in recent testing of modern aerospace-quality shell structures constructed using advanced materials and reliable manufacturing processes. In addition, the *NASA SP-8007* original monographs were limited to radius/thickness ratios currently driving design of modern structures, such as large integrally machined metallic cylinders or composite cylinders.

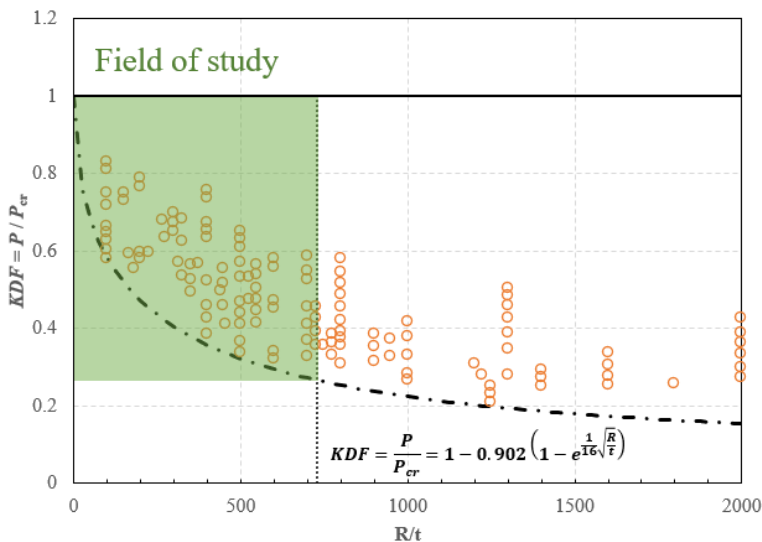


Fig. 1.1. NASA-SP8007 Knock-Down factor curve (Weingarten, 1968).

The main objective of the present Thesis is to extend the reliability of the Vibration Correlation Technique for assessment of imperfection sensitive composite cylindrical structure.

By conducting a largest experimental test campaign dedicated to VCT, a particular research aimed to provide a data set for both training and development of surrogate models in formulating a parametrical equation. As it was identified up to now, there is a major gap in statistically reliable set of experimental data, since the studies like NASA/SP-8007 took place in 1968 when composites were neglected. Therefore, assessing of manufacturing signature and testing equipment sensitivity was another objective of current research. Besides experimental research conducted, numerical simulations by Finite Element Method (FEM) and capacities of cloud computing were validated. Therefore, a range of both geometrical and mechanical properties has been covered to develop VCT guidelines assured by statistical credibility. In order to achieve this, there has been an effort to produce a series of CFRP hollow circular cross section columns and cylindrical shells with varying radius/thickness ratios and radius/free height (slenderness) ratios including ply lay-up orientation. It should be noted that R/t ratios are intentionally foreseen to vary between 100 to 750, while slenderness h/R could vary in the range from 8 to 1. With a selected number of lay-ups and boundary conditions, this ensured a statistically meaningful test production batch series (DESICOS, 2019) (NASA, 2019) (ESA, 2019).

1.3. **The research Goals**

Development of methodology to extend the reliability of the vibration correlation technique for assessment of imperfection sensitive composite cylindrical structure.

1.4. **Main statement**

The research hypothesis of this thesis was delineated as follows:

- 1) the correlation exists between the increment of compression load level and the decrease of eigen frequency for cylindrical shells;
- 2) the vibration correlation method is applicable for isotropic cylindrical shells as well as for orthotropic ones;
- 3) the modified Arbelo normalisation method for predicting critical load for cylindrical shell by vibration correlation technique is determined with high precision in comparison with the classic approach.

1.5. **Scientific novelty**

1. The novelty of the dissertation is the developed new method of experimental data normalisation, which is a logical continuation of the Arbelo approach.
2. A radically new approach has been developed and tested to determine the frequency shift under load for cylindrical shells.
3. The reliability of the vibration correlation technique for assessment of imperfection sensitive cylindrical structures has been significantly improved by analysis of results from a large number of experiments performed in this research.
4. Approbation of VCT has been employed for testing of the newest generation space launcher structure including a complex load case scenario.

1.6. Tasks

1. To confirm the correlation between the increase in load level and decrease in frequency for cylindrical shells.
2. To validate the VCT method by manufacturing and experimentally testing isotropic and orthotropic cylinders in a wide range of R/t and R/h ratios.
3. To increase the accuracy of critical load prediction by modifying the normalisation of experimental data.
4. To check the opportunities for applying the VCT method for predicting the critical load of cylindrical shells like evident geometrical defects or other load cases as internal pressure or bending loading.
5. To approbate the VCT method on real-scale objects.

1.7. Structure

Chapter 1: Overview. This chapter describes the scope of the dissertation research. In this chapter, the main research hypotheses and the importance of the novelty of research related to the VCT method are formulated. A brief description of the structure of the dissertation is also presented in this chapter. The list of publications and presentations at international conferences is also displayed in this chapter.

Chapter 2: Methodology. This chapter describes the basic factors necessary for successful prediction of critical load using the VCT method. Three main stages are outlined.

2.1. *Experimental Data Collection.* The experiment procedure is discussed in detail, which, in turn, could be divided into two sub-stages. The factors affecting the critical force are described. The equipment necessary for critical load prediction using the selected methodology is specified, problems faced during VCT data collection are discussed in detail.

2.2. *Data Analysis.* This chapter considers the normalisation options of experimental data to be applied to prediction of critical load using the VCT method.

2.3. *Vibration Correlation Technique Algorithm.* This chapter presents the algorithm for taking measurements using the VCT method

Chapter 3: Main results. This chapter represents publications which reflect the main results obtained during the research and application of the VCT method. The results are published in five cited sources, the total *Impact Factor* is **25** with a total of **155** (2022/09/01) citations in journals indexed in Scopus.

Chapter 4: Final remarks. This chapter represents the main conclusions and discussion of the challenges and their solutions with regard to practical application of the VCT method for critical load prediction.

1.8. Publications and approbation

Main results of the Thesis were summarised in five scientific publications. Results of the research were presented at five conferences.

Scientific publications:

1. Kalnins, K., Arbelo, M. A., Ozolins, O., **Skukis, E.**, Castro, S. G. P., Degenhardt R., Experimental non-destructive test for estimation of buckling load on unstiffened cylindrical shells using vibration correlation technique, *Shock and Vibration*, Volume **2015**, Article ID 729684.
2. Arbelo, M. A., Kalnins, K., Ozolins, O., **Skukis, E.**, Castro, S. G. P., Degenhardt, R., Experimental and numerical estimation of buckling load on unstiffened cylindrical shells using a vibration correlation technique, *Thin-Walled Structures*, Volume 94, 1 September **2015**, pp. 273–279.
3. **Skukis, E.**, Ozolins, O., Andersons, J., Kalnins, K., Arbelo, M. A., Applicability of the vibration correlation technique for estimation of the buckling load in axial compression of cylindrical isotropic shells with and without circular cutouts, *Shock and Vibration*, Volume **2017**, 29.
4. Franzoni, F., Odermann, F., Wilckens, D., **Skuķis, E.**, Kalniņš, K., Arbelo, M. A., Degenhardt, R. Assessing the axial buckling load of a pressurized orthotropic cylindrical shell through vibration correlation technique, *Thin-Walled Structures*, Volume 137, April **2019**, pp. 353–366.
5. **Skukis, E.**, Jekabsons, G., Andersons, J., Ozolins, O., Labans, E., Kalnins, K. Robustness of empirical vibration correlation techniques for predicting the instability of unstiffened cylindrical composite shells in axial compression, *Polymers*, Volume 12, Issue 12, December **2020**.

Results of the Thesis were presented at the following conferences:

1. **Skukis, E.**, Kalnins, K., Ozolins, O., *Assesment of the Effect of Boundary Conditions on Cylindrical Shell Modal Responses*, 4th International Conference CIVIL ENGINEERING'13, Proceedings Part I, STRUCTURAL ENGINEERING, Jelgava **2013**.
2. **Skukis, E.**, Kalnins, K., Chate, A., *Preliminary assessment of correlation between vibrations and buckling load of stainless-steel cylinders*, *Shell Structures: Theory and Applications – Proceedings of the 10th SSTA 2013 Conference, Volume 3*, **2014**, pp. 325–328, 10th Jubilee Conference on "Shell Structures: Theory and Applications", SSTA 2013, Gdansk, Poland, 16 October 2013.
3. **Skukis, E.**, Kalnins, K., Ozolins, O., *Application of vibration correlation technique for open hole cylinders*, Proceedings of the 5th International Conference on Nonlinear Dynamics, ND-KhPI2016, September 27–30, **2016**, Kharkov, Ukraine.
4. **Skukis, E.**, Ozolins, O., Adersons, J., Kalnins, K., Arbelo, M. A., *Experimental Test for Estimation of Buckling Load on Unstiffened Cylindrical Shells by Vibration Correlation Technique*, *Procedia Engineering*, Volume 172, **2017**, pp. 1023–1030, 12th International Conference Modern Building Materials, Structures and Techniques, MBMST 2016, Vilnius, Lithuania, 26 May 2016.
5. **Skukis, E.**, Kalnins, K., Jekabsons, G., Ozolins, O., *Benchmarking of vibration correlation techniques for prediction of buckling load of cylindrical shells*, 16th European Conference on Spacecraft Structures, Materials and Environmental Testing (ECSSMET), **2021**.

CHAPTER 2: METHODOLOGY

This section represents three main stages necessary for VCT prediction of the critical load:

- VCT experimental campaign: It is divided into two experimental approaches, which are necessary to carry out the prediction by the VCT method.
- Pre-selection of excitation, field of view of measurements and setting as well as other required data for further VCT analysis.
- Data analysis: This is the process of normalisation of experimental data, calculation and prediction of critical force using the method.

2.1. Experimental data collection

This section provides a description of the procedures executed during the experimental campaign, which can be divided into two main groups: shell buckling tests and experimental modal analysis, as shown in Fig. 2.1.

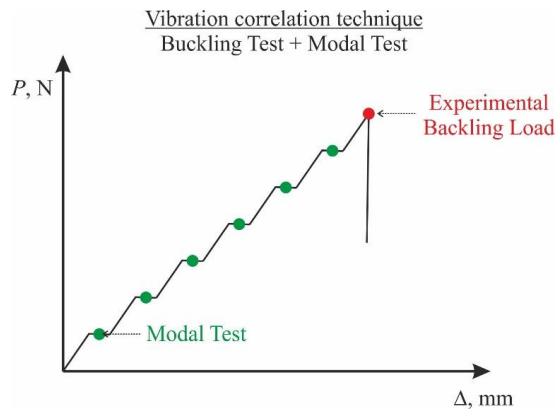


Fig. 2.1. Experimental VCT testing – step loading.

2.1.1. SHELL BUCKLING EXPERIMENTS

The universal quasi-static testing machine is necessary for conducting buckling tests (Degenhardt, 2007). The main task of this equipment is to load a sample until the set load is reached and to maintain this load over the time while the measurement of cylinder vibrations is made (Fig. 2.1). Another important aspect is preliminary determination of basic frequencies using a quasi-static testing machine to avoid resonance with the tested sample during testing. The opportunity to control the load via travel allows avoiding destruction of the tested piece during testing, which is also very relevant in order to be able to conduct a repeated experiment on the cylinders made from a composite material (Zimmermann, 2006; Wilckens, 2020).

The main machine used in the majority of experiments is the universal quasi-static testing machine Zwick 100. This equipment has certain limitations – the maximum diameter of the testable cylinder is 500 mm and maximum height is 1000 mm, the load also is limited to 100 kN.

Boundary conditions can be of two kinds. The first kind includes the boundary conditions for fixation of a cylinder in the testing machine. The first experiments were carried out with the cylinders placed between two plates. The upper plate was screwed tightly to the testing machine, a hemispherical joint was installed on the bottom plate, enabling rotation of the supporting plate, thus eliminating bending moments and, hence, promoting self-alignment of the cylinder axis with the loading direction, as shown schematically in Fig. 2.2.

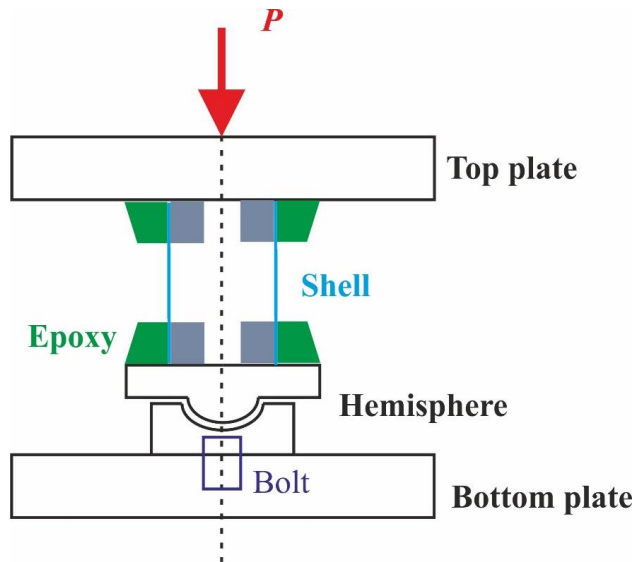


Fig. 2.2. Schematic of the setup for compression tests of cylinders, testing using a hemispherical joint.

Due to complexity of hemispherical modelling in the analytical model and the problems caused by single-side loading of a cylinder, i.e., at the moment of buckling, the sphere was compensating the load and further destruction was localised at the place with the biggest defect. In general terms, it was not possible to determine the buckling shapes over the whole surface of the cylinder. Thus, changes were made in the boundary conditions. Both the top and bottom edges of the shells resting on the respective machine plates were joined to the plates by means of potting with a resin/powder filler to eliminate loading imperfections and contact surface misalignments. The test set-up contained a shimmed interface at the lower machine plate (Fig. 2.3). Shimming was performed by placing very thin sheets of metal between the lower loading plate and the load-distributing washer attached to the load frame in order to eliminate the small gaps between both surfaces, so that an even distribution of load along the cylinder's circumference was ensured.

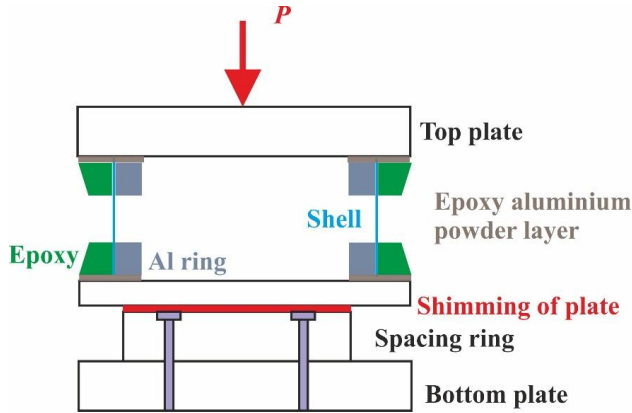


Fig. 2.3. Schematic of the setup for compression tests of cylinders, testing using the shimming of the plate.

Such an approach to boundary conditions results in dependence on an operator, a person who will install a cylinder for testing, and reduces the opportunity for repeatability of result. Having analysed the experiments conducted by the partners from DLR, boundary conditions were optimised, the bottom plate was bolted to the respective crosshead, as shown in Fig. 4.

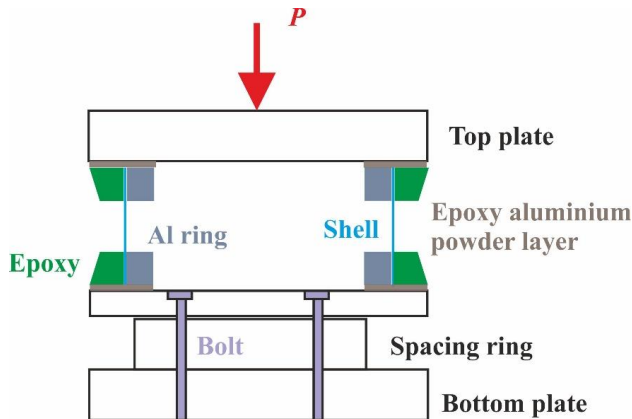


Fig. 2.4. Schematic of the setup for compression tests of cylinders, testing using the shimming of the plate.

The second kind includes the boundary conditions of the cylinder itself (Lancaster, 2000). Edges of the 100-mm-diameter shells were mounted between parallel steel rings, in 8 mm deep circular grooves with a V-shaped cross section, which were filled with a mixture of epoxy resin and fine sand, as schematically presented in Fig. 2.5 (a). The top and bottom edges of the 100-mm-diameter shells were both clamped by aluminium rings from the inside and potted with an epoxy mortar containing fine sand and slag (Fig. 2.5 (b)).

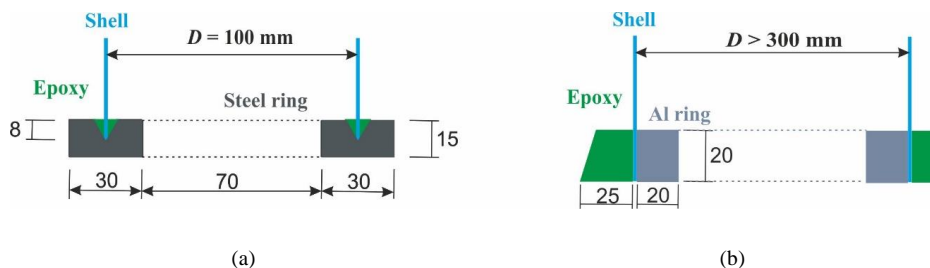


Fig. 2.5. Schematic of the mounting of cylinders: (a) in the groove of a steel ring; (b) potting onto plates of the test machine. Dimensions in the figure are given in mm.

The results and impact of these tests will be considered in the next chapter. Optimization of boundary conditions was carried out to increase the experimental critical load, as well as to simplify the finite element model. Calculation using the finite element method is necessary to determine the linear buckling load (Castro, 2014; Wagner, 2017), which further is applied to the VCT-based prediction of the critical load.

2.1.2. THE EXPERIMENTAL MODAL ANALYSIS

The experimental modal analysis (EMA) is the most widely used procedure for such investigations (Maia, 1997; Kjær, 2022). It provides the frequency response functions (FRFs) of the system using known input excitation forces and the corresponding measured output vibrational responses. The experimental equipment for the measurements of vibrations and building of shapes of fluctuations is manufactured in a great variety. One of the most widespread ways to measure vibrations is a vibrosensor – a contact method (ISO7626-2, 2015). Measurements are taken in a fixed place, with a vibrosensor installed inside (Zhang, 2008). Such an approach is relatively inexpensive, it allows acquiring continuous images of vibrations in a temporal response, but it features a range of bottlenecks, such as additional mass on the tested item (Wesolowski, 2010). The problem is to acquire the shapes of fluctuations, which are needed for control of the classical VCT method. The problem is that it is necessary to produce agitation in different pre-set locations, and this results in increased timing for the EMA.

There are also several different possibilities to start vibrations on a cylinder: piezoelectric actuator, modal shaker. All these actuators change boundary conditions and add mass to the tested item. Agitation produced by an impact hammer can result in an earlier buckling failure of a cylinder as well as increases the time required to acquire fluctuation shapes. Nevertheless, all options mentioned above are appropriate for application when there is a clear concept of the results to be obtained also within the limited budget. The solution to these problems is to use non-contact response transducers (sensing devices). The laser-based optical transducers can successfully substitute the traditional piezoelectric type of transducers and eliminate any additional mass coming from sensing devices. The most recently useable laser transducers are based on the Doppler velocimetry principle and they have attracted attention of many researchers dealing with experimental modal analysis. A highly sensitive optical system is therefore used for vibration sensing – POLYTEC Scanning Laser Vibrometer system PSV- 400

(Theory, 2008; Polytec, Laser Doppler vibrometry, 2022) Later, an opportunity to compare the performance of the Laser Vibrometer system PSV-500-3D appeared. Figure 2.6 shows a typical VCT set up.

The following parts are involved in the following measurement chain:

- source of excitation signal (generator);
- power amplifier;
- exciter-loudspeaker;
- vibrometer system PSV-400 and PSV-500-3D;
- analyser (PC system).



Fig. 2.6. Typical VCT test set up.

SCANNING LASER VIBROMETER: PSV-400

The PSV-400 operates on the Doppler effect measuring frequency changes of the back scattered light wave from a vibrating object. If a wave is reflected by the vibrating object and detected by the laser vibrometer, the measured frequency shift of the wave can be described as

$$\Delta f = \frac{2\vec{v} \cdot \vec{e}}{\lambda} = \frac{2v}{\lambda} \cos \theta, \quad (2.1)$$

where v is the object's velocity and $\lambda = 633 \text{ nm}$ is the wavelength of the emitted wave. To determine the velocity of an object, the Doppler frequency shift has to be measured at a known wavelength. This is done by a laser interferometer.

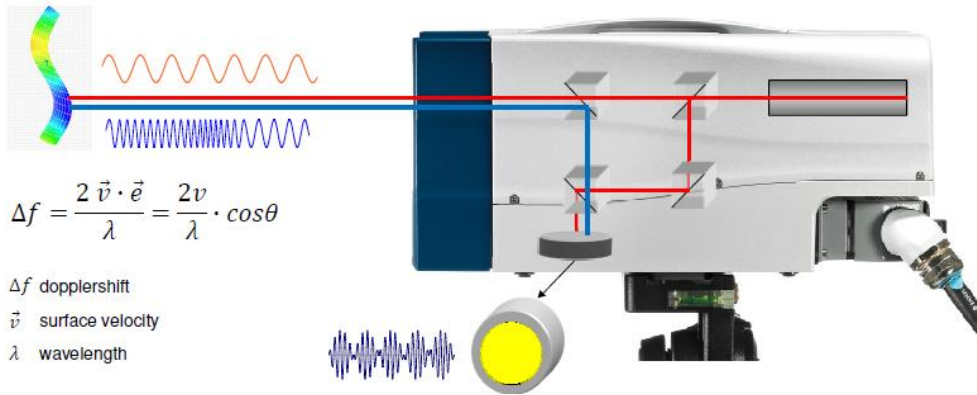


Fig. 2.7. Technological background (Polytec, Polytec Scanning Vibrometer, Theory Manual. PSV, PSV-3D, MSA/MSV, as of Software 8.5, 2001).

SCANNING LASER VIBROMETER PSV-500-3D

The main principle of the work of the scanning laser vibrometer PSV-500-3D is also based on the Doppler effect (Fig. 2.8). A distance gauge in the main head is an extra, which allows changing the object's geometry; this function was also available earlier, but it was necessary to integrate the distance gauge as a separate unit mounted outside the chamber. Scanning of the geometry has an accuracy of approximately 1 mm, depending on the quality of the reflected surface. The basic characterising features are:

- 3 synchronised laser scanners with the common control;
- laser beams intersect on the surface;
- geometry is imported or measured;
- simultaneous measurement of 3 vibration components;
- coordinate transformation in object coordinate system.

An additional difference is an opportunity to measure its own point with each head, i.e., to acquire three vibro results at a time. Also, only one head may be used for measurements, same as with the previous model PSV-400 with the only difference – the geometry data of the scanned cylinder will be acquired.

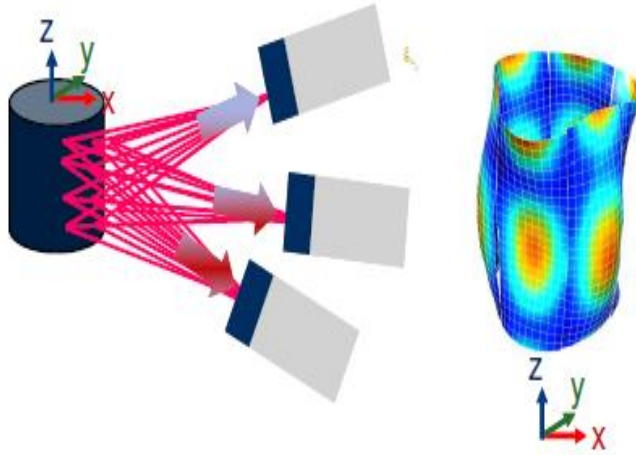


Fig. 2.8. Working principle of PSV-500-3D (Polytec, Polytec PSV-E-500 Operating Instructions Manual, 2016).

2.1.3. VIBRATION SPECTRA AND MODES

As it has been mentioned above, the VCT-based prediction needs measurements of the natural frequency at a fixed load, i.e., it is necessary to follow up the changes in the natural frequency under loading. As far as there are a great number of natural frequencies, the range of measurements is the first limitation (Hamidzadeh, 2009). The example of a frequency response is given in Fig. 2.9. Frequency peaks of low amplitude at the beginning of the response are exactly the natural frequencies of the structure, floors and walls. It is important to keep monitoring that during the testing the natural frequency of a cylinder does not approach them. After 200 Hz, for this sample, the natural frequencies to be monitored emerge.

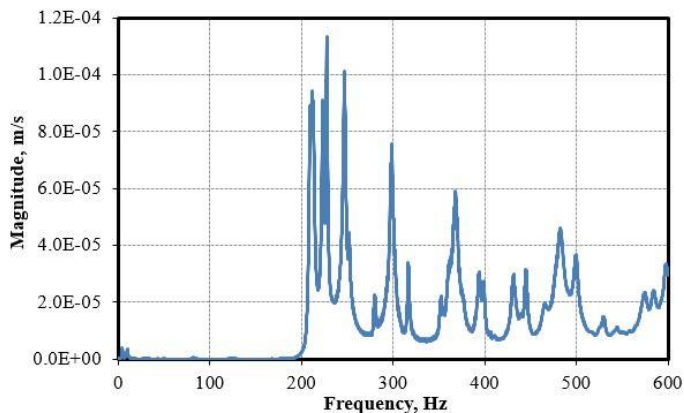


Fig. 2.9. Frequency response.

Every frequency has its shape of fluctuations and it is important to understand that at the changes under loading one and the same form of fluctuations is monitored. What kind of problems may occur here? There are indeed many bottlenecks. In the ideal world in the case of an ideal cylinder, the frequency will have two symmetric shapes of fluctuations. In the world of experiments, these shapes of fluctuations will be separated, i.e., will be distant, but it is not always the case, as these symmetric shapes also can be absent, see Fig. 2.10 a). In a similar manner, due to the vicinity of other shapes of fluctuations, changes in the sequence of shapes of fluctuations under loading can occur, which are complicated to monitor only by the frequency response (Fig. 2.10 b)).

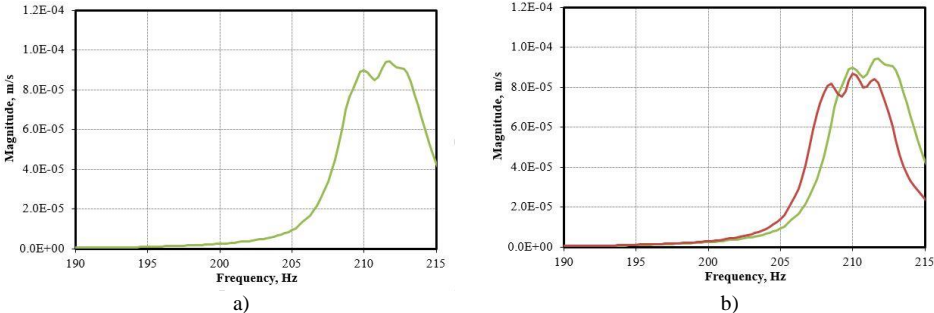


Fig. 2.10. Frequency response with two modes of one frequency.

Consequently, it is necessary to control the shape of fluctuations and its change under loading.

The following problem is in the fact that the chosen shape of fluctuations can disappear under loading, as shown in in Fig. 2.11. The higher the natural frequency, the higher is the chance of such an effect; besides, new natural frequencies appear at these high frequencies.

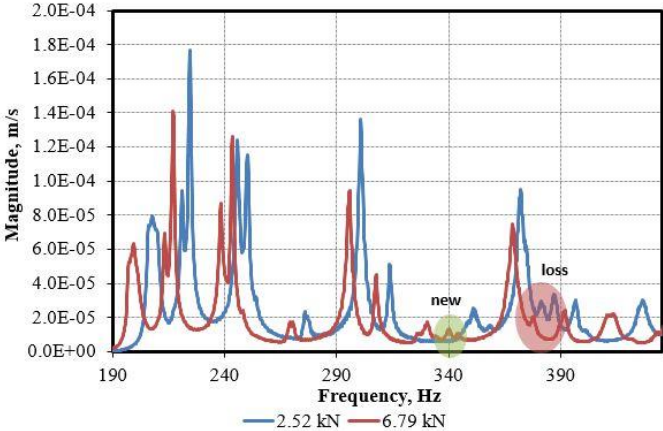


Fig. 2.11. Frequency response, example loss and new eigen frequency.

Every natural shape of fluctuations has its designation (m, n) – numbers of neutral lines by axis x and y . The example of such natural shapes of fluctuations under and without loading is shown in Fig. 2.12 (Avieable, 2022). The complexity of calculation of m – the number of vertical neutral lines from an experiment – is caused by the number of partial peaks, correlation of their surface areas to the total surface area of the cylinder. It is easier to calculate the number of horizontal lines n . Using PSV-500-3D, the natural shape of fluctuations can be acquired for the whole cylinder over the entire diameter, but the time required for this is disproportionately long compared to the benefits that can be gained from the acquired information.

There is a numerical algorithm based on the modal assurance criterion (MAC) (Pastora, 2012) used to identify the variation of each vibration mode during axial loading; the MAC index performs a comparison between two vectors of the same length and the index returns a value close to one if a linear relationship between the two vectors exists and near zero if they are linearly independent, which was applied to monitoring of a certain shape of fluctuations of a large number of cylinders. The result is available at vct.rtu.lv and published in one of the articles.

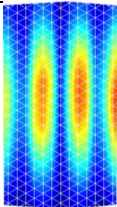
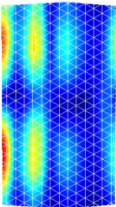
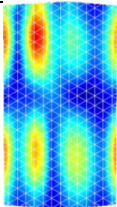
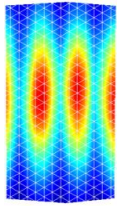
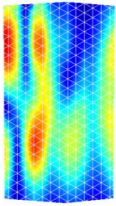
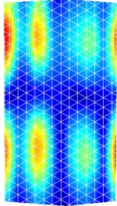
Load, kN	Mode	f , Hz	Mode	f , Hz	Mode	f , Hz
0.0		211.75		394.25		431.50
4.96		202.75		378.00		416.75

Fig. 2.12. Eigen modes without and with load.

The answer to the first question regarding the parameter to be measured is that the changes under loading of the first natural frequency for a certain shape of fluctuations acquired experimentally, which manifests itself over the entire range of loading, are measured or, actually, monitored. Indeed, it may be observed in the published works that the monitoring was performed also for other natural shapes of fluctuations, although it did not bring any significant improvement of the result with application of the normalisation technique, which will be discussed below.

The measurements are taken on the surface of the cylinder, as it has been described above, every shape has its zero lines, and it is logical that the information acquired from such sectors will be of a low quality. The example is shown on the frequency response presented in Fig. 2.13.

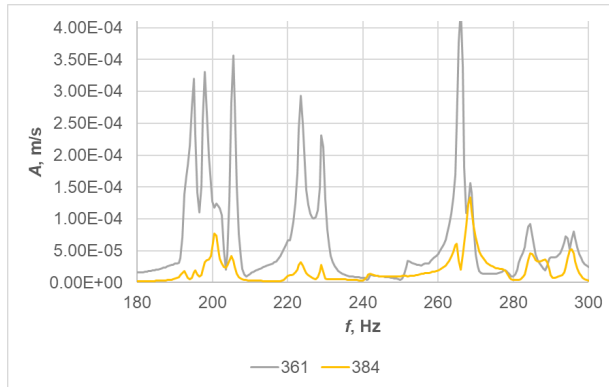


Fig. 2.13. Frequency response with bad and good measurement points.

The number of measured points has an impact on the time required to measure modal characteristics and accuracy of the shape of fluctuation. One more factor that influences the time of experiment is sampling frequency. This factor directly depends on the value of the first frequency. The lower the first frequency, the higher sampling frequency is required. A simple example may be presented: at $\Delta f = 0.25$ Hz the measurement must be made in one point at $(1/\Delta f)$ 4 sec. This value should be multiplied by the number of points, adding the time of transit from one point to another, adding a repeated measurement if the point differs from others by response. This makes the overall time required to measure one position for the VCT prediction. Thus, within 10-minute testing, approximately 120 points can be measured from the surface at $\Delta f = 0.25$ Hz. The questions whether 120 points are a lot or little and whether 10 minutes is a long time arise. There is no single answer to these questions. This parameter depends on the size of a tested item and sampling frequency. It is also necessary to account for load relaxation during testing, i.e., the load decreases during testing.

The number of positions is another important factor to measure the natural frequency at different loads. It is necessary to determine how close to the value of the experimental critical load measurement should be made. At the initial stage of familiarisation with the VCT method, measurements were taken at up to 50 % of the experimental critical load. Tolerance of prediction of the critical load exceeded 10 %, which was unacceptable. The bottle-neck is that before the buckling test, the experimental critical load is unknown. The experiments were carried out on the metal cylinders that may not be retested after buckling failure, but the main goal of the research was to determine the maximum critical load and to become aware of an opportunity to measure the data for the VCT prediction. Later, the testing was carried out on the carbonic cylinders appropriate for multiple testing. It has been discovered that the VCT method is becoming more precise in predictions of the critical load approaching to the experimental critical force in terms of load, as shown in Fig. 2.14, at the experimental critical load of 25.04kN.

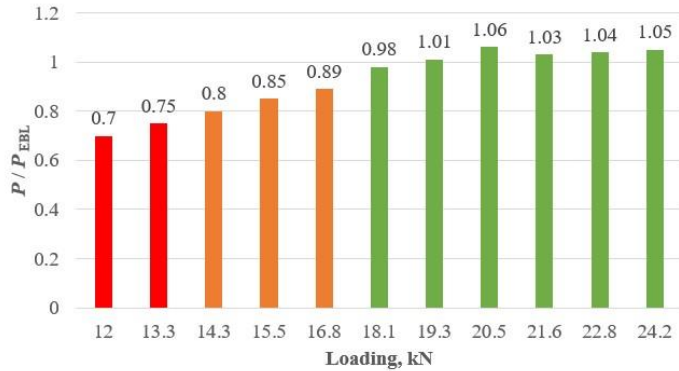


Fig. 2.14. Buckling load prediction using the VCT approach for different loading ranges.

One more important factor to be considered is the first data used in the VCT-based prediction at low loading close to 0 kN. It was noticed that during some experiments, frequency at loading was higher than that at a lower loading, see Fig. 2.15 for data on Cyl.6N. Besides, demonstrative behaviour at the initial stage can be observed in case of Cyl.4N, when abrupt decrease of frequency occurs compared to further loading. Such behaviour, most likely, points at some problems in the boundary conditions.

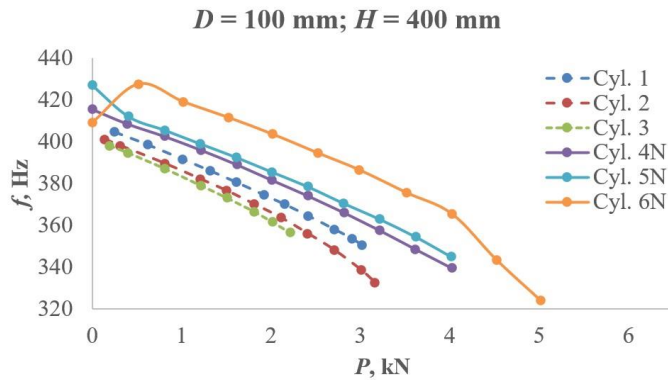


Fig. 2.15. Anomaly at the initial testing stage.

2.2. Data analysis

The concept of relating the buckling load of the structure to the load level in which the fundamental natural frequency is zero has been known for more than a century, it is attributed to Sommerfeld (Sommerfeld, 1905). Nevertheless, only in the 1950s, this concept was first considered for estimating the buckling load through a non-destructive experimental procedure (Lurie, 1952; Johnson, 1953). The first VCT studies were based on the linear relationship between the axial load level and the square of the loaded natural frequency, which can be demonstrated for fully simply supported columns, plates (Johnson, 1953), and cylindrical shells (Leissa, 1973; Virgin, 2007):

$$f^2 + p = 1, \quad (2.2)$$

where f is the ratio between the loaded natural frequency $\underline{\omega}_{mn}$ and the unloaded natural frequency ω_{mn} , both associated with the same vibration mode defined by axial half-waves m and circumferential waves n (for cylindrical shells), and p is the ratio between the applied load P and the linearized buckling load P_{CR} (from an eigenvalue buckling analysis or theoretical buckling equations).

Based on Eq. (2.2), direct and indirect VCT approaches were proposed throughout the last 7 decades (Singer, 2002); a complete review of this research effort is available in the quoted book. The indirect methods imply assessing the actual boundary conditions through the VCT test campaign aiming to update an initial model. This methodology improves the estimation of the buckling load; an example of an indirect method based on Eq. (2.2) is found in (Singer, 1979). The direct methods are based on an experimentally determined functional relationship between the applied load and the loaded natural frequency to directly estimate the buckling load, see (Radhakrishnan, 1973; Souza, 1983; Arbelo, 2014) among others.

The classic direct VCT method consists of plotting the characteristic chart f^2 versus p and calculating the best-fit linear relationship between the experimental data. In this method, the buckling load is extrapolated as the load level associated with zero magnitude of the loaded natural frequency (Lurie, 1952; Johnson, 1953; Singer, 2002). Even considering that the linear relationship does not hold in the presence of other than fully simply supported boundary conditions, the method presented proper estimations for columns with different boundary conditions in the experimental campaigns (Lurie, 1952; Burgreen, 1961; Chailleux, 1975).

Based on the detailed bibliographic review provided in (Singer, 2002), it may be concluded that the classic VCT approach applied to plate structures is straightforward in case of imperfection-insensitive structures. For examples, Lurie (Lurie, 1952) did not validate it considering simply supported flat plates during the 1950s, Chailleux et al. (Chailleux, 1975) succeed in estimating the buckling load of simply supported flat plate specimens with small imperfections during the 1970s and, recently, Chaves-Vargas et al. (Chaves-Vargas, 2015) applied the linear approach for flat carbon fibre-reinforced polymer stiffened plates.

Different authors proposed modified VCT approaches addressing imperfection-sensitive structures like curved panels and cylindrical shells (Singer, 2002). In the 1970s, Radhakrishnan (Radhakrishnan, 1973) proposed a method based on the extrapolation of the final linear path of the classical characteristic chart to the applied load axis; the author obtained exact results considering the last two measured points for tubes made of Hostaphan®.

Segal (Segal, 1980) investigated 35 existing VCT experiments of stiffened cylindrical shells. The author adjusted an optimal parameter q_{OPT} to raise the natural frequency F , in which a linear best-fit would lead the load level associated with zero natural frequency magnitude to the experimental buckling load:

$$F^{q_{OPT}} = A - BP, \quad (2.3)$$

where A and B are fitting constants.

A functional relationship between the optimal parameter q_{OPT} and the main geometric characteristics of stiffened cylindrical shells was proposed. This study achieved a substantial

reduction in the scatter of the VCT estimated knock-down factors (KDF) when compared to the indirect VCT method based on Eq. (2.2). The same Eq. (2.3) was investigated for upper and lower bounds of the optimal parameter q_{OPT} and, hence, of the estimated buckling load.

A novel approach for imperfection-sensitive stiffened cylindrical shells was proposed in (Souza, 1983). The authors suggested a modified characteristic chart based on the parametric forms $(1-p)^2$ and $1-f^4$, in which a linear relationship is expected, as presented in Fig. 2.16, the schematic view of the VCT proposed in (Souza, 1983), that reproduces the results from (Souza, 1983) for illustrating the VCT.

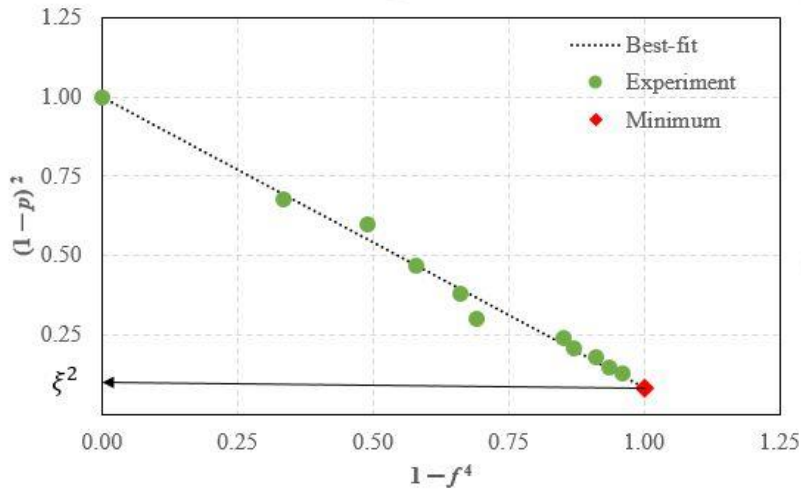


Fig. 2.16. Schematic view of the VCT proposed in (Souza, 1983).

In this VCT method, the linear relationship is obtained through a best fit procedure and it is considered for evaluating the parametric form $(1-p)^2$ when the loaded natural frequency is zero $1-f^4 = 1$ in the frequency parametric form therefore, the method can be expressed as:

$$(1-p)^2 + (1-\xi^2)(1-f^4) = 1, \quad (2.4)$$

where ξ^2 is the magnitude of $(1-p)^2$ when $1-f^4$ equates one and it represents the square of the drop of the load-carrying capacity due to initial imperfections. Based on ξ^2 , the VCT estimation of the buckling load P_{VCT} is:

$$P_{VCT} = P_{CR} \left(1 - \sqrt{\xi^2}\right). \quad (2.5)$$

From Eq. (2.5), the term $1 - \sqrt{\xi^2}$ can be considered as an experimental estimation of the KDF γ of conventional sizing approaches (Weingarten, (Revised 1968), 1965). Another method considering stiffened cylindrical shells was proposed in (Souza, 1991). The authors approximated the classic characteristic chart as a cubic parametric curve. They also suggested the Hermite form for defining the parametric equations. The described methods (Souza, 1983;

1991) were both validated considering the experimental results of stiffened cylindrical shells tested at Technion (Singer, 1980).

Similarly, the classic characteristic chart was represented by a second-order equation in (Abramovich, 2015). The authors adjusted the second-order best-fit relationship applied to curved stiffened panels. An assessment of the estimated buckling load accounting for load levels up to 50 % of the linear buckling load showed reasonable results. Nevertheless, for improving the estimations, the authors suggested load levels near the typical sharp bend of the classic characteristic chart.

In 2014, Arbelo et al. (Arbelo, 2014) modified the work done by Souza et al. (Souza, 1983) proposing a novel VCT based on the characteristic chart between the parametric forms $(1 - p)^2$ and $1 - f^2$. The authors empirically verified a second-order relationship as illustrated in Fig. 2.17, which reproduces the results from (Arbelo, 2014) for a schematic view.

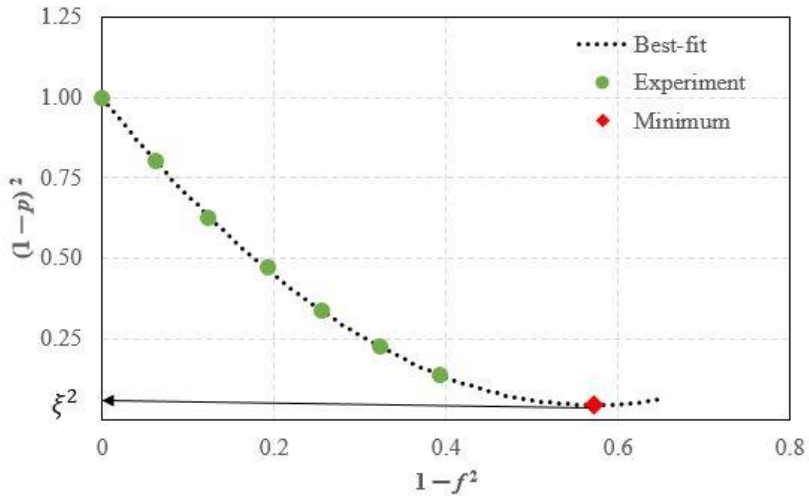


Fig. 2.17. Schematic view of the VCT proposed in (Arbelo, 2014).

The second-order equation is obtained through the best-fit procedure and it is considered to evaluate ξ^2 as the minimum value of the $(1 - p)^2$ axis. Mathematically, the method is formulated as:

$$(1 - p)^2 = C_2(1 - f^2)^2 + C_1(1 - f^2) + C_0, \quad (2.6)$$

where A , B and C are the fitting coefficients and ξ^2 is calculated as:

$$(1 - p)^2 = \xi^2 = -\frac{B^2}{4A} + C. \quad (2.7)$$

The estimated ξ^2 is considered for the buckling load estimation as presented in Eq. (2.5). It is worth mentioning that this method does not depend on the similarities between the buckling and the vibration modes but on the effects of the initial imperfections on the loaded frequency magnitude.

The above-presented method has been validated through 8 experimental campaigns (Arbelo, 2015; Kalnins, 2015; Skukis, 2017; Franzoni, 2019; Shahgholian Ghahfarokhi, 2018; Labans, 2019; Franzoni, 2019) considering metallic and laminated composite cylindrical shells with different design details: unstiffened (Arbelo, 2015; Kalnins, 2015; Skukis, 2017; Franzoni, 2019), with and without cut-outs (Skukis, 2017), grid-stiffened (Shahgholian Ghahfarokhi, 2018), with closely-spaced stringers and internal pressure (Labans, 2019), and manufactured considering variable angle tow (Franzoni, 2019).

In 2020, Skukis et al. (Skukis, 2020) modified the work done by Arbelo et al. (Arbelo, 2014) proposing a novel VCT based on the characteristic chart between the parametric forms $(1 - p)^2$ and $1 - f$. The authors empirically verified a second-order relationship as illustrated in Fig. 2.17, which reproduces the results from (Skukis, 2020) for a schematic view.

Since the form of the right-hand side of Eq. (2.6) has been arrived at empirically, it appears plausible that similar functions with this property can be used to locate the instability onset. An empirical modification of Eq. (2.6) employing a second-order polynomial of $1 - f$ was considered:

$$(1 - p)^2 = c_2(1 - f^2)^2 + c_1(1 - f) + c_0. \quad (2.8)$$

Then, the minimum value of $(1 - p)^2$ as a function of $1 - f$ is given by

$$\frac{d(1 - p)^2}{d(1 - f)} = 2(1 - p) \frac{dp}{df}, \quad (2.9)$$

i.e., the condition $dp/df = 0$ holds at the critical load. The relationship is illustrated in Fig. 2.18.

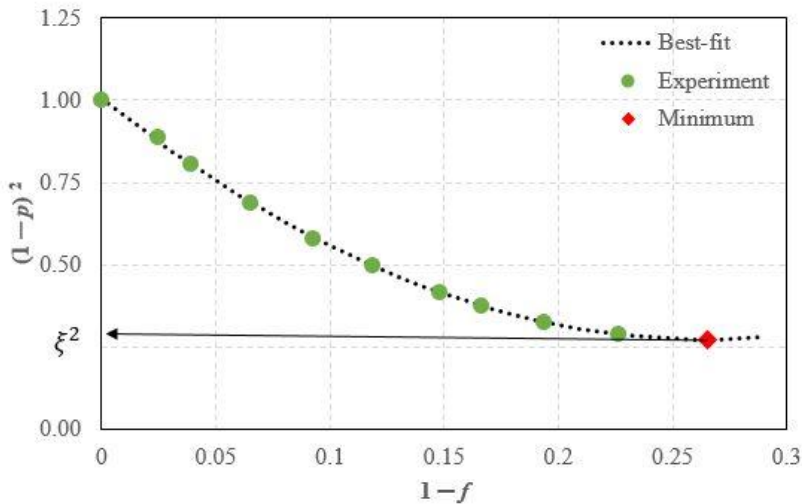


Fig. 2.18. Schematic view of the VCT proposed in (Skukis, 2020).

2.3. The sequence of vibration correlation technique

Based on the information presented in this chapter, the algorithm for taking measurements using the VCT method has been developed.

1. **To determine critical load $P_{CR,FEM}$ and the value of the first natural frequency $f_{P=0N,FEM}$** using the finite element method. The value of critical load is needed for the VCT-based prediction of the critical load. The value of the first natural frequency acquired using FEM is needed for verification of the computational model with a real tested item, as well as for determination of modal parameters of the experiment.
2. **To determine loading step** depending on the calculated critical load $P_{CR,FEM}$ specified in Chapter 1. The minimum number of steps for the calculation to predict the critical force is 3 qt. $\Delta P = \frac{P_{CR,FEM}}{n}$. My recommendation is to use at least $n = 10$ qt.
3. To determine **the value of the first natural frequency under loading $f_{P=\Delta P}$** using the finite element method.
4. To determine the parameters of the model experiment:
 - **Frequency range:** $0 \cdots 5 \cdot f_{P=0N,FEM}$
 - **Resolution:** $\max \Delta f = \frac{f_{P=0N,FEM} - f_{P=\Delta P}}{2}$
 - **Scanning point:** it should be selected so that the overall time of scanning does not exceed 15 minutes or the time set by the commissioner.
5. To take experimental modal measurements without loading. Compare the acquired first natural frequency with the calculated frequency. **Make sure that all measurements correspond to expected ones** and the quality of the acquired shapes of fluctuations is appropriate for use.
6. Two experimental modal measurements under the load equal to Δf , $2\Delta f$ should be taken additionally. This is a mandatory minimum data set to begin the VCT-based prediction of the critical load.
7. To make a VCT-based prediction of the critical load.
8. If the following changes in the loading step do not exceed the calculated critical load P_{cr} , then increase the load on ΔP and repeat the measurement, otherwise assume that the critical force has been determined.

A schematic representation of the VCT method algorithm is presented in Fig. 2.19.

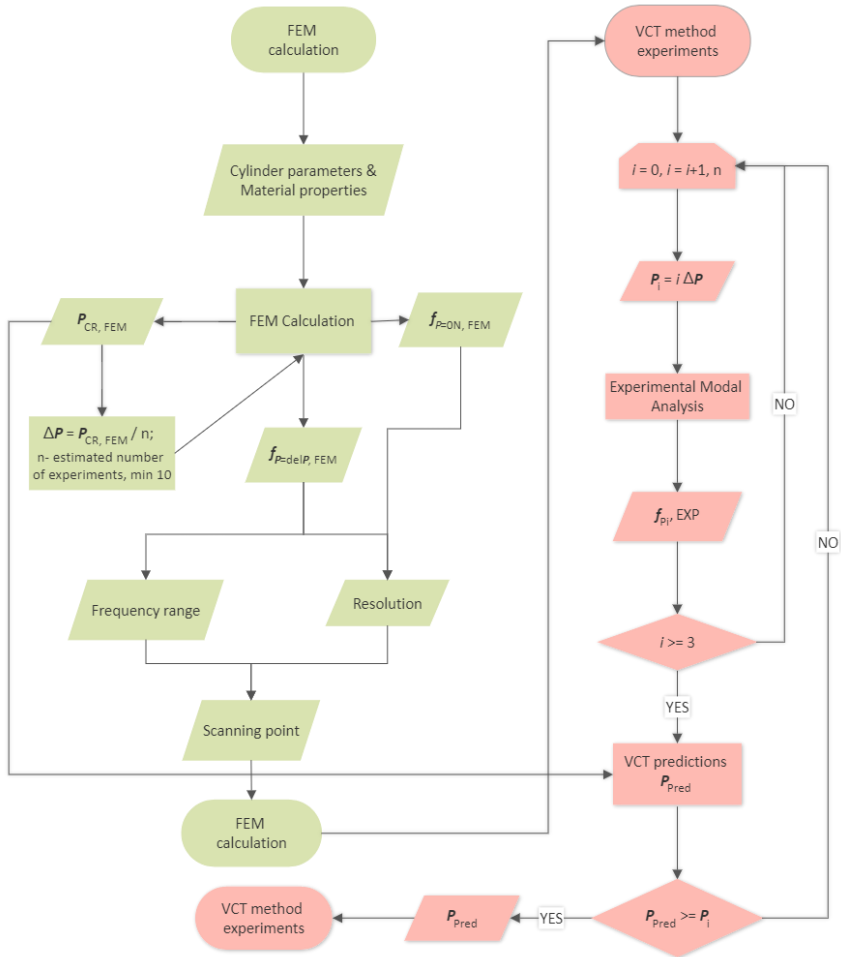


Fig. 2.19. Flowchart of the VCT method.

CHAPTER 3: MAIN RESULTS

Familiarisation and testing for natural frequency decrease under loading in thin-walled cylindrical structures by the vibration correlation technique (VCT) was carried out on two cylinders. A set of cylinders with the diameter of 300 mm and 500 mm was manufactured, they were rolled from ASI 304 0.5 mm thick sheet and then joined by plasma welding. First, the experiment was modelled with the finite element method (FEM) code ANSYS. Modelling VCT with finite elements can be subdivided into two stages. Initially, the calculation is carried out introducing the static load at the axis of the shell and restricting displacements at the other end of the shell. At the second stage, the modal analysis of the shell is carried out by accounting the shell's pre-stressed state from the initial analysis. Next, a physical experiment was carried out. The detailed results are presented in article by *Skukis, E., Kalnins, K., Chate, A. "Preliminary assessment of correlation between vibrations and buckling load of stainless-steel cylinders", Shell Structures: Theory and Applications – Proceedings of the 10th SSTA 2013 Conference, Volume 3, 2014, pp. 325–328, 10th Jubilee Conference on "Shell Structures: Theory and Applications", SSTA 2013, Gdansk, Poland, 16 October 2013.*

The main finding of this paper is the statement that the natural frequency under loading decreases for thin-walled cylindrical structures both in the physical experiment and the finite element method simulation.

The following very important step was to enhance the accuracy of critical force prediction. Analysis of the research in this field shows that the acquired experimental data should be preliminarily normalised. The approach to normalisation suggested by Arbelo is an experimental verification of a novel approach using vibration correlation technique for prediction of realistic buckling loads of unstiffened cylindrical shells loaded under axial compression. Four different test structures were manufactured and loaded up to buckling: two composite laminated cylindrical shells and two stainless steel cylinders. In order to characterise a relationship with the applied load, the first natural frequency of vibration and mode shape is measured during testing using a 3D laser scanner. The proposed vibration correlation technique allows predicting the experimental buckling load with a very good approximation without actually reaching the instability point. The detailed results are presented in article by *Kalnins, K., Arbelo, M. A., Ozolin, O., Skukis, E., Castro, S. G. P., Degenhardt, R., "Experimental non-destructive test for estimation of buckling load on unstiffened cylindrical shells using vibration correlation technique", Shock and Vibration, Volume 2015, Article ID 729684.*

Based on the experience gained from experiments conducted using the VCT method and the opportunity to produce cylinders similar to those used by other researchers, three identical cylinders were produced and tested. They were normalised using the method suggested by Arbelo. The data acquired within this research are presented in the article by *Arbelo, M. A., Kalnins, K., Ozolins, O., Skukis, E., Castro, S. G. P., Degenhardt, R., "Experimental and numerical estimation of buckling load on unstiffened cylindrical shells using a vibration correlation technique", Thin-Walled Structures, Volume 94, 1 September 2015, pp. 273–279.*

The main finding of this paper is that the first frequency shall be used to ensure the most efficient prediction of the critical force. Further, this statement will be disproved, as there are

the frequencies, which disappear during the experiment, those may be also the first frequencies, depending on the geometry and size of a sample. This is why the first frequencies, which remain throughout the VCT testing, should be used.

The normalisation method suggested by Arbelo is not the only one, its comparison with the method suggested by Souza in 1983 is presented in the work by Skukis, E., Ozolins, O., Andersons, J., Kalnins, K., Arbelo, M. A., “*Experimental Test for Estimation of Buckling Load on Unstiffened Cylindrical Shells by Vibration Correlation Technique*”, *Procedia Engineering, Volume 172, 2017, pp. 1023–1030, 12th International Conference Modern Building Materials, Structures and Techniques, MBMST 2016, Vilnius, Lithuania, 26 May 2016.*

This paper also presents optimized boundary conditions for experiments. Optimization excludes the impact of an operator on the final result. Comparison of the impact of boundary conditions is presented in the article by Skukis, E., Ozolins, O., Andersons, J., Kalnins, K., Arbelo, M. A., “*Applicability of the vibration correlation technique for estimation of the buckling load in axial compression of cylindrical isotropic shells with and without circular cutouts*”, *Shock and Vibration, Volume 2017, 29.* The main aims of this paper is to test the opportunities to predict critical force in cylindrical shells with evident defects.

The main finding of this paper is the conclusion that the changed boundary conditions increase the bearing capacity avoiding deterioration of the accuracy in prediction of critical force using the VCT method. This work also represents a simplified and enhanced production process of cylindrical shells by replacing a welded joint for an adhesive bond, which also increases the bearing capacity by 35 %. Furthermore, same as in the earlier works, the most precise prediction is observed within the range close to the critical force. Predictions of the critical force with defects require adjustments and, most likely, another approach to predictions of the critical force.

Application of VCT prediction of the critical force for double load caused by inner pressure and central compression was tested on an orthotropic cylinder. These results are presented in the article by Franzoni, F., Odermann, F., Wilckens, D., Skukis, E., Kalniņš, K., Arbelo, M. A., Degenhardt, R. “*Assessing the axial buckling load of a pressurised orthotropic cylindrical shell through vibration correlation technique*”, *Thin-Walled Structures, Volume 137, April 2019, pp. 353–366.*

The studies on a more advanced method of VCT test data normalisation are partly discussed in the paper by Skukis, E., Jekabsons, G., Andersons, J., Ozolins, O., Labans, E., Kalnins, K. “*Robustness of empirical vibration correlation techniques for predicting the instability of unstiffened cylindrical composite shells in axial compression*”, *Polymers, Volume 12, Issue 12, December 2020.* This work compares two normalisation techniques: the one suggested by Arbelo and the other developed by RTU.

During the work supported by the grant from the Latvian Council of Science, grant number LZP-2018/2-363, a web-site <http://vct.rtu.lv/> was designed to report about all testing procedures, the technique and the equipment, as well as the test results for 59 cylinders. All cylinders were produced of a composite material in three diameters – 100, 300, 500 mm, with various heights from 150 mm to 750 mm and two kinds of layering optimised for the maximum bearing capacity with 3 and 4 layers, respectively. The data are available at <http://vct.rtu.lv/>.

A review of the critical force prediction using the VCT method is presented in the work by Skukis, E., Kalnins, K., Jekabsons, G., Ozolins, O., “Benchmarking of vibration correlation techniques for prediction of buckling load of cylindrical shells”, 16th European Conference on Spacecraft Structures, Materials and Environmental Testing (ECSSMET), 2021.

The process of the implementation of the VCT method is described in Fig. 3.1.



Fig. 3.1. The main results of the implementation of the VCT method presented in the publications.

CHAPTER 4: FINAL REMARKS

In this final chapter, the main achievements of the Thesis are discussed in Section 4.1, whereas Section 4.2 provides critical recommendations and Section 4.3 gives a perspective for future research.

The main work in the presented dissertation can be summarized as follows:

1. As a first step correlation between increment of load level and decrease of frequency has been experimentally confirmed for cylindrical shells. This proof of hypothesis enabled us to further study the applicability of the VCT method for cylinders with and without damage. Nevertheless, initial trials also outlined findings that eigen frequencies do not tend to be equal to 0 Hz upon reaching the buckling load level, which requires a redefinition of criteria or new solutions for normalisation of correlation assumptions.
2. In the present research, a total of 76 cylinders were produced and experimentally tested using the VCT method. Out of particular test campaigns 17 specimens were isotropic while 59 specimens were orthotropic. The dimensional ranges covered R/t ratio 100...2000, given minimum cylinder diameter is 100 mm, the maximum is 8000 mm. Similarly, experimentally assessed series ranges for $R/h = (1/1 \text{ to } 1/4)$. Minimum height is 200 mm, maximum 6000 m.
3. Five different testing equipment and set-ups have been assessed including electromagnetic and hydraulic testing jigs as well as axial compression, axial & bending and axial & internal pressure setups. These test series cover four testing laboratories: RTU Institute of Materials and Structures, Forest and Wood Products Research and Development Institute in Jelgava, DLR Institute of Composite Structures and Adaptive Systems in Braunschweig –, and IMA Materialforschung und Anwendungstechnik GmbH in Dresden.
4. Approbation of the VCT method has been demonstrated on a real scale object – the cryogen tank of the Ariane-6, the newest generation European launcher during its certification testing campaign. Two separate load cases have been investigated and VCT applicability approved. Full-scale tests have confirmed requirements and settings for frequency measurement resolution, location of measurement equipment and ability for seamless integration in certification procedures for full-scale structural tests.
5. As a benchmark both ANSYS and ABAQUS commercial finite element code parametric models have been developed and correlated providing an open source code for the research community as a validated benchmark example on an open data web portal <https://vct.rtu.lv/ansys.html>. Numerous boundary conditions, multilayer stacking sequence combinations and material models are made available and tested.
6. It has been confirmed that testing with hydraulic force actuators should be done with diligence, as equipment excites a phantom frequency which does not diminish throughout load level increment. Therefore, it is very important to isolate the source of vibration.

4.1 Main conclusions

1. It has been confirmed that a classical approach leading buckling/self-frequency correlation to 0 Hz is not valid for composite cylindrical shells. A new normalisation approach for VCT prediction originally has been applied and approached by Souza in 1983. An experimental work has led to contribution of normalisation method also referred as Arbelo (2014) and further improvement Skukis (2020) of developed method based on statistical dataset approved during the presented research work.
2. It was found that the prediction accuracy of the buckling load using either VCT approach proposed by Arbelo or its empirical modification approach proposed by Skukis was virtually insensitive to shell geometry and mounting and loading methods. Moreover, the VCT methods also appeared robust with respect to a lack of natural frequency data for an unloaded shell caused, e.g., by the need for a preload to reliably fix the shell in the test rig. Both VCT methods tended to slightly underestimate the critical load for shells with relatively large experimental KDF values, thus providing not only close but also conservative estimates of the limit load for high-quality shells.
3. The modified VCT has been demonstrated to be an efficient tool for nondestructive prediction of the load-carrying capacity of intact shells. The discrepancy of the predicted and experimental critical load of less than about 10 % was attained when the reduction of fundamental frequency of a shell was monitored under axial loads in excess of 60 % of the buckling load. By contrast, appearance of a local buckling at the cutout, preceding the global buckling of a shell, was found to invalidate the considered VCT for shells with holes.

4.2 Critical recommendations

A testing guidance has been formulated for scaling up vibration correlation technique drawing several critical recommendations:

- A batch of several frequencies should be analysed simultaneously during the load application process by monitoring overall frequency shift estimating statistically proved dependency.
- The best structural excitation and frequency response capture for cylindrical structures could be realised by loudspeaker localization avoiding contact with the testing surface. This reduces both added mass and contact induced frequency mode shape divergence compared to other means of excitation.
- A laser scanning is the best suited method for non-contact frequency and is both scalable and time sensitive during a testing campaign.
- A zero-load level should not be considered, as frequency response may vary compared to actual load distribution pattern. Therefore, a load level of 5 % of linear buckling load should be considered as a first reference point for estimation of VCT.

- Statistical indicators, e.g., modal assurance criteria or modified modal assurance criteria, are a must in monitoring of response in order to clear out structural ghost frequencies from testing grounds or dissipating and merging of frequencies.
- A way to visualise experimental progress has been proposed by plotting frequencies versus oscillation amplitude intensity, therefore providing a comprehensive overview of test campaigns progress.

4.3 Further outlook

Several aspects have been identified for further extension of current research:

- The obtained experimental data set should be further elaborated in development of a frequency shift method including application of machine learning processes for VCT method, thus determining the unloaded waveforms, the safest state for the design and the optimal points for scanning of structural frequencies. It has to be done in order to speed up and simplify the testing process and at the same time to increase the prediction accuracy.
- For a practical applicability, a dedicated (vibration sensor + GSM or WiFi module) IoT sensor can be developed for monitoring a set critical frequency shift and for structural health monitoring.

ACKNOWLEDGMENT

I would like to thank the following people for their help in this research project, without whom I would not have been able to complete this research: the team of the Materials and Construction Research Institute and my colleagues who have come to terms with the peculiarities of my character and love of sports.

Thanks to Olģerts Ozoliņš, a large number of samples were produced, which I then tested. Olģerts also made an invaluable contribution to the creation of new equipment and taught me how to use it.

Thanks go to Mariano Arbelo and his normalisation approach, which is still used in predicting critical strength by the VCT method. In this study, many samples were tested by this method.

The contribution of Gints Jēkabsons in the study was mathematical processing of a large volume of experimental data and helping me to create new normalisation approaches. Thanks to Gints, I discovered the possibilities of Matlab, which were previously hidden for me.

The experience of Jānis Andersons in the analysis and presentation of experimental data, which were successfully applied in this study, was invaluable.

Professor Richard Degenhardt's interest in this study made it possible to conduct experiments on a real design used in the space industry.

Special thanks go to my supervisor Kaspars Kalniņš. Thanks to him, I resumed my doctoral studies. He provided an opportunity to participate in projects that were interesting and brought this study closer to the logical finale. I am also grateful to Kaspars for his constant support and guidance.

And most of all, many thanks to my family for the support you have given me in this study. To my wife Irina, without whom I would have stopped these studies a long time ago. I promise that now I will remove all the papers from the kitchen table!

Finally, many thanks to all the participants who took part in the study and made it possible.

This research was funded by Latvian Council of Science, grant number LZP-2018/2-363.

BIBLIOGRAPHY

- Abramovich, H. G. D. (2015). Buckling prediction of panels using the vibration correlation technique. *Prog. Aerosp. Sci.* 78, 62–73.
- Arbelo, M. A. (2014). Vibration correlation technique for the estimation of real boundary conditions and buckling load of unstiffened plates and cylindrical shells. 79.
- Arbelo, M. A. (2015). Experimental and numerical estimation of buckling load on unstiffened cylindrical shells using a vibration correlation technique. 94.
- Avieable P. (2022). *Modal Analysis of Cylindrical Structures*. Retrieved from https://www.uml.edu/docs/s-v-jan2001_modal_analysis_tcm18-189939.pdf
- Bisagni, C. (2015). Composite cylindrical shells under static and dynamic axial loading: An experimental campaign. *Progress in Aerospace Sciences* 78, pp. 107–115.
- Burgreen, D. (1961). End-fixity effect on vibration and instability. *Trans. Am. Soc. Civil Eng.* 126 (1), 1058–1073.
- Castro, S. G. (2014). Geometric imperfections and lower-bound methods used to calculate knock-down factors for axially compressed composite cylindrical shells. *Thin-Walled Structures*, 118–132.
- Chailleux, A. H. Y. (1975). Experimental study of the buckling of laminated composite columns and plates. *Int. J. Mech. Sci.* 17, 489–498.
- Chaves-Vargas, M., Dafnis, A., Reimerdes, H.-G., Schröder, K.-U. (2015). Modal parameter identification of a compression-loaded CFRP stiffened plate and correlation with its buckling behaviour. *Prog. Aerosp. Sci.* 78, 39–49.
- Chu, T. H. (1949). *Determination of Buckling Loads by Frequency Measurements, Ph.D. Thesis*. California Institute of Technology, Pasadena, CA, USA.
- Composites, H. (2013). *HexPly® 8552 Product Data*.
- Datta, P. K. (1973). Buckling and vibration of a thin tensioned sheet with an elliptical hole. *Experimental Mechanics* 13(7), 280–286.
- Datta, P. K. (1979). Static stability behaviour of plate elements with non-uniform, in-plane stress distribution. *Journal of Mechanical Engineering Science* 21(5), 363–365.
- Degenhardt, R. K. (2007). Experiments on buckling and postbuckling of thin-walled CFRP structures using advanced measurement systems. *International Journal of Structural Stability and Dynamics* 7(02), 337–358.
- DESICOS. (2019, 05 05). *Shell Buckling Knockdown Factor project by NASA*. Retrieved from <https://s.dlr.de/index.php/sbkf-by-nasa>
- ESA. (2019). *NASA Has a Crush on You, NASA's Shell Buckling Knockdown Factor (SBKF) project*. Retrieved from <https://www.nasa.gov/topics/technology/features/sbkf.html>
- Evkin, A. (2019). Dynamic energy barrier estimation for spherical shells under external pressure. *International Journal of Mechanical Sciences* 160, 51–58.
- Evkin, A. K. (2019). Local buckling of axially compressed cylindrical shells with different boundary conditions. *Thin-Walled Structures* 141, 374–388.
- Experimental Mechanics 10(11). (1970). *Recent Experimental Studies on the Buckling of Stringer-Stiffened Cylindrical Shells (Eng. Report TAE No 100)*. Israel Institute of Technology, Haifa, IL.
- Franzoni, F. (2019). Nondestructive vibration-based method for buckling prediction of unstiffened composite cylindrical shells: experimental study and parametric analysis. *Compos. Struct.*
- Franzoni, F. D. (2019). Vibration correlation technique for predicting the buckling load of imperfection-sensitive isotropic cylindrical shells: An analytical and numerical verification. 140.

- Hamidzadeh, H. R., Jazar, R. N. (2009). *Modal Analysis of Cylindrical Structures*. Boston, MA: Springer.
- Horton, W. H. (1977). Determination of the critical loads of shells by nondestructive methods. *Experimental Mechanics* 17(4), 154–160.
- ISO7626-2. (2015). *Vibration and shock – Experimental determination of mechanical mobility – Part 2: Measurements using single-point translation excitation with an attached vibration*.
- Johnson, E. G. (1953). The determination of the critical load of a column. 11(1).
- Kalnins, K. A. (2015). Experimental Nondestructive Test for Estimation of Buckling Load on Unstiffened Cylindrical Shells Using Vibration Correlation Technique.
- Kennedy, D. a. (2018). Critical buckling predictions for plates and stiffened panels from natural frequency measurements. *Conference Series 1106*, (Journal of Physics).
- Kjær, B. (2022). *Sound & Vibration Measurement*. Retrieved from <http://hnutest.hnu.edu.cn/pdf/20150826110815181.pdf>
- Labans, E. A. (2019). An experimental vibration-buckling investigation on classical and variable angle tow composite shells under axial compression. 449.
- Lancaster, E. R., Calladine, C.R., Palmer, S.C., (2000). Paradoxical buckling behaviour of a thin cylindrical shell under axial compression. *International Journal of Mechanical Sciences*, 42, 843–864.
- Leissa, A. (1973). *Vibration of Shells (NASA SP-288)*. Washington: US Government Printing Office.
- Leissa, A. W. (1973). *Vibration of Shells (NASA SP-288), tech. rep.* Washington: US Government Printing Office.
- Lurie, H. (1951). Effective end restraint of columns by frequency measurements. *Journal of the Aeronautical Sciences* 18(8), 566–567.
- Lurie, H. (1952). Lateral vibrations as related to structural stability. *ASME J. Appl. Mech.*
- Maia N., Silva., J. (1997). *Theoretical and Experimental Modal Analysis*. UK: Research Studies Press.
- Mandal, P. (2002). Prediction of buckling load from vibration measurements in New Approaches to Structural Mechanics. *Shells and Biological Structures (eds. Drew, H. and Pellegrino, S.), Solid Mechanics and Its Applications, Vol. 104*, 175–188.
- NASA. (2019). *NASA Has a Crush on You, NASA's Shell Buckling Knockdown Factor (SBKF) project*. Retrieved from <https://www.nasa.gov/topics/technology/features/sbkf.html>
- Pastora, M., Binda., M. (2012). Modal Assurance Criterion. *MMaMS 2012, Procedia Engineering* 48, pp. 543–548.
- Polytec. (2001). *Polytec Scanning Vibrometer, Theory Manual. PSV, PSV-3D, MSA/MSV, As Of Software 8.5*. Germany: Polytec.
- Polytec. (2016). *Polytec PSV-E-500 Operating Instructions Manual*. Germany: Polytec.
- Polytec. (2022). *Laser Doppler vibrometry*. Retrieved from <https://www.polytec.com/int/vibrometry/technology/laser-doppler-vibrometry>
- Radhakrishnan, R. (1973). Prediction of buckling strengths of cylindrical shells from their natural frequencies. 2.
- Segal, Y. (1980). *Prediction of buckling load and loading conditions of stiffened shells*. Faculty of Aeronautical Engineering, Technion – Israel Institute of Technology.
- Shahgholian Ghahfarokhi, R. (2018). Buckling load prediction of grid-stiffened composite cylindrical shells using the vibration correlation technique. *Compos. Sci. Tech.* 167, 470–481.
- Singer, J. (1980). *Buckling Experiments on Shells – A Review of Recent Developments*. Technion Israel Institute of Technology.

- Singer, J., Abramovich, H. (1979). Vibration correlation techniques for definition of practical boundary conditions in stiffened shells. *AIAA J.* 17 (7), 762–769.
- Singer, J., Arbocz, J., Weller, T., (2002). *Buckling Experiments: Experimental Methods in Buckling of Thin-Walled Structures, Shells, Built-up Structures, Composites and Additional Topics Vols 2*. New York: John Wiley & Sons.
- Skukis, E., Ozolins, O., Andersons, J., Kalnins, K., Arbelo, M.A., (2017). Applicability of the Vibration Correlation Technique for Estimation of the Buckling Load in Axial Compression of Cylindrical Isotropic Shells with and without Circular Cutouts. *Shock and Vibration*.
- Skukis, E., Ozolins, O., Kalnins, K., Arbelo, M.A., (2017). Experimental test for estimation of buckling load on unstiffened cylindrical shells by vibration correlation technique. *Procedia Eng.* 172, pp. 1023–1030.
- Skukis, E. J. (2020). Robustness of empirical vibration correlation techniques for predicting the instability of unstiffened cylindrical composite shells in axial compression.
- Somerfeld, A. (1905). Eine einfache Vorrichtung zur Veranschaulichung des Knickungsvorganges.
- Souza, M. A., Fok, W.C., Walker, A.C., (1983). Review of experimental techniques for thin-walled structures liable to buckling: neutral and unstable buckling. *Exp. Tech.* 7 (9).
- Souza, M. A. (1991). A new technique for the prediction of buckling loads from nondestructive vibration tests.
- Theory, M. (2008). *Polytec Scanning Vibrometer*.
- Virgin, L. (2007). *Vibration of Axially Loaded Structures*. Cambridge University Press: Cambridge.
- Wagner, H. N. (2017). Robust design criterion for axially loaded cylindrical shells—Simulation and validation. *ThinWalled Structures* 115, 154–162.
- Wang, L. R.-A. (1966). Effect of boundary conditions on shell buckling. *Journal of the Engineering Mechanics Division* 92(6), 101–116.
- Weingarten, V. I., Seide, P., Peterson, J.P. (1968). *Buckling of Thin-Walled Circular Cylinders*. NASA-SP-8007.
- Weingarten, V. I., Seide, P., Peterson, J. P. ((Revised 1968), 1965). Buckling of Thin-walled Circular Cylinders (NASA SP-8007). *NASA Space Vehicle Design Criteria – Structures*.
- Weller, T. a. (1970). Experimental studies on buckling of ring-stiffened conical shells under axial compression. *Experimental Mechanics* 10(11), 449–457.
- Wesolowski, M. (2010). *Dissertation thesis, Development and validation of an effective inverse technique for characterisation of advanced composite material properties*. Riga, Latvia: RTU.
- Wilckens, D. (2020). *Buckling tests on unstiffened cylindrical shells (ITOBUCK WP 3) tech. rep.*
- Zhang Y. H., Xie, S. L., Zhang, X., N. (2008). Vibration control of a simply supported cylindrical shell using a laminated piezoelectric actuator. *Acta Mechanica volume 196*, 87–101.
- Zimmermann, R. K. (2006). Buckling and postbuckling of stringer stiffened fibre composite curved panels – Tests and computations. *Composite Structures* 73, 150–161.

ANNEX / PUBLICATIONS

I

Skukis E., Kalnins K., Chate

“Preliminary assessment of correlation between vibrations and buckling load of stainless steel cylinders”

"Shell Structures: Theory and Applications", SSTA 2013; 2013, 325-328.

Parameters (2022/09/01)

ISBN	978-113800082-7
Citations in Scopus	10
FWCI	4.56
IF	-

Preliminary assessment of correlation between vibrations and buckling load of stainless steel cylinders

E. Skukis, K. Kalnins & A. Chate
Riga Technical University, Riga, Latvia

ABSTRACT: The current research focuses on the preliminary assessment of correlation between the shift of modal response due to compression stresses and its influence in estimation of buckling load. Such a methodology is known as Vibration Correlation Technique (VCT) and has a potential for estimation of limit load for axially loaded structures from a set of self-frequency measurements. For a particular study a finite element eigenvalue analysis involving axially loaded state of the structure was compared with modal tests of axially loaded cylinders. A set of cylinders has been manufactured with the radius/thickness ratios of 300/500 and rolled from ASI 304 0.5mm thick sheet, then joined by plasma welding. Obtained preliminary vibration results confirmed the trend required for identification of the buckling load. However, it has been noted that the sensitivity of obtained results are highly dependent on the technique applied for excitation of the structure. Therefore a set of recommendations for further study is proposed.

1 INTRODUCTION

Stability is one of most important failure modes of thin-walled structures subjected to compressive loading. In practice it is sufficiently difficult to experimentally determine the buckling load of thin-walled structures by exploiting static test methods. Since even the smallest amount of imperfection of the specimen or boundary conditions can have an apparent impact on the buckling behaviour, thus diverging obtained results from theoretical estimates. There is a need for an alternative approach in order to determine buckling loads for such structures. One of the major aspects of non-destructive testing techniques is the ability to accurately predict buckling loads without damaging the tested specimen itself. In present study the Vibration Correlation Technique (VCT) was explored to derive buckling loads for thin-walled structures.

A research by Lurie (Lurie, H., 1950) showed that for columns in the form of rigid rectangular frames the relationship between the square of the frequency and the load is almost linear, and that the extrapolated load corresponding to a zero frequency coincides with the buckling load. In the case of a flat plate, tests showed that such linear behaviour may not be achieved in physical tests because plate equations are not valid due to initial curvatures of actual plates. More recently (Sukajit, P. & Singhatanadgid, P 2007) studied the analytical relationship between the buckling and vibration behaviour of thin plate. The relationship between applied in-plane load and the natural frequency of plates were derived from the differential governing equations of both problems. The relationship (the square of the natural frequency is linearly related to the applied load) was verified by applying the Ritz method. Research has been extended (Singhatanadgid, P. & Sukajit 2011) in the form of modal test series by employing VCT. A set

of rectangular plates has been tested for natural frequencies by utilizing an impact test method. The measured buckling load was determined from the plot of square of the measured natural frequency versus an in plane load (tensile). The buckling loads from the measured vibration data come to good agreement with the numerical solutions. Souza and Assaid (Souza, M. A. & Assaid, L. 1991), Abramovich and Singer (Abramovich, H. & Singer, J. 1978) and Singer and Abramovich (Singer, J. & Abramovich, H. 1979) have extended the VCT approach to thin wall shell structures. Singer, Arboez and Weller provided the most detailed descriptions about the application of VCT for non-destructive buckling testing of the thin-walled cylindrical structures.

2 VIBRATION CORRELATION TECHNIQUES.

The VCT method is aimed to reduce the scatter in prediction of buckling loads for thin-walled shells. This approach determines the real natural frequencies of the in-situ shell as a function of the applied axial load. Nevertheless, it hasn't been fully exploited so far as it requires implementation of both destructive and non-destructive testing means as well as high – fidelity measurements.

Both theoretical and experimental research reported in the literature had shown that in some cases a linear descending relationship may be observed. Thus this relationship can be expressed as

$$\frac{P}{P_{cr}} + \left(\frac{f_m}{f_0}\right)^2 = 1 \quad (1)$$

where P is the applied load, P_{cr} is the buckling load, f_0 is the frequency without any load applied, and f_m is the frequency at load prestress state P . The above equation states that for structure reaching the

buckling load level the natural frequency of the structure (f_m) would become zero (see Fig. 1).

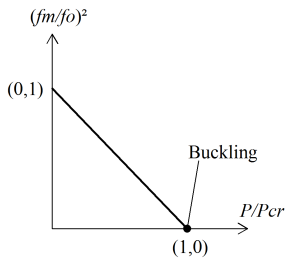


Figure 1. Relationship between dimensionless squared frequency and buckling load.

3 MATERIALS AND METHODS

3.1 Test specimens

For current study two thin-walled stainless steel cylinders with the following geometrical and material characteristics were selected:

- 1st cylinder (D300): the cylinder length was 400 mm; the cylinder radius was 150 mm;
- 2nd cylinder (D500): the cylinder was 500 mm in length; the cylinder radius was 250mm.

Both cylinders share the same characteristics: the thickness of both cylinders was 0.5 mm, Young's modulus 204 GPa, Poisson's ratio of 0.3, material density 8000 kg/m³ were considered. The shells, which are pinned in both ends, are examined in this study.

3.2 Finite element analysis

All numerical calculation has been performed employing the finite element method (FEM) code ANSYS. A SHELL281 8-node finite element has been selected for the current study, which is suitable for analysis of thin to moderately-thick shell structures. The element has eight nodes with six degrees of freedom at each node.

Modelling VCT with finite elements (see Fig.2) can be subdivided into two stages. Initially, the calculation is carried out as static load introduced at the axis of the shell and restricting displacements at other end of the shell. At the second stage the shell modal analysis is carried out, by accounting the shell's pre-stressed state from initial analysis.

Typical mode shapes, which were obtained during the modal analysis, are shown for 1st cylinder in Fig. 3 (shell D300). Where index m corresponds to the number of half waves in the longitudinal direction and n indicates the half waves in the radial direction. The obtained relationship between the compressive load and the appropriate shell natural vibration frequencies square is displayed in Fig. 4 (shell D300) and in Fig. 6 (shell D500). As one may observe from

derived graphs, both the VCT and FEM approaches tend to result in, similar buckling load level $P_{cr}=220$ kN for both shells. Nevertheless, each cylinder has its unique natural frequency level. Moreover, in addition a non-linear postbuckling FEM analysis (see Fig. 5) has been performed applying side perturbation load at different load levels. In these analyses the buckling load level may reach up to $P_{cr}= 200$ kN, however even with slight side load the buckling load of the shell may decrease by 40%.

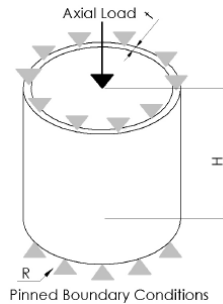


Figure 2. Specimen geometrical variables and test set-up

Modes	Front view	Isometric view
$m=1; n=14$		
$m=1; n=12$		
$m=2; n=18$		
$m=2; n=16$		

Figure 3. Finite element model (mode shapes) for shell D300.

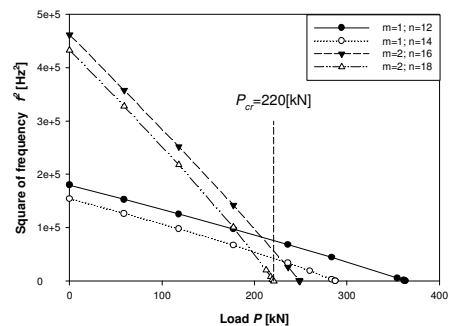


Figure 4. VCT analytical experiments on cylinder (D300).

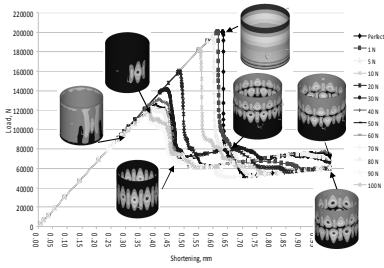


Figure 5. Postbuckling analytical experiment on cylinder (D300).

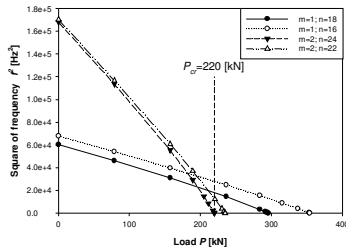


Figure 6. VCT correlation obtained with FE analysis of (D500) cylinder.

3.3 Experimental Modal Analysis

For the purpose of the experiment the testing equipment Zwick Z100 and vibrometer Polytech PSV-400 have been employed for current research. The PSV-400 vibrometer is a laser-based measurement tool for non-contact measurements, visualization and analysis of structural vibrations. In a modal test entire surfaces can be scanned and probed automatically by applying flexible and interactive measurement grids. Moreover, measurements can be made over a wide frequency bandwidth. Excitation of the structure has been introduced by software controllable shaker or loudspeaker, depending on the structure stiffness. Structural responses has been captured by a laser vibrometer and converted to graphical mode shapes for visual matching with FEM eigenmode results.

Experimental procedure has been performed in a following sequence of steps. Initially, the cylinder structure has been pinned in testing support plates with spherical support and preloaded to the load level of 1kN. Thus assuring that natural frequency mode corresponding to the boundary conditions as determined from FE analysis. Then the load level has been increased by 20kN step with corresponding natural frequency measurement. These steps have been repeated on different cylinders and varying the vibration excitation means. The experimental set-up of VCT is shown in Fig. 7 where the numbers indicate the following items: 1) test sample; 2) Zwick Z100 testing equipment; 3) Polytech PSV-400 modal vibrometer; 4) modal data controller; 5) light source; 6) tested specimen; 7) spherical support.

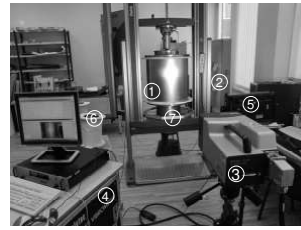


Figure 7. Experimental VCT set-up at Riga Technical University, Institute of Materials and Structures.

Obtained preliminary results – pre-stress load level with corresponding modes have been summarised for the cylinders D300 (see Fig.8) and D500 (see Fig.9).

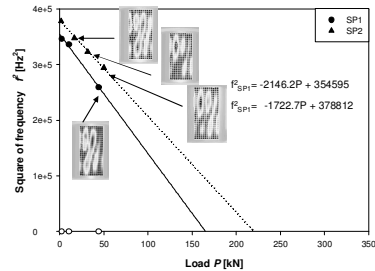


Figure 8. VCT graph with natural frequency modal shapes on cylinder (D300).

4 RESULTS

Obtained results from numerical eigenfrequencies confirm expected correlation between the natural frequency shifts towards the zero once it has been axially loaded up to the buckling of the structure. Even though vibration correlation technique is not limited to the only first eigenfrequency in numerical and experimental results was particularly difficult to follow the initial mode shape as due pre-stress a mode shift may cause merging even an additional local mode development. Therefore, a particular attention was given to follow the same mode pattern with corresponding half-waves in longitudinal and radial directions. Moreover, from a non-linear buckling analysis with minor perturbation load it has been identified that buckling load is neither robust nor associated with the only one mode shape. Therefore, buckling load should be correlated with both vibration modes having longitudinal half waves $m=2$ and $m=1$.

Furthermore experimental natural frequency measurements have been plotted and buckling load determined by linear regression as shown in Fig.8. As it has been suggested by other researcher in literature a different regression models have been examined in order to assess the robustness of a correlation approach as outlined in Figure 9. One may see that at least a second order polynomial function would be the most suitable for a more reliable determination of

experimental buckling load. However, function type and corresponding coefficient should be further elaborated in more detail once the number of samples would be sufficient to allow the test sample to buckle. For preliminary analysis cylinders were not subjected to buckling due to the limit load stress level close to the plasticity of stainless steel.

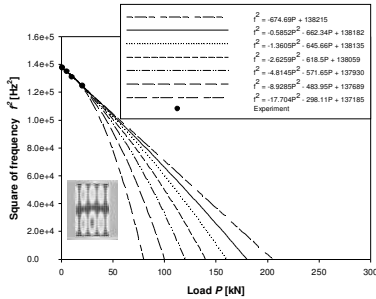


Figure 9. Extrapolation of VCT versus physical experiments of cylinder (D500)

It should be noted that for the improvement of reliability of vibration tests some further considerations should be taken. For vibration excitation a contactless means should be considered as loudspeaker or micro fibre composite actuators as even few newton perturbation load levels can cause mode shift and decrease of the buckling load in the imperfection-sensitive cylindrical structure. For samples with small a diameter, a 2D measurement of natural frequency modes causing significant scatter. Moreover, some load relaxation can be observed and this issue should be addressed during further studies. These are just of a few considerations for further experimental and numerical study of vibration correlation technique applicability on isotropic and orthotropic cylindrical shells.

5 CONCLUSIONS

It has been demonstrated from preliminary analysis that vibration correlation technique may be successfully applied for determination of buckling load of axially compressed cylindrical structures. Moreover a non-destructive control may be stated as main advantage of this method as it provides the opportunity of suspending the loss of shell stability during physical

experiment as well as it provides possibility to assess the level of pre-stress or even to determine the shell load carrying capacity. A further quantitative study would evaluate reliability of this approach as it requires a series of specimens loaded to the highest stress/strain level.

ACKNOWLEDGEMENTS

The research leading to these results has received the funding from the European Community's 7th Framework Programme (FP7/2007-2013) under grant agreement 282522 a project DESICOS (www.desicos.eu).

REFERENCES

- Abramovich, H. & Singer, J. 1978. Correlation between vibrations and buckling of cylindrical shells under external pressure and combined loading. *Israel J. of Technology* (16): 34-44.
- Lurie, H. 1950. Lateral vibrations as related to structural stability. *PhD Thesis, California Institute of Technology: Pasadena, California, USA.*
- Singer, J. & Abramovich, H. 1979. Vibration correlation techniques for definition of practical boundary conditions in stiffened shells. *AIAA J.*, 17(7): 762- 769.
- Singer, J., Arbocz, J. & Weller, T. 2002. *Buckling experiments: Experimental methods in buckling of thin-walled structures. Vol.2* New York: John Wiley & Sons.
- Singhatanadgid, P. & Sukajit, P. 2011. Experimental determination of the buckling load of rectangular plates using vibration correlation technique. *An International Journal Structural Engineering & Mechanics* 37(3): 331-349.
- Souza, M.A. & Assaid, L.M.B. 1991. A new technique for the prediction of buckling loads from nondestructive vibration tests. *Experimental Mechanics* 31(2): 93-97.
- Sukajit, P. & Singhatanadgid, P. 2007. Identification of buckling load of thin plate using the vibration correlation technique. Proc. of the 21st Conference of Mechanical Engineering Network of Thailand, Chonburi, Thailand, 17 -19 October 2007: 520-525.

II

Kalnins K., Arbelo M.A., Ozolins O., **Skukis E.**, Castro S.G.P., Degenhardt R.

“Experimental non-destructive test for estimation of buckling load on unstiffened cylindrical shells using vibration correlation technique”

Shock and Vibration, Open access, Volume 2015, Article ID 729684.

Parameters (2022/09/01)

DOI	10.1155/2015/729684
Citations in Scopus	24
FWCI	0.54
IF	1.59

Research Article

Experimental Nondestructive Test for Estimation of Buckling Load on Unstiffened Cylindrical Shells Using Vibration Correlation Technique

Kaspars Kalnins,¹ Mariano A. Arbelo,² Olgerts Ozolins,¹ Eduards Skukis,¹ Saullo G. P. Castro,³ and Richard Degenhardt⁴

¹Riga Technical University (RTU), Institute of Materials and Structures, Azenes 16, Riga LV-1048, Latvia

²Department of Aeronautics, Aeronautics Institute of Technology (ITA), 12228-900 São José dos Campos, SP, Brazil

³Embraer (Brazilian Aerospace Company), 12227-901 São José dos Campos, SP, Brazil

⁴DLR, Institute of Composite Structures and Adaptive Systems, Lilienthalplatz 7, 38108 Braunschweig, Germany

Correspondence should be addressed to Mariano A. Arbelo; arbelom@gmail.com

Received 4 June 2015; Accepted 27 July 2015

Academic Editor: Matteo Aureli

Copyright © 2015 Kaspars Kalnins et al. This is an open access article distributed under the Creative Commons Attribution License, which permits unrestricted use, distribution, and reproduction in any medium, provided the original work is properly cited.

Nondestructive methods, to calculate the buckling load of imperfection sensitive thin-walled structures, such as large-scale aerospace structures, are one of the most important techniques for the evaluation of new structures and validation of numerical models. The vibration correlation technique (VCT) allows determining the buckling load for several types of structures without reaching the instability point, but this technique is still under development for thin-walled plates and shells. This paper presents and discusses an experimental verification of a novel approach using vibration correlation technique for the prediction of realistic buckling loads of unstiffened cylindrical shells loaded under axial compression. Four different test structures were manufactured and loaded up to buckling: two composite laminated cylindrical shells and two stainless steel cylinders. In order to characterize a relationship with the applied load, the first natural frequency of vibration and mode shape is measured during testing using a 3D laser scanner. The proposed vibration correlation technique allows one to predict the experimental buckling load with a very good approximation without actually reaching the instability point. Additional experimental tests and numerical models are currently under development to further validate the proposed approach for composite and metallic conical structures.

1. Introduction

Southwell [1] proposed one of the first nondestructive methods to predict the buckling load of simple structures such as slender beams, which was modified by Galletly and Reynolds [2] in order to be applicable for stiffened cylindrical shells. The main disadvantage of the latter is the need of high applied loads, close to the onset of buckling, in order to provide a reliable prediction of the buckling load.

Vibration correlation methods can also be used as a nondestructive technique. The concept of relating vibration characteristics to buckling loads was considered at the beginning of the 20th century for Sommerfeld, 1905 [3], but only in the 50s some experimental investigations were conducted by Chu, 1949 [4], Lurie, 1952 [5], and Meier, 1953 [6], among

others. A very detailed review of the theory, application, experimental setup, and results of the vibration correlation technique (VCT) approach on different structures can be found in the work of Singer et al. [7] (Chapter 15).

For a better understanding of the applications of VCT on plates and shells it is important to classify the method according to its purpose: (1) determination of actual boundary conditions for numerical calculation purposes; (2) direct estimation of buckling load. This paper deals with the direct determination of the buckling load on cylindrical shells.

There is no established procedure about how to apply the VCT for unstiffened cylindrical shells, commonly used in space applications for launcher structures. This type of structure is usually associated with a high imperfection sensitivity, requiring the application of empirical guidelines in order

TABLE I: Geometric parameters for tested cylinders.

	R15	Z37	SST-1	SST-2
Free length (L) [mm]	500	800	500	800
Radius (R) [mm]	250	400	250	400
Thickness (t) [mm]	0.523	0.785	0.5	0.5
Layup [in-out]	$[(\pm 24^\circ)/(\pm 41^\circ)] \pm 1^\circ$	$[(\pm 34^\circ)/0_2/(\pm 53^\circ)] \pm 1^\circ$		

to calculate the design buckling load, currently leading to conservative estimations (Degenhardt et al., 2010 [8]). Skukis et al., 2013 [9], presented a preliminary assessment correlating the vibration modes with the buckling load of stainless steel cylinders. If a relationship between the buckling load and the variation of the natural frequencies of vibration exists, it is possible to use the VCT as a nondestructive technique for estimating the real knockdown factor of space structures. Moreover, for this type of structures, there is a remarkable influence of the boundary conditions on the buckling load (see Zimmermann, 1996 [10], and Hühne et al., 2002 [11]), where the VCT could be used for a better characterization of the actual boundary conditions in order to provide reliable data for numerical simulation, such as finite element models (see Hilburger et al., 2004 [12], Degenhardt et al., 2008 [13], and Degenhardt et al., 2010 [8]).

Recent efforts to improve the work done so far on the VCT field are presented by Jansen et al., 2014 [14], where new semi-analytical tools are introduced to extend the existing semiempirical VCT for shells, considering both the nonlinear effect of the static state and the nonlinear effect of the geometric imperfections.

The current paper will present and discuss an experimental verification of a new VCT approach presented by Arbelo et al., 2014 [15]. This approach is based on the observations made by Souza et al., 1983 [16]. The original approach proposed by Souza is a linear fit between $(1-p)^2$ and $(1-f^4)$, where $p = (P/P_{cr})$ and $f = (f_m/f_0)$; P is the applied axial load, P_{cr} is the critical buckling load for a perfect shell, f_m is the measured frequency at P load, and f_0 is the natural frequency of the unloaded shell. Souza states that the value of $(1-p)^2$ corresponding to $(1-f^4) = 1$ would represent the square of the drop of the load carrying capacity (ξ^2), due to the initial imperfections. However, if this approach is applied to unstiffened cylindrical shells, the results will be negative values of the drop of the load carrying capacity (ξ^2), which does not have a coherent physical meaning (see Arbelo et al., 2014 [15]).

Instead of plotting $(1-p)^2$ versus $(1-f^4)$, Arbelo proposed to plot $(1-p)^2$ versus $(1-f^2)$ and represented the points by a second-order fitting curve. Therefore, the minimum value of $(1-p)^2$ obtained using this approximation represents the square of the knockdown of the load carrying capacity (ξ^2) for unstiffened cylindrical shells. Then, the buckling load can be estimate by

$$P_{\text{imperfect}} = P_{cr} \left(1 - \sqrt{\xi^2} \right). \quad (1)$$

For the validation of the proposed empirical VCT approach, this paper presents four experimental tests

conducted on composite and metallic unstiffened cylinders with clamped boundary conditions. The applied load and the first natural frequency of vibration and mode shape are measured and correlated. The initial geometric imperfection shape of each cylinder is measured using a 3D noncontact laser scan.

The main goal on this work is to compare the predicted buckling load versus the real buckling load measured on samples with different materials, geometries (radius, thickness, and height) and fabrication technologies. More details about each study case are given in the following section.

2. Experimental Test: Materials and Methods

2.1. Test Specimen: Overview. Two laminated composites and two stainless steel cylindrical shells are fabricated and tested. Details of each specimen are described in the following.

2.1.1. Composite Cylindrical Shell "R15" with $R/t = 478$. The R15 cylinder is fabricated at RTU by hand-layup, using 4 plies of unidirectional (UD) carbon fiber prepreg Hexcel IM7/8552, and cured out of autoclave. The geometry and layup are presented in Table 1. The material properties were measured according to the ASTM D3039 [17], D3410 [18], and D3518 [19] standards for tension, compression, and shear, respectively. The results are presented in Table 2, where E_i^j is the elastic modulus along the fiber direction ($i = 1$) or matrix direction ($i = 2$) in tension ($j = T$) or compression ($j = C$). G_{12} is the shear modulus and ν_{12} is the Poisson ratio. S_i^j is the maximum strength along the fiber direction ($i = 1$) or matrix direction ($i = 2$) in tension ($j = T$) or compression ($j = C$). S_{12} is the shear strength. t -ply is the ply thickness.

After fabrication the top and bottom edges are trimmed and clamped using a resin potting and metallic rings. The final radius over thickness (R/t) ratio is about 478.

2.1.2. Composite Cylindrical Shell "Z37" with $R/t = 510$. The Z37 cylinder is fabricated at DLR-Braunschweig by hand-layup, using 6 plies of the same unidirectional (UD) carbon fiber prepreg Hexcel IM7/8552. The geometry and layup are presented in Table 1. This cylinder is clamped on both ends using a sand-resin concrete and the final R/t radius is about 510.

2.1.3. Stainless Steel Cylindrical Shell "SST-1" with $R/t = 500$. The stainless steel cylinder SST-1 is manufactured and tested at RTU. The cylinder is manufactured from a flat plate of AISI 304 stainless steel, rolled up to the desired curvature, and closed forming a top joint which is laser-welded. The

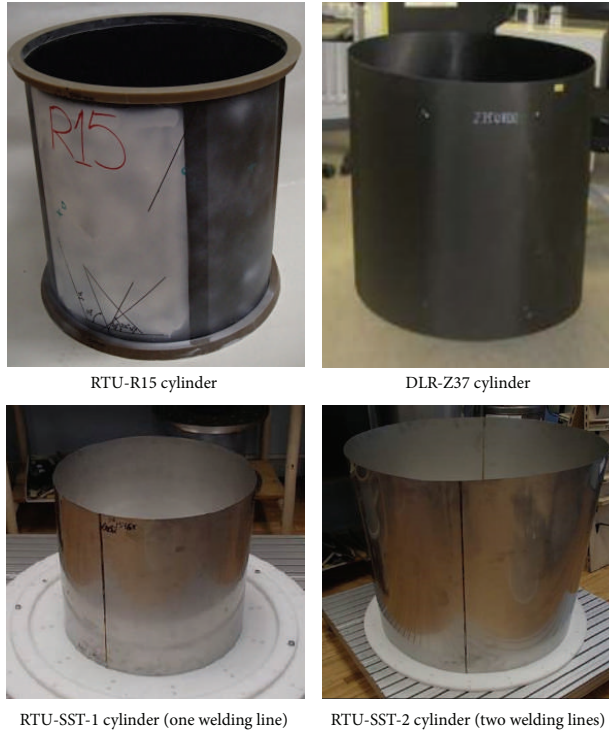


FIGURE 1: Overview of tested cylindrical shells.

geometric parameters are presented in Table 1. The material properties are detailed in Table 3, where S_Y is the yield strength and S_U is the ultimate strength.

The laser welding technique used to join both ends of the specimen generates a characteristic imperfection signature, not observed on the composite specimens, which is discussed in the next sections.

After fabrication, the top and bottom edges are clamped using a resin potting supported by metallic rings.

2.1.4. Stainless Steel Cylindrical Shell “SST-2” with $R/t = 800$. The stainless steel cylinder SST-2 is also manufactured and tested at RTU. The cylinder is manufactured from two flat plates of the same AISI 304 stainless steel material used on SST-1, rolled up to the desired curvature, and closed using laser welding between the ends. In this case, each plate is half of the cylinder’s perimeter long, resulting in a symmetrical imperfection signature due to the two welding lines. The geometric parameters are presented in Table 1.

Figure 1 shows a general view of each tested specimen.

2.2. Characterization of Initial Geometric Imperfection. A laser scan (Panasonic HL-G1 sensor) is used to measure the geometric imperfection on the inner surface of R15, SST-1, and SST-2 cylinders at RTU. The laser scan is controlled

TABLE 2: Measured material properties of UD prepreg Hexcel IM7/8552.

	Mean value		Std. deviation [%]
E_1^T	171.5	GPa	2.6
E_1^C	150.2	GPa	4.6
E_2^T	8.9	GPa	4.2
E_2^C	9.4	GPa	10.9
G_{12}	5.1	GPa	7.8
ν_{12}	0.32		13
S_1^T	2300	MPa	13.8
S_1^C	857	MPa	10.1
S_2^T	40	MPa	20.4
S_2^C	203	MPa	3.9
S_{12}	51	MPa	8.4
t -ply	0.125	mm	

using an in-house software and the acquired data is exported in real time to a plain text file for further analysis and postprocessing.

For Z37 cylinder DLR uses ATOS 3D measurement system in order to characterize the initial geometric imperfections from the outer surface.

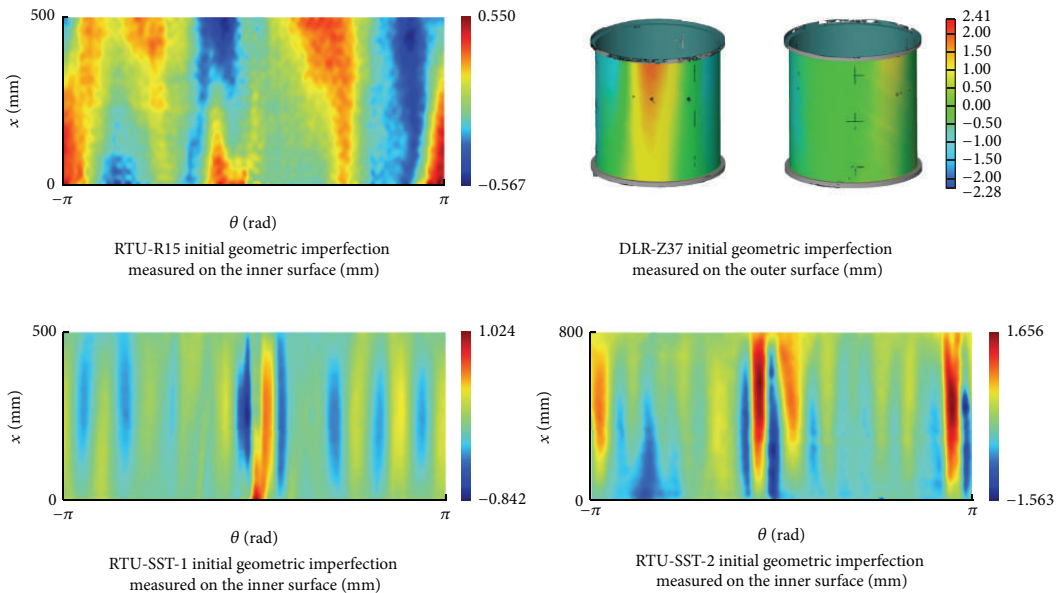


FIGURE 2: Initial geometric imperfection on the studied cylinders.

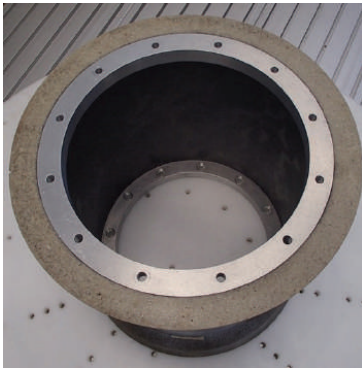


FIGURE 3: Boundary conditions on top and bottom edges.

For all cases the best-fit-cylinder algorithm is applied afterwards over the raw data to eliminate the rigid body motion modes from the measurements. The results are presented in Figure 2, where the imperfection pattern generated by the welding process on SST-1 and SST-2 cylinders can be seen.

2.3. Experimental Test Setup and Boundary Conditions. Because the tests are performed using different testing machines and laboratories (RTU and DLR facilities), the boundary conditions and test setups vary between the studied cases, allowing the authors to verify the robustness of

TABLE 3: Material properties of AISI 304 stainless steel.

E	193	GPa
G	77	GPa
ν	0.29	
S_Y	215	MPa
S_U	505	MPa

the proposed VCT approach. In general, the top and bottom cylinder edges are clamped for all cases using a resin potting that is 25 mm height for RTU and 20 mm for DLR cylinders, together with metallic rings placed at the inner face, as presented in Figure 3. For testing, each cylinder is placed between two metallic plates and glued with epoxy resin. For R15, SST-1, and SST-2 a spherical joint is placed between the crosshead of the testing machine and the loading plate, in order to avoid bending moments (see Figures 4 and 5). DLR test setup for Z37 cylinder uses special loading tables that can be adjusted in order to avoid loading imperfection and bending introduction along the cylinder edges (see Figure 6).

The compression tests for R15 and SST-1 cylindrical shells are performed using a Zwick 100 kN testing machine. Because SST-2 is too large to be fitted on the same machine, an Instron SATEC 600 kN testing machine is used in this case. Z37 cylinder is tested at DLR, using its own hydraulic testing machine. In all cases the compressive load is measured using a load cell and it is applied using displacement control at a constant velocity of 0.5 mm/min.



FIGURE 4: Experimental test setup for compressive loading on R15 and SST-1 cylindrical shells (RTU).

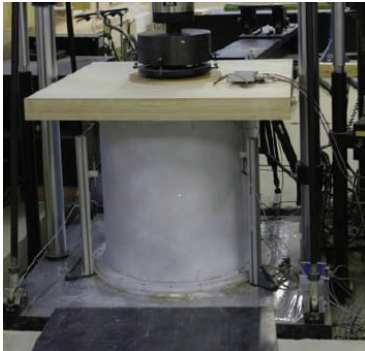


FIGURE 5: Experimental test setup for compressive loading on SST-2 cylindrical shell (RTU).

For the composite cylindrical shells R15 and Z37 two types of tests are carried out in order to verify the proposed VCT approach. First, the cylinder is loaded in compression up to buckling. Notice that the cylinders are designed to buckle in the elastic regime in order to minimize accumulated damage during repeated tests. Once the onset of buckling is found, a second test is performed using a Polytec laser vibrometer to characterize the first natural frequency of vibration and mode shape for different values of applied compressive load, below the onset of buckling. For this test, the cylinder surface is excited with a periodic chirp signal using a loudspeaker placed perpendicularly to the cylinder's surface and the laser is positioned in a rectangular grid of points in order to map the vibration mode for the whole signal spectrum.

The stainless steel cylinders SST-1 and SST-2 must be tested following a different approach. Since the buckling event will produce plastic deformation, no further test can be



FIGURE 6: Experimental test setup for compressive loading on Z37 cylindrical shell (DLR).

TABLE 4: Experimental buckling load of tested cylinders.

Cylinder	Experimental buckling load [kN]
R15	24.2
Z37	59.0
SST-1	70.2
SST-2	49.9

carried out once the onset of buckling is reached. For these cases the compressive load is applied in small increments and the frequencies and vibration modes are measured using the laser vibrometer. This procedure is followed up to buckling, when the structure collapses and is no longer useful.

2.4. Experimental Results. The buckling load obtained for each tested cylinder is summarized in Table 4.

The variation of the first natural frequency of vibration measured on each cylinder is presented in Table 5. Additionally, for the SST-2 cylinder, the second vibration mode is measured (see Table 6) in order to compare the predicted buckling load with the one obtained using the variation of the first vibration mode. An example of the vibration mode shape obtained from the laser vibrometer and overlaid on top of the test specimen Z37 is shown in Figure 7.

3. Validation of the Proposed VCT Approach

In order to predict the onset of buckling following the proposed VCT approach, first presented by Arbelo et al. [15], one needs to know the evolution of the first vibration mode with a growing axial compression on the prebuckling regime, as presented in the previous section, and the critical buckling load of the perfect cylinder (P_{cr}). The latter can be obtained through a linear eigenvalue analysis of a simple finite element model.

For the present study, the finite element model (FEM) is generated using Abaqus. For all four cylinders the mesh adopted after the convergence analysis uses 160 S8R5 [20] square elements distributed along the circumference. The critical buckling loads obtained for a perfect cylindrical shell with the layup, dimensions, materials properties, and

TABLE 5: Variation of the 1st vibration frequency with the applied load.

R15 cylinder		Z37 cylinder		SST-1 cylinder		SST-2 cylinder	
Compressive load [kN]	1st vibration mode [Hz]	Compressive load [kN]	1st vibration mode [Hz]	Compressive load [kN]	1st vibration mode [Hz]	Compressive load [kN]	1st vibration mode [Hz]
0.09	216.75	0	152.5	0	232.75	0	117.5
2.18	212.25	1.2	151.5	4.94	231.75	5.2	116.5
4.16	208	10.2	148.75	10.02	230.5	10.22	115.25
6.16	203.5	20.2	143	20.05	226.5	15.24	113.75
8.2	198.75	30.2	137.25	30.1	222.5	20.24	112.5
10.55	193.5	40.2	130.75	40.04	218.5	24.97	110
12.77	188.25	50.2	123.25	50.2	213.5	30.24	109.75
15	182.75	55.2	119	55.07	211	35.23	107.25
17.57	175.5	58.2	115.5	60.25	208	40.22	106.5
19.42	170					45.23	102.5
20.63	166.25						
22.4	159.75						

TABLE 6: Variation of the 2nd vibration frequency with the applied load on the SST-2 cylinder.

SST-2 cylinder	
Compressive load [kN]	1st vibration mode [Hz]
0	122
5.2	121.25
10.22	120.25
15.24	119.25
20.24	118.25
24.97	117
30.24	114.75
35.23	113.25
40.22	112.25
45.23	109.75

TABLE 7: Critical buckling load of tested cylinders.

Cylinder	Critical buckling load [kN]
R15	35.1
Z37	89.8
SST-1	183.1
SST-2	183.1

boundary conditions used on the studied cases are summarized in Table 7.

The proposed VCT approach can be plotted in function of the dimensionless parameters $(1 - p)^2$ versus $(1 - f^2)$, as shown in Figure 8, for each study case.

The minimum value of $(1 - p)^2$ obtained using this approximation represents the square of the drop of the load carrying capacity (ξ^2). Using (1), the predicted buckling load obtained from the proposed VCT approach for each case is presented in Table 8. A very good correlation can be noticed with the experimental buckling load measured during testing

TABLE 8: Buckling load prediction using the VCT approach for the different studied cases.

Cylinder	Predicted buckling load using VCT [kN]	Deviation from experimental results [%]
R15	26.62	10
Z37	58.41	1
SST-1	70.2	0
SST-2	52.5	5

(see Table 4), with less than 10% of deviation (in most of the studied cases the deviation is lower than 5%).

Additional studies are carried out for the SST-2 structure, where the proposed VCT approach is applied using the second vibration mode. The predicted buckling load in this case is 47.96 kN, with a deviation of 3.9% from the experimental results. It must be mentioned that this result correlates better than the original approach, where the first vibration mode is used (see Table 8). Another important observation is that using the second vibration mode makes the proposed VCT approach more conservative.

The predicted buckling load for R15 cylinder presents a fairly good correlation, despite being clearly not as good as the other studied cases. The authors found out that the load around the top and bottom edges was not evenly distributed along the circumference during testing. In this way, the vibration analysis can give nonconservative results depending on the relative position of the laser scan and the measured surface region. Further studies are currently being conducted in order to quantify a relationship between the initial loading imperfection around the edges and the buckling loads predicted using the VCT.

Furthermore, it is interesting to investigate the minimum threshold of compressive load needed to achieve a good correlation with the proposed VCT approach, with less than 10% deviation from the experimental buckling load.

TABLE 9: Buckling load prediction using the VCT approach for different loading ranges on Z37 cylinder.

Max. load used for VCT [% of experimental buckling load]	Predicted buckling load using VCT [kN]	Deviation from experimental results [%]
98.6%	58.41	1
93.6%	56.58	4.1
85.1%	53.19	9.8
68.1%	45.35	23.1 (fail)

TABLE 10: Buckling load prediction using the VCT approach for different loading ranges on SST-1 cylinder.

Max. load used for VCT [% of experimental buckling load]	Predicted buckling load using VCT [kN]	Deviation from experimental results [%]
85.8%	70.22	0
78.4%	67.11	4.4
71.5%	63.34	9.8
57%	53.74	23.4 (fail)

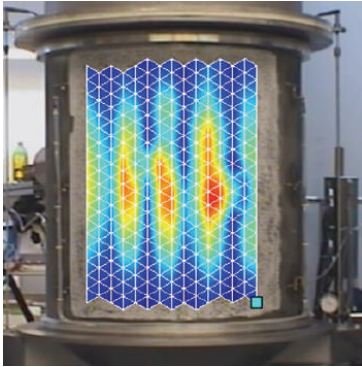


FIGURE 7: First vibration mode shape measured during testing (DLR-Z37).

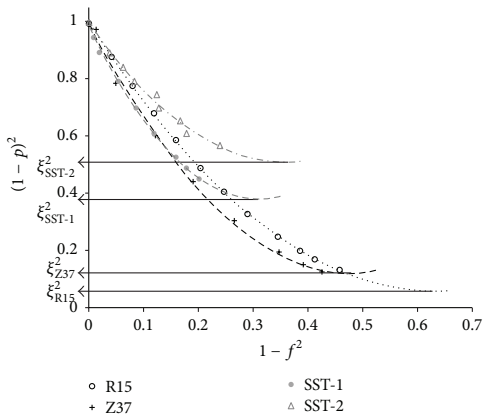


FIGURE 8: Plot of $(1 - p)^2$ versus $(1 - f^2)$ and 2nd-order fit for each tested cylinder.

Tables 9–11 present the VCT results obtained for Z37, SST-1, and SST-2 cylinders, using different ranges of applied load (always starting from the unloaded state).

It is clear that the correlation degrades when the maximum load is lower than 70% of the buckling load.

From these results one concludes that the present approach could be applied as an experimental nondestructive method to estimate the buckling load on unstiffened cylindrical shells loaded in compression. In addition, the authors recommend monitoring also the second vibration mode during the vibration tests, since a better correlation has been found for SST-2 cylinder using the second vibration mode. Further experimental investigations are being addressed by the authors in order to verify the proposed VCT approach for cylindrical shells with different levels of loading imperfections and initial geometric imperfections.

4. Summary and Concluding Remarks

In this paper a validation of a novel empirical approach using the vibration correlation technique as a nondestructive method to estimate the buckling load of unstiffened cylindrical shells is presented. Four tests are carried out in order to verify the robustness of the proposed approach for different structures under different test setups. The material properties and initial geometric imperfections are measured using state-of-the-art techniques. The variation of the first natural frequency of vibration with the applied compressive load on four cylindrical shells is measured up to buckling. The proposed approach presents a very good correlation when the maximum load adopted in the VCT is higher than 80% of the buckling load obtained with tests. If no failure occurs at this maximum load, the proposed approach characterizes a truly nondestructive methodology. Furthermore, it is observed that the use of the second vibration mode for the estimation of the buckling load can provide better predictions in some cases. Therefore, the authors recommend monitoring the evolution of the first and second vibration modes with the increase of the compressive load.

TABLE II: Buckling load prediction using the VCT approach for different loading ranges on SST-2 cylinder (second vibration mode).

Max. load used for VCT [% of experimental buckling load]	Predicted buckling load using VCT [kN]	Deviation from experimental results [%]
90.6%	47.96	3.9
80.6%	42.77	14.3 (fail)
70.6%	36.38	27.1 (fail)

Further experimental investigations are being addressed by the authors in order to verify this new methodology for cylindrical shells with different levels of load imperfection and initial geometric imperfection. Additional experimental tests are currently under development to further validate the proposed approach for composite and metallic conical structures.

Disclaimer

The information in this paper reflects only the author's views and the European Community is not liable for any use that may be made of the information contained therein.

Conflict of Interests

The authors declare that there is no conflict of interests regarding the publication of this paper.

Acknowledgments

The research leading to these results has received funding from the European Community's Seventh Framework Programme (FP7/2007-2013), Grant Agreement no. 282522 (<http://www.desicos.eu/>).

References

- [1] R. V. Southwell, "On the analysis of experimental observations in problems of elastic stability," *Proceedings of the Royal Society of London A*, vol. 135, pp. 601–616, 1932.
- [2] G. D. Galletly and T. E. Reynolds, "A simple extension of Southwell's method for determining the elastic general instability pressure of ring stiffened cylinders subjected to external pressure," *SESA Proceedings*, vol. 12, no. 2, pp. 141–153, 1956.
- [3] A. Sommerfeld, "Eine einfache Vorrichtung zur Veranschaulichung des Knickungsvorganges," in *Zeitschrift des Verein Deutscher Ingenieure (ZVDI)*, pp. 1320–1323, 1905.
- [4] T. H. Chu, *Determination of buckling loads by frequency measurements [Ph.D. thesis]*, California Institute of Technology, Pasadena, Calif, USA, 1949.
- [5] H. Lurie, "Lateral vibrations as related to structural stability," *Journal of Applied Mechanics*, vol. 19, pp. 195–204, 1952.
- [6] J. H. Meier, "The determination of the critical load of a column or stiffened panel in compression by the vibration method," *Proceedings of the Society for Experimental Stress Analysis*, vol. 11, pp. 233–234, 1953.
- [7] J. Singer, J. Arbocz, and T. Weller, *Buckling Experiments, Experimental Methods in Buckling of Thin-Walled Structures, Volume 2*, chapter 15, John Wiley & Sons, New York, NY, USA, 2002.
- [8] R. Degenhardt, A. Kling, A. Bethge et al., "Investigations on imperfection sensitivity and deduction of improved knock-down factors for unstiffened CFRP cylindrical shells," *Composite Structures*, vol. 92, no. 8, pp. 1939–1946, 2010.
- [9] E. Skukis, K. Kalnins, and A. Chate, *Preliminary Assessment of Correlation between Vibrations and Buckling Load of Stainless Steel Cylinders. Shell Structures Theory and Applications*, CRC Press, London, UK, 2013.
- [10] R. Zimmernann, "Buckling research for imperfection tolerant fiber composite structures," in *Proceedings of the Conference on Spacecraft Structures, Materials and Mechanical Testing*, Noordwijk, The Netherlands, March 1996.
- [11] C. Hühne, R. Zimmermann, R. Rolfes, and B. Geier, "Sensitivities to geometrical and loading imperfections on buckling of composite cylindrical shells," in *Proceedings of the European Conference on Spacecraft Structures, Materials and Mechanical Testing*, pp. 11–13, Toulouse, France, December 2002.
- [12] M. W. Hilburger, M. P. Nemeth, and J. H. Starnes Jr., "Shell buckling design criteria based on manufacturing imperfection signatures," NASA Report TM-2004-212659, NASA, 2004.
- [13] R. Degenhardt, A. Bethge, A. King et al., "Probabilistic approach for improved buckling knock-down factors of CFRP cylindrical shells," in *Proceedings of the 1st CEAS European Air and Space Conference*, Berlin, Germany, September 2008.
- [14] E. L. Jansen, H. Abramovich, and R. Rolfes, "The direct prediction of buckling loads of shells under axial compression using VCT—towards an upgraded approach," in *Proceedings of the 27th Congress of the International Council of the Aeronautical Sciences*, St. Petersburg, Russia, September 2014.
- [15] M. A. Arbelo, S. F. M. de Almeida, M. V. Donadon et al., "Vibration correlation technique for the estimation of real boundary conditions and buckling load of unstiffened plates and cylindrical shells," *Thin-Walled Structures*, vol. 79, pp. 119–128, 2014.
- [16] M. A. Souza, W. C. Fok, and A. C. Walker, "Review of experimental techniques for thin-walled structures liable to buckling, part I—neutral and unstable buckling," *Experimental Techniques*, vol. 7, no. 9, pp. 21–25, 1983.
- [17] American Society for Testing and Materials, *ASTM D3039/D3039M-08. Standard Test Method for Tensile Properties of Polymer Matrix Composite Materials*, American Society for Testing and Materials, West Conshohocken, Pa, USA, 2011.
- [18] ASTM, "Standard test method for compressive properties of polymer matrix composite materials with unsupported gage section by shear loading," ASTM D3410/D3410M-03, American Society for Testing and Materials, Philadelphia, Pa, USA, 2011.
- [19] American Society for Testing and Materials, *ASTM D3518/D3518M-94. Standard Test Method for In-Plane Shear Response of Polymer Matrix Composite Materials by Tensile Test of a $\pm 45^\circ$ Laminate*, American Society for Testing and Materials, West Conshohocken, Pa, USA, 2011.
- [20] ABAQUS User's Manual, Abaqus Analysis User's Manual, 2011.



The Scientific World Journal



International Journal of
Rotating Machinery



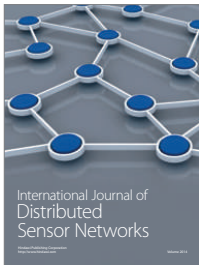
Journal of
Engineering



Journal of
Sensors



Advances in
Mechanical Engineering



International Journal of
Distributed Sensor Networks

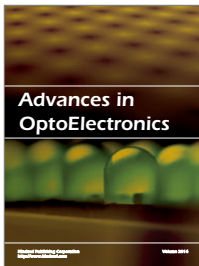


Hindawi

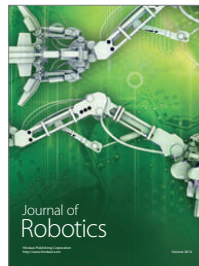
Submit your manuscripts at
<http://www.hindawi.com>



Advances in
Civil Engineering



Advances in
OptoElectronics



Journal of
Robotics



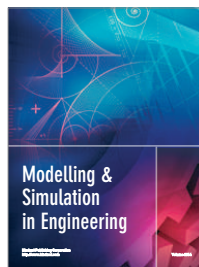
International Journal of
Chemical Engineering



VLSI Design



International Journal of
Navigation and Observation



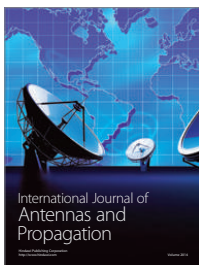
Modelling &
Simulation in Engineering



Advances in
Acoustics and Vibration



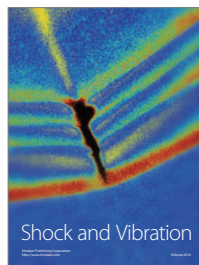
Active and Passive
Electronic Components



International Journal of
Antennas and Propagation



Journal of
Control Science and Engineering



Shock and Vibration



Journal of
Electrical and Computer Engineering

III

Arbelo M.A., Kalnins K., Ozolins O., **Skukis E.**, Castro S.G.P., Degenhardt R.

“Experimental and numerical estimation of buckling load on unstiffened cylindrical shells using a vibration correlation technique”

Thin-Walled Structures, Volume 94, Pages 273 – 279, 1 September 2015.

Parameters (2022/09/01)

DOI	10.1016/j.tws.2015.04.024
Citations in Scopus	42
FWCI	1.81
IF	4.0



Contents lists available at ScienceDirect

Thin-Walled Structures

journal homepage: www.elsevier.com/locate/tws

Experimental and numerical estimation of buckling load on unstiffened cylindrical shells using a vibration correlation technique



Mariano A. Arbelo^{a,*}, Kaspars Kalnins^b, Olgerts Ozolins^b, Eduards Skukis^b, Saullo G.P. Castro^c, Richard Degenhardt^d

^a ITA, Aeronautics Institute of Technology, Department of Aeronautics, São José dos Campos, SP, Brazil

^b RTU, Riga Technical University, Institute of Materials and Structures, Riga, Latvia

^c Embraer, Brazilian Aerospace Company, São José dos Campos, SP, Brazil

^d DLR, Institute of Composite Structures and Adaptive Systems, Braunschweig, Germany

ARTICLE INFO

Article history:

Received 11 March 2015

Accepted 21 April 2015

Available online 14 May 2015

Keywords:

Vibration correlation technique

Buckling

Thin-walled structures

Finite element model

Cylindrical shells

Composite materials

ABSTRACT

Nondestructive methods, to calculate the buckling load of imperfection sensitive thin-walled structures, are one of the most important techniques for the validation of new structures and numerical models of large scale aerospace structures. The vibration correlation technique (VCT) allows determining the buckling load for several types of structures without reaching the instability point, but this technique is still under development for thin-walled plates and shells.

This paper presents and discusses an experimental and numerical validation of a novel approach, using the vibration correlation technique, for the prediction of realistic buckling loads on unstiffened cylindrical shells loaded in compression. From the experimental point of view, a batch of three composite laminated cylindrical shells are fabricated and loaded in compression up to buckling. An unsymmetric laminate is adopted in order to increase the sensitivity of the test structure to initial geometric imperfections. In order to characterize a relationship with the applied load, the first natural frequency of vibration and mode shape is measured during testing using a 3D laser scanner. The proposed vibration correlation technique allows one to predict the experimental buckling load with a very good approximation, without actually reaching the instability point. Furthermore, a series of numerical models, including non-linear effects such as initial geometric and thickness imperfection, are carried-out in order to characterize the variation of the natural frequencies of vibration with the applied load and compare the results with the experiment findings. Additional experimental tests are currently under development to further validate the proposed approach for metallic and balanced composite structures.

© 2015 Elsevier Ltd. All rights reserved.

1. Introduction

The concept of relating vibration characteristics to buckling loads was considered at the beginning of the 20th century for Somerfeld [1], but only in the 50s some experimental investigations were conducted by Chu [2], Lurie [3] and Meier [4], among others. A very detailed review of the theory, application, experimental setup and results of the vibration correlation technique (VCT) approach on different structures can be found in Singer et al. [5 (Chapter 15)].

For a better understanding of the applications of VCT on plates and shells it is important to classify the method according to its use: 1) determination of actual boundary conditions for numerical calculation purposes; 2) direct estimation of buckling load. This

paper will deal with the direct determination of the buckling load on cylindrical shells.

There is not full understanding of how to apply the VCT for unstiffened cylindrical shells, commonly used in space applications for launcher structures. This type of structure is usually associated with a high imperfection sensitivity, which requires the application of empirical guidelines in order to calculate the design buckling load, currently leading to conservative estimations (Degenhardt et al. [7]). Skukis et al. [8] presented a preliminary assessment correlating the vibration modes with the buckling load of stainless steel cylinders. If a relationship between the buckling load and the variation of the natural frequencies of vibration exists, it is possible to use the VCT as a non-destructive technique for estimating the real knock-down factor of space structures. Moreover, for this type of structures there is a remarkable influence of the boundary conditions on the buckling load (see Zimmermann [9] and Hühne et al. [10]), where the VCT could be

* Corresponding author. Tel.: +54 12 3947 5945.

E-mail address: marbelo@ita.br (M.A. Arbelo).

used for a better characterization of the actual boundary conditions, providing reliable data for numerical simulation, such as finite element models (see Hilburger et al. [11], Degenhardt et al. [12], and Degenhardt et al. [7]).

Recent efforts to improve the work done so far on the VCT field are presented by Jansen et al. [13], where new semi-analytical tools are introduced to extend the existing semi-empirical VCT for shells, considering both the non-linear effect of the static state and the nonlinear effect of the geometric imperfections.

The current manuscript will present and discuss an experimental and numerical validation of a new VCT approach presented by Arbelo et al. [14]. This approach is based on the observations made by Souza et al. [15]. The original approach proposed by Souza is a linear fit between $(1-p)^2$ versus $(1-f^4)$, where $p = (P/P_{cr})$, $f = (f_m/f_0)$; P is the applied axial load, P_{cr} is the critical buckling load for a perfect shell, f_m is the measured frequency at P load and f_0 is the natural frequency of the unloaded shell. Souza states that the value of $(1-p)^2$ corresponding to $(1-f^4) = 1$ would represent the square of the drop of the load carrying capacity (ξ^2), due to the initial imperfections. However, if this approach is applied on unstiffened cylindrical shells the results will be negative values of the drop of the load carrying capacity (ξ^2), which does not have a physical meaning (see Arbelo et al. [14]).

Instead of plotting $(1-p)^2$ versus $(1-f^4)$, Arbelo proposed to plot $(1-p)^2$ versus $(1-f^2)$ and represented the points by a second order fitting curve. Moreover, the minimum value of $(1-p)^2$ obtained using this approximation represents the square of the drop of the load carrying capacity (ξ^2), for unstiffened cylindrical shells, due to the initial imperfections. Then, the buckling load can be estimate by Eq. (1):

$$P_{\text{imperfect}} = P_{cr} \left(1 - \sqrt{\frac{\xi^2}{5}} \right) \quad (1)$$

Focused on the validation of the new VCT approach, this manuscript presents a series of experimental test, conducted on 500 mm diameter cylinders, fabricated with composite materials, in order to identify the range of applicability of the VCT for unstiffened cylindrical shells. The applied load and the first natural frequency of vibration and mode shape are measured and correlated. The results are compared with numerical simulations including initial geometric and thickness imperfection. After an initial finite element assessment for the design of the test structures, an unsymmetric laminate setup is adopted in order to increase the sensitivity of the test structure to initial geometric imperfections (see Zimmermann [16]), increasing the loss of load carrying capacity, which is more difficult to predict using standard experimental tests or conventional finite element approaches.

2. Experimental test: materials and methods

2.1. Test specimen: overview

Three identical unstiffened cylindrical shells (named R07, R08 & R09) are fabricated by hand-layup using 6 plies of unidirectional (UD) carbon fiber Unipreg 100 g/m². The geometry and lay-up are presented in Table 1. The material properties were measured according to the ASTM D3039 [17], D3410 [18] and D3518 [19]

Table 1
Geometric parameters for R07 to R09 cylinders.

Length [mm]	500 ± 1
Radius [mm]	250 ± 1
Thickness [mm]	0.6264 ± 0.11
Lay-up [in-out]	$[0_2 / (\pm 45^\circ)_2] \pm 1^\circ$

Table 2
Material properties of UD prepreg Unipreg 100 g/m².

E_1^T	116.44 ± 8.71	GPa
E_2^T	91.65 ± 7.58	GPa
E_1^C	6.73 ± 0.23	GPa
E_2^C	6.39 ± 0.81	GPa
G_{12}	3.63 ± 0.2	GPa
ν_{12}	0.34 ± 0.04	
S_1^T	1771.82 ± 177.88	MPa
S_2^T	478.22 ± 17.3	MPa
S_1^C	40.48 ± 2.67	MPa
S_2^C	122.87 ± 7.48	MPa
S_{12}	61.53 ± 0.67	MPa
t	0.1044 ± 0.0015	mm

standards for tension, compression and shear respectively and the results are presented in Table 2; where E_i^j is the elastic modulus along the fiber direction ($i=1$) or matrix direction ($i=2$) in tension ($j=T$) or compression ($j=C$). G_{12} is the shear modulus and ν_{12} is the Poisson ratio. S_i^j is the maximum strength along the fiber direction ($i=1$) or matrix direction ($i=2$) in tension ($j=T$) or compression ($j=C$). S_{12} is the shear strength. t is the ply thickness.

After fabrication, the top and bottom edges are trimmed and clamped using a resin potting and metallic rings. The final radius over thickness (R/t) ratio is about 400.

2.2. Characterization of initial thickness imperfection using ultrasonic scan

In order to characterize the thickness imperfection inherent of the material and fabrication process, an ultrasonic scan is performed on each test specimen. The obtained thickness imperfection distribution is used afterwards to improve the correlation of the finite element models, since the buckling mechanism can be triggered by local imperfections along the shell. Furthermore, imperfections like gaps or overlaps between plies (due to the fabrication process) can be quantified using ultrasonic scanning. Fig. 1 shows the results of the thickness imperfection for each cylinder. A 10 MHz probe is used to perform the thickness measuring, which provides a good balance between resolution and thickness range.

2.3. Characterization of initial geometric imperfection using laser scan (inner surface)

A laser scan (Panasonic® HL-G1 sensor) is used to measure the initial geometric imperfection on the inner surface of each cylinder. The laser scan is controlled using an in-house software and the acquired data is exported in real time to a plain text file for further analysis and postprocessing. The best-fit-cylinder algorithm is applied afterwards over the raw data to eliminate the rigid body motion modes from the measurements. The results are presented in Fig. 2, where it can be seen as approximately 12 half-waves distributed along the circumference of the inner surface. The maximum amplitude observed from the measurements is less than 0.2% of the cylinder diameter.

It must be noticed that the geometric imperfection of the first 50 mm from both top and bottom edges is not measured due to hardware limitations of the laser scan system, and in this region the imperfection data is extrapolated from the closest cross-section containing measured data.

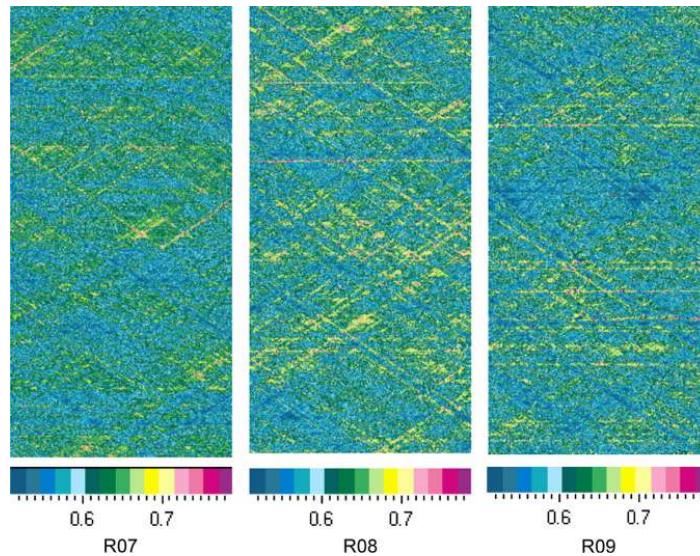


Fig. 1. Thickness imperfection pattern of the studied cylinders [mm].

2.4. Experimental test setup and boundary conditions

The top and bottom cylinder edges are clamped using a 25 mm height resin potting from the outside and metallic rings from the inside, as presented in Fig. 3. For testing, each cylinder is placed between two metallic plates and glued with epoxy resin to them. Moreover, a spherical joint is placed between the cross-head of the testing machine and the lower plate, in order to assure axial loading only (see Fig. 4). The compressive load is measured using a load cell and it is applied using displacement control at a constant velocity of 1.5 mm/min. Two types of tests are carried-out in order to validate the proposed VCT approach. First the cylinder is loaded in compression up to buckling. Notice that the cylinders are designed to buckle in the elastic regime in order to avoid damage accumulated during repeated tests. Once the onset of buckling is found, a second test is performed using a Polytec[®] laser vibrometer to characterize the first natural frequency of vibration and mode shape for different values of applied compressive load, below the onset of buckling. For this test, the cylinder surface is excited with a random signal using a loudspeaker placed inside the cylinder and the laser is positioned in a mesh of 15×25 points in order to map the vibration mode for the whole signal spectrum.

2.5. Experimental results

Several buckling test were conducted on each cylinder to check the reliability of the test results and to assure the absence of accumulative damage on the structure. The average buckling load obtained for each cylinder is summarized in Table 3.

The variation of the first natural frequency of vibration measured on each cylinder when loaded in compression is presented in Table 4. The vibration mode shape obtained from the laser vibrometer and overlaid on top of the test specimen is shown in Fig. 5.

3. Validation of the proposed VCT approach

In order to predict the onset of buckling following the proposed VCT approach, presented by Arbelo et al. [14], it is needed to know:

- The evolution of the first vibration mode on the cylindrical shell with the applied load on the prebuckling regime. These results are carried-out on the previous section of this manuscript.
- The critical buckling load of the perfect cylinder. This value can be obtained through a finite element model. An eigenvalue analysis of a perfect cylindrical shell is fast, simple and provides such information. More details about the modeling tools and techniques are discussed in the following sections. For the study case, the critical buckling load obtained for a perfect cylindrical shell with the lay-up, dimensions, materials properties and boundary conditions of the study case is $P_{cr} = 34.17$ kN.

Since the experimental results presented in Table 4 correspond to cylinders with the same characteristics, one can use all this data at once, plotting $(1-p)^2$ versus $(1-f^2)$ and performing a 2nd order fit, as shown in Fig. 6.

The minimum value of $(1-p)^2$ obtained using this approximation represents the square of the drop of the load carrying capacity (ξ^2). Using Eq. (1), the predicted buckling load obtained from the proposed VCT approach is 22.84 kN, which correlates very well with the average value of the experimental buckling load measured during testing (see Table 3), with less than 3% of deviation.

Furthermore, one can apply the VCT approach on each study case to investigate the minimum threshold of compressive load needed to achieve a good correlation, with less than 10% deviation from the experimental buckling load. Tables 5–7 present the VCT results obtained for each cylinder, using different ranges of applied load (always starting from the unloaded state). In general very good results are obtained for all the studied cases and in particular for the cylinder R08, where the correlations are remarkably good even with a very low maximum load used in the VCT measurements (only 49.3% of the buckling load), because in this case more points are

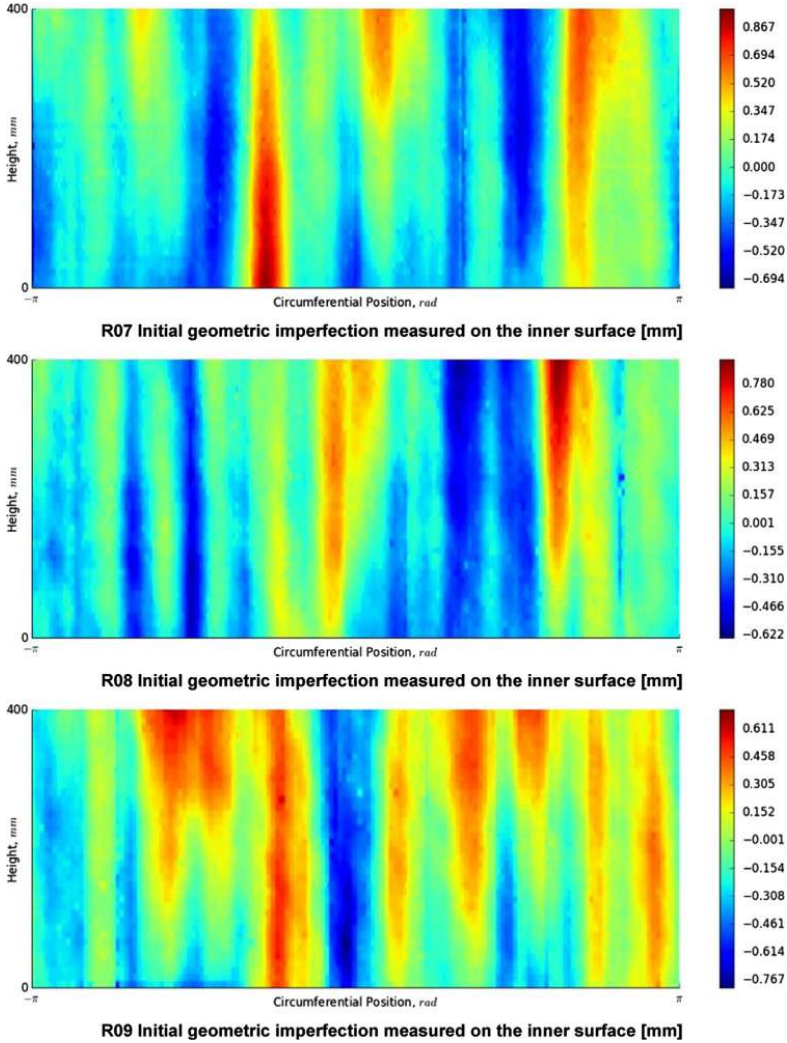


Fig. 2. Initial geometric imperfection results from the laser scan on the studied cylinders (inner surface).

measured up to the maximum load, improving the resultant 2nd order fitting curve.

It is clear that the correlation degrades (in general) when the maximum load is lower than 50% of the buckling load. From these results one can conclude that the present approach could be applied as an experimental non-destructive method to estimate the buckling load on unstiffened cylindrical shells loaded in compression. Further experimental investigations are being addressed by the authors in order to validate the proposed VCT approach for cylindrical shells with different geometries/materials/lay-up, including isotropic shells.

4. Finite element analysis

A finite element model (FEM) is implemented using Abaqus[®]. For all three cylinder the mesh adopted after the convergence

analysis uses 140 S8R5 [20] elements distributed along the circumference. Three different analyses are carried-out:

- Eigenvalue analysis, to calculate the linear buckling load (P_{cr}) of the perfect cylinder.
- Non-linear analysis considering geometric and thickness imperfections, followed by a frequency analysis to characterize the variation of the vibration frequencies when the cylinders are loaded under axial compression. The geometric imperfection is imported into the finite element model through shifting the radial position of each node, using an inverse weighted interpolation rule with the five closest measured points from the imperfection data file. In a similar way, the thickness imperfection is applied to the finite element model changing the total thickness of each element and shifting the medium-plane, considering that the inner surface is equal for all the elements.



Fig. 3. Boundary conditions on top and bottom edges.



Fig. 4. Experimental test setup for compressive loading on cylindrical shells.

- c) Non-linear analysis considering geometric and thickness imperfection up to buckling to calculate the buckling load of the imperfect shell ($P_{imperfect}$). For this particular case, the Newton–Raphson iteration solver is used with artificial damping. This methodology is less computationally demanding than

Table 3
Experimental buckling load of R07 to R09 cylinders.

Cylinder	Experimental buckling load [kN]
R07	22.44 ± 0.13
R08	22.74 ± 0.14
R09	21.55 ± 0.11
Average	22.24

dynamic relaxation methods, but has the inconvenience to define the correct damping factor for each model, since this is not a physical parameter and can only be estimated after a convergence analysis. The selected damping factor should be the smallest that allows overcoming the global buckling and in the presented cases the value of $1 \cdot 10^{-7}$ is used.

4.1. Numerical buckling load characterization

The results of linear buckling load (P_{cr}) and non-linear buckling load ($P_{imperfect}$) are presented in Table 8. It can be seen that the drop of load carrying capacity due to the consideration of initial imperfection can be up to 44% on R09 cylinder.

An overall good correlation can be found between the numerical prediction of the buckling load, considering geometric and thickness imperfection, and the experimental buckling load measured during testing (see Table 9).

4.2. The VCT applied to the finite element model

Using the modeling technique described in previous sections, the natural frequency of vibration of the first vibration mode is extracted, for each cylinder, at different levels of applied compressive load. As an example, the plot of $(1-p)^2$ versus $(1-f^2)$ for cylinder R08 is presented in Fig. 7.

The predicted buckling load using the VCT approach on the numerical model is presented in Table 10 for each cylinder. Notice that the deviation from the experimental buckling load obtained from previous test is only 6.3% and 2.2% for cylinders R07 and R08, respectively. On the other hand, for R09 the obtained error is 12%, with a poorer correlation which can be associated with non-characterized imperfections, such as non-uniform load distributions. Since such imperfections are not included in the proposed modeling technique, the predicted buckling loads may be overestimated.

From the previous analysis it is important to remark that the same behavior observed during the experimental test is present on the results carried-out from the finite element models. Despite the proposed VCT is intended to be applied as an experimental non-destructive method, it is shown that good results can be obtained from numerical simulations, when all the initial imperfections are taken into account.

5. Summary and concluding remarks

In this paper, the advantages of using vibration correlation techniques as a non-destructive method to estimate the buckling load of unstiffened cylindrical shells are presented. A test campaign is defined in order to validate a novel VCT approach on composite laminated cylindrical shells, with a radius over thickness ratio of 400. The material properties, initial geometric and thickness imperfections are measured using the state-of-the-art techniques. The variation of the first natural frequency of vibration with the applied compressive load on three cylindrical shells is

Table 4
Variation of the 1st vibration frequency with the applied load.

R07 Cylinder		R08 Cylinder		R09 Cylinder	
Compressive load [kN]	1st vibration mode [Hz]	Compressive load [kN]	1st vibration mode [Hz]	Compressive load [kN]	1st vibration mode [Hz]
0.18	208.25	0	213	0	212.5
1.55	205.5	1.19	210.75	3.49	207.5
4.2	200.5	3.15	207	6.47	201.5
6.7	196	5.16	202.75	9.37	195.5
9.63	190	7.21	198.5	13.94	184.5
12.5	183	9.15	194.5	18.2	174
15.03	176.75	11.22	189.75	20.24	165.5
18.12	168	13.19	185		
		15.15	180.5		
		17.08	175.5		
		18.33	171.75		
		20.98	163.25		

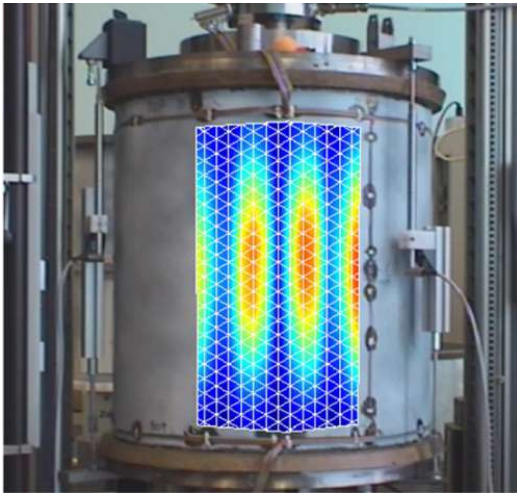


Fig. 5. First vibration mode shape measured during testing.

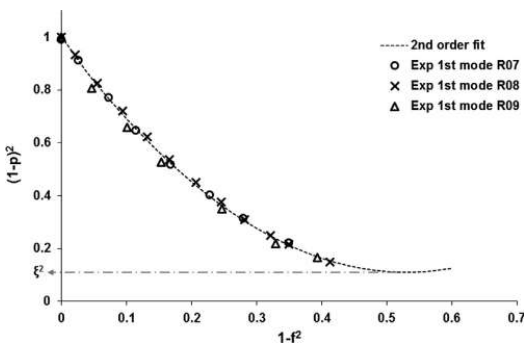


Fig. 6. Plot of $(1-p)^2$ versus $(1-f)^2$ and 2nd order fit based on all the experimental data.

measured up to buckling. The proposed approach presents a very good correlation when the maximum load adopted in the VCT is higher than 50% of the buckling load obtained with tests. If no failure occurs at this maximum load, the proposed approach characterizes a truly nondestructive methodology.

Table 5
Buckling load prediction using the VCT approach for different loading ranges on R07 cylinder.

Max. load used for VCT [% of experimental buckling load]	Predicted buckling load using VCT [kN]	Deviation from experimental results [%]
80	21.28	5.1
67	20.25	9.8
55.7	19.88	11.4 (Fail)

Table 6
Buckling load prediction using the VCT approach for different loading ranges on R08 cylinder.

Max. load used for VCT [% of experimental buckling load]	Predicted buckling load using VCT [kN]	Deviation from experimental results [%]
92.2	24.33	7
80.6	24.52	7.8
75.1	24.89	9.4
66.6	24.46	7.5
58	23.01	1.2
49.3	23.97	5.4
40.2	25.55	12.3 (Fail)

Table 7
Buckling load prediction using the VCT approach for different loading ranges on R09 cylinder.

Max. load used for VCT [% of experimental buckling load]	Predicted buckling load using VCT [kN]	Deviation from experimental results [%]
93.9	21.05	2.3
84.4	20.37	5.5
64.6	16.4	23.9 (Fail)

Table 8
Critical buckling load and non-linear buckling load obtained from the FEM analysis.

Linear buckling analysis (P_{cr})	34.17 kN
Non-linear buckling load of R07	22.94 kN
Non-linear buckling load of R08	21.1 kN
Non-linear buckling load of R09	19.2 kN
Average non-linear buckling load	21.1 kN

Table 9

Comparison between the buckling load obtained through a non-linear finite element model and experimental testing.

Deviation numerical - experimental R07	2.2
Deviation numerical - experimental R08	7.2
Deviation numerical - experimental R09	10.9

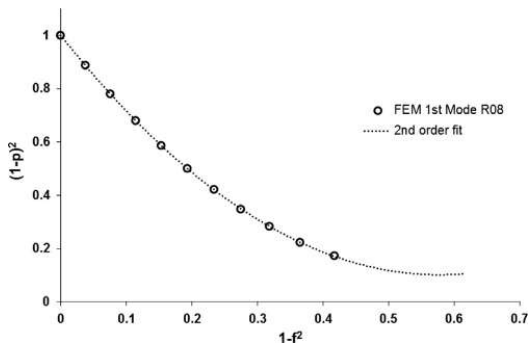


Fig. 7. Plot of $(1-p)^2$ versus $(1-f^2)$ for cylinder R08 (Numerical results).

Table 10

Comparison between numerically predicted buckling load using VCT and experimental results.

	Estimated buckling load [kN]	Deviation [%]
FEM R07 cylinder	23.86	+6.3
FEM R08 cylinder	23.25	+2.2
FEM R09 cylinder	24.21	+12.3

Additionally, a series of non-linear finite element analyses are presented. The results show a very good correlation if the inherent initial imperfections are taken into account, with a deviation of the predicted buckling load less than 7% on most of the studied cases. For future studies, load imperfections should be taken into account in order to improve the accuracy of the numerical results. Further experimental investigations are being addressed by the authors in order to validate this new methodology for cylindrical shells with different geometries/materials, including isotropic shells.

Acknowledgments

The research leading to these results has received funding from the European Community's Seventh Framework Programme

(FP7/2007–2013), under Priority ERDF (European Regional Development Fund), Grant Agreement number WA3-80123539 and collaboration from the European Community's Seventh Framework Programme (FP7/2007–2013), Grant Agreement number 282522 (www.DESICOS.eu). The information in this paper reflects only the author's views and the European Community is not liable for any use that may be made of the information contained therein.

References

- [1] Sommerfeld A. Eine einfache Vorrichtung zur Veranschaulichung des Knickungsvorganges. *Z Ver Dtsch Ing* 1905;49:1320–3.
- [2] Chu TH. Determination of buckling loads by frequency measurements. (Thesis). Pasadena, Calif: California Institute of Technology; 1949.
- [3] Lurie H. Lateral vibration as related to structural stability. *ASME J Appl Mech* 1952;19:195–204.
- [4] Meier JH. Discussion of the paper entitled "the determination of the critical load of a column or stiffened panel in compression by the vibration method". *Proc Soc Exp Stress Anal* 1953;11:233–4.
- [5] Singer J, Arbocz J, Weller T. Buckling experiments, experimental methods in buckling of thin-walled structures. New York: John Wiley & Sons; 2002.
- [7] Degenhardt R, Kling A, Bethge A, Orf J, Kärger L, Rohwer K, et al. Investigations on imperfection sensitivity and deduction of improved knock-down factors for unstiffened CFRP cylindrical shells. *Compos Struct* 2010;92(8):1939–46.
- [8] Pietraszkiewicz W, Górski J, editors. *Shell Structures: Theory and Applications*, Vol. 3. London: Taylor & Francis Group; 1980. ISBN978-1-138-00082-7, pp 325–328.
- [9] Zimmermann, R. Buckling research for imperfection tolerant fiber composite structures. In: Proceedings of the conference on spacecraft structures, materials and mechanical testing. Noordwijk (The Netherlands); 27–29 March 1996.
- [10] Hühne, C, Zimmermann, R, Rolfes, R and Geier, B. Sensitivities to geometrical and loading imperfections on buckling of composite cylindrical shells. In: Proceedings of the European conference on spacecraft structures, materials and mechanical testing. Toulouse; 11–13 December 2002.
- [11] Hilburger, MW, Nemeth, MP and Starnes, JH Jr. Shell buckling design criteria based on manufacturing imperfection signatures. NASA Report TM-2004-212659; 2004.
- [12] Degenhardt, R, Bethge, A, King, A, Zimmermann, R, Rohwer, K, Teßmer, J and et al. Probabilistic approach for improved buckling knock-down factors of CFRP cylindrical shells. In: Proceedings of the first CEAS European air and space conference. Berlin (Germany); 10–13 September 2008.
- [13] Jansen, EL, Abramovich, H, Rolfes, R. The direct prediction of buckling loads of shells under axial compression using VCT—towards an upgraded approach. In: Proceedings of 27th congress of the international council of the aeronautical sciences. St. Petersburg (Russia); 7–12 September 2014.
- [14] Arbelo MA, de Almeida SFM, Donadon MV, Rett SR, Degenhardt R, Castro SGP, et al. Vibration correlation technique for the estimation of real boundary conditions and buckling load of unstiffened plates and cylindrical shells. *Int J Thin-Walled Struct* 2014;79:119–28.
- [15] Souza MA, Fok WC, Walker AC. Review of experimental techniques for thin-walled structures liable to buckling, Part I - Neutral and unstable buckling. *Exp Tech* 1983;7:21–5.
- [16] Zimmermann, R. Optimierung axial gedrückter CFK-Zylinderschalen. *Fortschrittsberichte VDI-Reihe 1, Nr.207*. Düsseldorf VDI Verlag; 1992.
- [17] American Society for Testing and Materials, ASTM D3039/D3039M-08. Standard test method for tensile properties of polymer matrix composite materials. Pennsylvania; 2011.
- [18] American Society for Testing and Materials, ASTM D3410/D3410M-03. Standard test method for compressive properties of polymer matrix composite materials with unsupported gage section by shear loading. Pennsylvania; 2011.
- [19] American Society for Testing and Materials, ASTM D3518/D3518M-94. Standard test method for in-plane shear response of polymer matrix composite materials by tensile test of a $\pm 45^\circ$ laminate. Pennsylvania; 2011.
- [20] ABAQUS user's manual, Abaqus analysis user's manual; 2011.

IV

Skukis E., Ozolins O., Kalnins K., Arbelo M.A.

“Experimental test for estimation of buckling load on unstiffened cylindrical shells by vibration correlation technique”

Procedia Engineering, Open access, Volume 172, Pages 1023 – 1030, 2017, 12th International Conference Modern Building Materials, Structures and Techniques, MBMST.

Parameters (2022/09/01)

DOI	10.1016/j.proeng.2017.02.154
Citations in Scopus	33
FWCI	14.81
IF	0.97



Modern Building Materials, Structures and Techniques, MBMST 2016

Experimental test for estimation of buckling load on unstiffened cylindrical shells by vibration correlation technique

Eduards Skukis^a, Olgerts Ozolins^a, Kaspars Kalnins^a, Mariano A. Arbelo^b.

^aRTU, Riga Technical University, Institute of Materials and Structures, Riga, Latvia

^bITA, Aeronautics Institute of Technology, Department of Aeronautics, São José dos Campos-SP, Brazil

Abstract

Non-destructive methods to estimate the actual buckling load in particularly for imperfection sensitive thin-walled structures, are of severe interest among many fields. Particular techniques for validation of structural limit state and numerical model predictions for large scale structures are getting momentum. The vibration correlation technique (VCT) allows to correlate the ultimate load our instability point with rapid decrement of self-frequency response. Nevertheless this technique is still under development for thin-walled shells and plates. The current research discusses an experimental verification of extended approach, using vibration correlation technique, for the prediction of actual buckling loads on unstiffened cylindrical shells loaded in axial compression. Validation study include two laminated composite cylinders which were manufactured and repeatedly loaded up to instability point.

In order to characterize a correlation with the applied load, several initial natural frequencies and mode shapes were measured during tests by 3D laser scanner. Results demonstrate that proposed vibration correlation technique allows one to predict the experimental buckling load with high reliability, without actually reaching the instability point. Additional experimental tests and numerical models are currently under development to further validate the proposed approach to extended composite and metallic structures.

© 2016 The Authors. Published by Elsevier Ltd.

Peer-review under responsibility of the organizing committee of MBMST 2016.

Keywords: Vibration correlation technique, buckling, thin-walled structures, cylindrical shells ;

1. Introduction

Since beginning of the 20th century a concept correlating vibration characteristics with stability was considered initially only by theoretical studies Somerfeld, [1]. Nevertheless it took more than half a century to start to conduct initial experimental knowledge and to summarize previous achievements which were reviewed in great detail of the

theory, application, experimental setup and results of the vibration correlation technique (VCT) approach on different structures by Singer et al [2]. Initial findings suggested that main application of VCT on plates and shells may be classified according to its application: assurance of actual boundary conditions and for validation of stability load in comparison with numerical analyses. Even though a conventional vibration tests with accelerometers are still industry standard a non-contact laser scanning tests enable a new dimension on data acquisition and visualization. Therefore extend the reliability of VCT method and its sole potential for determination of the buckling load on cylindrical shells.

Currently there is limited knowledge on application of VCT for unstiffened cylindrical shells, commonly used in aerospace applications or as silos in building sector. This type of structures typically are associated with a high imperfection sensitivity, which requires the application of empirical guidelines /design codes in order to calculate the design buckling load and currently leading to over conservative estimations. Even though the Eurocode 3 [3] dealing with strength and stability of cylindrical structures and silos particularly [4] include less conservative safety factors if design analysis involve known our measured geometrical/material imperfections boundary conditions etc. related to the manufacturing process. Nevertheless there is not much discussion given how those input variables could be assessed with confident level of reliability. Therefore in common engineering practice those softened safety factors are neglected and over conservative knock-down factors are implemented (Degenhardt et al, 2010 [5]). Preliminary assessment of correlating the vibration modes with the buckling load of stainless steel cylinders obtained by non-contact measurements was presented by Skukis et al, 2013 [6]. It was shown that it is possible to observe a relationship between the buckling load and the variation of the natural frequencies of vibration, therefore highlighting the potential of a VCT as a non-destructive technique for estimating the real knock-down factor of unstiffened structures. Moreover, for this type of structures there is a remarkable influence of the boundary conditions on the buckling load [7, 8, 9], where the VCT could be used to assess the actual boundary conditions, providing reliable data for numerical simulation, such as finite element models [10, 11, 6].

Recent efforts to improve the work done so far on the VCT field are presented by Abramovich et al, 2015 [12], where new semi-analytical methods was experimentally verified for shells, considering both the non-linear effect of the static state and the nonlinear effect of the geometric imperfections. The current research will present and discuss an experimental verification of a modified VCT approach originally presented by Arbelo et al, 2014 [13]. This approach is based on the observations made by Souza et al, 1983 [14]. The original approach proposed by Souza is a linear fit between $(1 - p)^2$ versus $(1 - f^4)$, where $p = P/P_{cr}$, $f = f_m/f_0$; P is the applied axial load, P_{cr} is the critical buckling load for a perfect shell, f_m is the measured frequency at P load and f_0 is the natural frequency of the unloaded shell. Souza states that the value of $(1 - p)^2$ corresponding to $(1 - f^4) = 1$ would represent the square of the drop of the load carrying capacity (ξ^2), due to the initial imperfections. However, if this approach is applied on unstiffened cylindrical shells the results will be negative values of the drop of the load carrying capacity (ξ^2), which doesn't have any physical meaning [14].

Therefore in modified VCT approach instead of plotting $(1 - p)^2$ versus $(1 - f^4)$, Arbelo proposed to plot $(1 - p)^2$ versus $(1 - f^2)$ and represented the points by a second order fitting curve (which could be further improved). Moreover, the minimum value of $(1 - p)^2$ obtained using this approximation represents the square of the drop of the load carrying capacity (ξ^2), for unstiffened cylindrical shells, due to the initial imperfections. Then, the buckling load can be estimate by Eq. 1:

$$P_{imperfect} = P_{cr}(1 - \sqrt{\xi^2}) \quad (1)$$

Focused on the verification of modified VCT approach, this research presents a series of two experimental test, conducted on composite benchmark cylinders [11, 15, 16], in order to identify the range of applicability of the VCT for unstiffened composite cylindrical shells. The applied load and the first natural frequency of vibration and mode shape are measured and correlated. The initial geometric imperfection shape of each cylinder is measured by a 3D non-contact laser scan.

The main goal on this research is to compare the predicted buckling load versus the real buckling load measured on samples with different materials, geometries (radius, thickness, height) and fabrication technologies. More details about each study case are given in the following section.

Nomenclature

P	is the applied axial load
P_{cr}	Critical buckling load for a perfect shell
f_0	is the natural frequency of the unloaded shell
f_m	is the measured frequency at P load
ζ^2	the load carrying capacity
L	Free length
R	Radius
t	Thickness
E_1^T	Elastic modulus along the fiber direction, tension
E_1^C	Elastic modulus along the fiber direction, compression
E_2^T	Elastic modulus along the matrix direction, tension
E_2^C	Elastic modulus along the matrix direction, compression
G_{12}	is the shear modulus
ν_{12}	is the Poisson ratio
S_1^T	is the maximum strength along the fiber direction, tension
S_1^C	is the maximum strength along the fiber direction, compression
S_2^T	is the maximum strength along the matrix direction, tension
S_2^C	is the maximum strength along the matrix direction, compression
S_{12}	is the shear strength

2. Experimental test: materials and methods*2.1. Test specimen: Overview*

Two identical composite laminated cylindrical shells corresponding to German Aerospace set benchmark study [11] was fabricated and tested. The R15 and R16 cylinder were fabricated at RTU by hand-layup, using 4 plies of unidirectional (UD) carbon fiber prepreg Hexcel® IM7/8552, and cured out of autoclave. The material properties were measured according to the ASTM D3039 [17], D3410 [18] and D3518 [19] standards for tension, compression and shear respectively and the results are presented in 1. Compared with material properties given by material producer in data sheet and other research articles [11, 20, 21, 23] show slight discrepancies mainly in shear strength values, therefore it was concluded that even thought out of autoclave is not a proper manufacturing method obtained material properties are valid for comparison with benchmark tests [11].

Table 1 – Measured material properties of out of autoclave manufacturing of UD prepreg Hexcel® IM7/8552.

	Stiffness				Strength			
	Mean value		Std. Deviation [%]		Mean value		Std. Deviation [%]	
E_1^T	171.5	GPa	2.6	S_1^T	2300	MPa	13.8	
E_1^C	150.2	GPa	4.6	S_1^C	857	MPa	10.1	
E_2^T	8.9	GPa	4.2	S_2^T	40	MPa	20.4	
E_2^C	9.4	GPa	10.9	S_2^C	203	MPa	3.9	
G_{12}	5.1	GPa	7.8	S_{12}	51	MPa	8.4	
ν_{12}	0.32		13	t_{ply}	0.125	mm		

The detailed geometry and optimised – imperfection sensitive lay-up are presented in Table . It should be noted that after fabrication, the top and bottom edges are trimmed and clamped using a resin potting and metallic rings. The final radius over thickness (R/t) ratio is about 478.

Table 2 - Geometric parameters for tested cylinders.

Free length [mm]	500
Radius [mm]	250
Total thickness [mm]	0.523
Lay-up [in-out]	[+24°/-24°/+41°/-41°] ± 1°

2.2. Experimental test setup and boundary conditions

The universal quasi static testing machine Zwick 100 was used to apply axial compressive load on the cylinder. Starting from zero, the compressive load was increased at 2 kN step up to 85% of predetermined buckling load. During each increment the natural frequencies and vibration modes were measured using *Polytec* laser vibrometer on a grid of points distributed along a small area of the cylinder (white area figure 1a). For structural excitation a loudspeaker placed 180° opposite the measured area was used. Measured sector of cylinder was approximately 72 deg wide in frequency range from 0 to 400Hz. The scanned area consisted of 300 grid points which was found as a good tradeoff between the scanning time and the level of detail of modal response.

In general, the top and bottom cylinder edges are clamped by a resin potting from the outside 25 mm in height and internal metallic rings, as shown in Figure 1a. For testing, each cylinder is placed between two metallic plates and the narrow gap filled with reinforced epoxy resin (see Figure 1b).

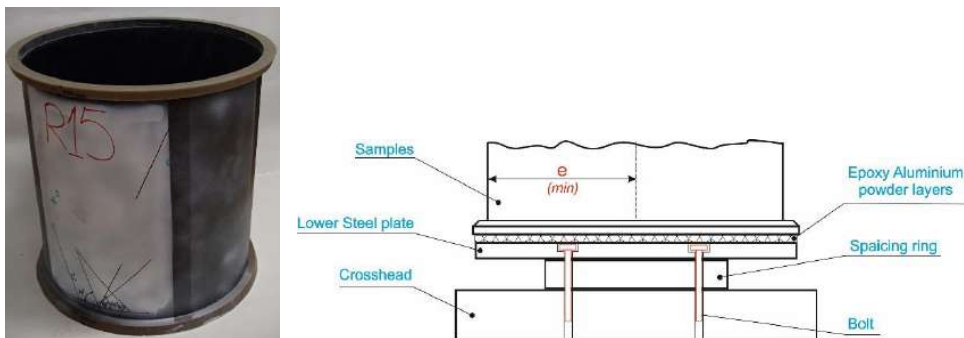


Fig. 1. (a) Boundary conditions on top and bottom edges; (b) Experimental test setup for compressive loading.

2.3. Experimental results

It should be noted that for composite cylinders the buckling tests could be repeated for several configurations without scarifying the test specimen response. Therefore besides initial tests there has been a several repeated series of experimental assessment of robustness of test set up. One should note that once specimen has been repeatedly tested following all set up procedure obtained buckling load has increased by 3-4%. Nevertheless the buckling load and mode shape obtained for each tested cylinder is summarized in Table 3. It is worth to mention that obtained experimental buckling load compared to series average of benchmark study by Degenhard et al. [5] show result compatibility with

upper limit loads obtained in benchmark study. Therefore confirming the material and specimen processing technology and testing set up compatibility with numerical predictions by finite element method.

Table 3 - Experimental buckling load of tested cylinders.

Cylinder	Experimental buckling load [kN]	Experimental buckling mode
R15	25.04	
R16	25.20	

The dependency between natural frequency and applied compression load is shown in Figure 2 (a). One may see that throughout test the self-frequency and amplitude decreases while wavelength increase. This may indicate that once amplitude of the response has leveled the structure has reached a bifurcation point. This correlation is easy to observe in Figure 2 (b) where magnitude of excitation almost merge before reaching the buckling point.

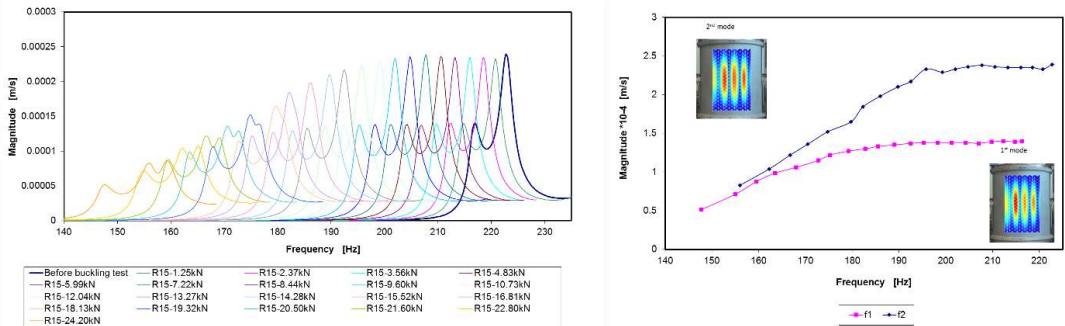


Fig. 2. Natural frequency response of cylinder R15 (a) Decrement of natural frequency due axial compression; (b) First versus second natural frequency magnitude decrement.

3. Verification of the proposed VCT approach

As a next step in order to predict the onset of buckling following the modified VCT approach, presented by Arbelo et al, 2014 [13, 14, 22], it is required to follow: a) The evolution of the first vibration mode on the cylindrical shell with the applied load on the pre buckling regime. This procedure is briefly described in previous section of this manuscript.

b) Numerical determination of linear buckling load (eigenbuckling) of the perfect cylinder (P_{cr}). This value can be obtained through a finite element model. An eigenvalue analysis of a perfect cylindrical shell is fast, simple and

provides such estimate. Even though there is little correlation with experimental results thus knock down factors should be added. For this study, a finite element model (FEM) is implemented by commercial software ANSYS [24]. The critical buckling loads obtained for a perfect cylindrical shell with the lay-up, dimensions, materials properties and boundary conditions used as a reference was 38.75kN. Obtained eigenbuckling load was 55% higher than the experimental load.

The proposed VCT approach can be plotted in function of the dimensionless parameters $(1 - p)^2$ versus $(1 - f^2)$ or $(1 - f^4)$ for modified approach as shown in Figure 3. Obtained vibration correlation approximation function for both R15 and R16 cylinders show strong correlation. Furthermore result assessment in table 4 confirms that the best estimate by modified VCT method gives overestimate by 5-8% whereas classical VCT diminish by 4-12%.

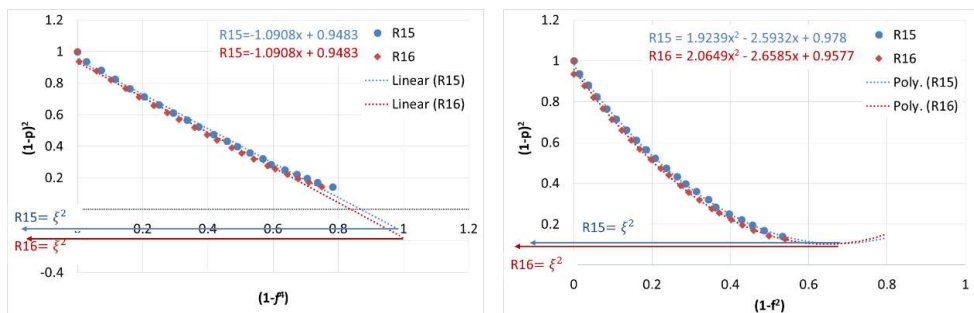


Fig. 3. a) Plot of $(1-p)^2$ versus $(1-f^2)$ by stepwise axial load increment; b) Plot of $(1-p)^2$ versus $(1-f^2)$ by stepwise axial load increment.

Table 4 - Buckling load prediction using the VCT approach for the different studied cases.

Cylinder	Predicted buckling load by modified VCT [kN]	Deviation from modified VCT and experimental results [%]	Predicted buckling load by modified VCT [kN]	Deviation from modified VCT and experimental results [%]
R15	24.1	- 3.7	26.2	+ 4.8
R16	22.3	- 11.9	27.3	+ 8.4

More detailed analysis should be given to Figure 4 where approximation of response with every axial load step. It should be noted that pre-stress from axial compression up to 50% of buckling load gives reliability up to 75% of predicted buckling load. Further increase to 65% of buckling load gives prediction reliability close to 90%. One should note that some loading imperfections has been found around the top and bottom edges along the circumference during testing. In this way, the vibration analysis can give non-conservative results depending on the relative position of the laser scan and the measured surface section. Further studies are currently been conducted in order to quantify a relationship between the initial loading imperfection around the edges and the predicted VCT buckling load.

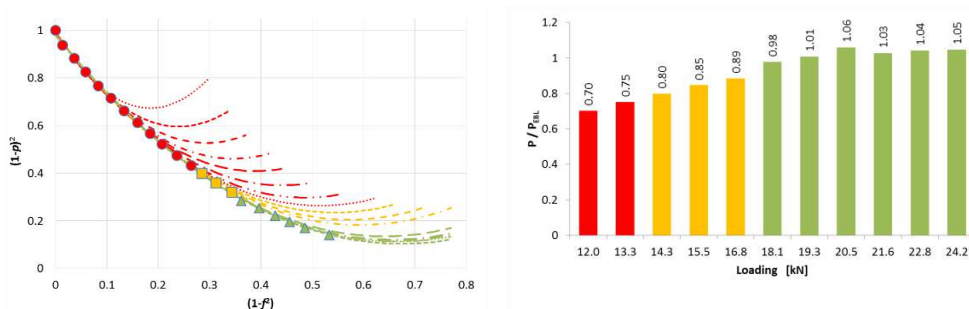


Fig. 4. Buckling load prediction using the VCT approach for different loading ranges on R15 cylinder.

From these results one can conclude that the present modified vibration correlation approach could be applied as an experimental non-destructive method to estimate the buckling load on unstiffened cylindrical shells loaded in compression. This indicates that modified VCT procedure show potential capacity to estimate ultimate load carrying capacity of real structures in real loading conditions.

4. Summary and concluding remarks

In this paper, a verification of an empirical approach applying modified vibration correlation techniques as a non-destructive/ non-contact method to estimate the buckling load of unstiffened cylindrical shells is presented. A series of benchmark tests are carried-out with two similar cylindrical shells in order to verify robustness of modified and classical VCT approach. The material properties and initial geometric imperfections are measured using the state-of-the-art techniques. The variation of the first and second natural frequency in conjunction with the applied compressive load for cylindrical shells is measured up to buckling. The proposed approach presents a very good correlation when the maximum load adopted in the VCT is higher than 80% of the buckling load obtained with tests. Nevertheless tests up to 65% of buckling load can give a 90% fidelity in estimation of buckling load. If no failure occurs at this maximum load, the proposed approach characterizes a truly nondestructive methodology. Furthermore it is observed that the use of the second natural frequency mode for the estimation of the buckling load can provide result with smaller deviation on some particular cases. The authors recommend to monitor the variation of amplitude for the first and second vibration mode when while axial compression load is applied.

Further experimental investigations are being addressed by the authors in order to verify this modified methodology for cylindrical shells with different levels of load imperfection and initial geometric imperfection. Additional experimental tests are currently under development to further validate the proposed approach for composite and metallic cylindrical structures.

References

- [1] A. Sommerfeld, Eine einfache Vorrichtung zur Veranschaulichung des Knickungsvorganges, Zeitschrift des Verein Deutscher Ingenieure (ZVVDI), 1905, 1320-1323.
- [2] J. Singer, J. Arbocz, T. Weller, Buckling experiments, Experimental methods in buckling of thin-walled structures, Volume 2. New York, John Wiley & Sons, 2002.
- [3] Eurocode 3 - Design of steel structures - Part 1-6: Strength and stability of shell structures (2007). Comite European de Normalisation (CEN).
- [4] Eurocode 3 - Design of steel structures - Part 4-1: Silos (2007). Comite European de Normalisation (CEN).
- [5] R. Degenhardt, A. Kling, A. Bethge, J. Orf, L. Kärger, K. Rohwer, R. Zimmermann, A. Calvi, Investigations on imperfection sensitivity and deduction of improved knock-down factors for unstiffened CFRP cylindrical shells, *Composite Structures*, 92 (8), 2010, 1939–1946.
- [6] E. Skukis, K. Kalnins, A. Chate, Preliminary assessment of correlation between vibrations and buckling load of stainless steel cylinders. *Shell Structures Theory and applications*. CRC Press, London 2014, 325-328.
- [7] R. Zimmermann, H. Klein, A. Kling, Buckling and postbuckling of stringer stiffened fibre composite curved panels - Tests and computations. *Composite Structures*, Volume 73, Issue 2, May 2006, Pages 150-161
- [8] B. Kriegesmann, R. Rolfes, C. Hühne, J. Tessmer, J. Arbocz, Probabilistic design of axially compressed composite cylinders with geometric and loading imperfections. *International Journal of Structural Stability and Dynamics*, Volume 10, Issue 4, October 2010, Pages 623-644
- [9] H.N.R. Wagner, C. Hühne, S. Niemann, Constant single-buckle imperfection principle to determine a lower bound for the buckling load of unstiffened composite cylinders under axial compression. *Composite Structures*, Volume 139, April 01, 2016, Pages 120-129
- [10] M. W. Hilburger, M. P. Nemeth, and J. H. Jr. Starnes, Shell buckling design criteria based on manufacturing imperfection signatures, NASA Report TM-2004-212659, 2004.
- [11] R. Degenhardt, A. Kling, A. Bethge, J. Orf, L. Kärger, R. Zimmermann, K. Rohwer, A. Calvi, Investigations on imperfection sensitivity and deduction of improved knock-down factors for unstiffened CFRP cylindrical shells. *Composite Structures*, Volume 92, Issue 8, July 2010, Pages 1939-1946
- [12] H. Abrampvich, D. Govich, A. Grunwald, Buckling prediction of panels using the vibration correlation technique. *Progress in Aerospace Sciences*. Volume 78, October 2015, Pages 62-73.
- [13] M.A. Arbelo, S.F.M. de Almeida, M.V. Donadon, S.R. Rett, R. Degenhardt, S.G.P. Castro, K. Kalnins, O. Ozolins, Vibration correlation technique for the estimation of real boundary conditions and buckling load of unstiffened plates and cylindrical shells, *Int. Journal of Thin-Walled Structures*, 2014, 79, 119–128.

- [14] K. Kalnins, M.A. Arbelo, O. Ozolins, E. Skukis, S.G.P. Castro, R. Degenhardt, Experimental nondestructive test for estimation of buckling load on unstiffened cylindrical shells using vibration correlation technique, *Shock and Vibration*, Volume 2015, 2015, Article number 729684
- [15] H.N.R. Wagner, C. Hühne, S. Niemann, Constant single-buckle imperfection principle to determine a lower bound for the buckling load of unstiffened composite cylinders under axial compression. *Composite Structures*, Volume 139, April 01, 2016, Pages 120-129
- [16] M.A. Arbelo, A. Herrmann, S.G.P. Castro, R. Khakimova, R. Zimmermann, R. Degenhardt, Investigation of Buckling Behavior of Composite Shell Structures with Cutouts. *Applied Composite Materials*, Volume 22, Issue 6, 1 December 2015, Pages 623-636
- [17] American Society for Testing and Materials, ASTM D3039/D3039M-08. Standard test method for tensile properties of polymer matrix composite materials. Pennsylvania, 2011.
- [18] American Society for Testing and Materials, ASTM D3410/D3410M-03. Standard test method for compressive properties of polymer matrix composite materials with unsupported gage section by shear loading. Pennsylvania, 2011.
- [19] American Society for Testing and Materials, ASTM D3518/D3518M-94. Standard test method for In-plane shear response of polymer matrix composite materials by tensile test of a $\pm 45^\circ$ laminate. Pennsylvania, 2011.
- [20] E. Clarkson. A comparison of Equivalence Criteria and Basis Values for HEXCEL 8552 IM7 Unidirectional Tape computed from the NCAMP shared database, NCP-RP-2013-015 N/C.
- [21] G. Jacobsen. Mechanical characterization of stretch broken carbon fiber materials – IM7 fiber in 8552 resin. HEXCEL corp.
- [22] M.A. Arbelo, K. Kalnins, O. Ozolins, E. Skukis, S.G.P. Castro, R. Degenhardt, Experimental and numerical estimation of buckling load on unstiffened cylindrical shells using a vibration correlation technique. *Thin-Walled Structures*, Volume 94, 1 September 2015, Pages 273-279
- [23] http://www.hexcel.com/Resources/DataSheets/Prepreg-Data-Sheets/8552_eu.pdf
- [24] ANSYS® Academic Research, Release 16.2.

V

Skukis E., Ozolins O., Andersons, J., Kalnins, K., Arbelo, M.A.

“Applicability of the vibration correlation technique for estimation of the buckling load in axial compression of cylindrical isotropic shells with and without circular cutouts”

Shock and Vibration, Open access, Volume 2017, 29 November 2017, Article ID 2983747.

Parameters (2022/09/01)

DOI	10.1155/2017/2983747
Citations in Scopus	26
FWCI	1.39
IF	1.59

Research Article

Applicability of the Vibration Correlation Technique for Estimation of the Buckling Load in Axial Compression of Cylindrical Isotropic Shells with and without Circular Cutouts

Eduards Skukis,¹ Olgerts Ozolins,¹ Janis Andersons,²
Kaspars Kalnins,¹ and Mariano A. Arbelo³

¹Riga Technical University (RTU), Institute of Materials and Structures, Kipsalas 6A, Riga, LV-1048, Latvia

²University of Latvia (LU), Institute for Mechanics of Materials, Aizkraukles 23, Riga, LV-1006, Latvia

³Aeronautics Institute of Technology (ITA), 12228-900 Sao Jose dos Campos, SP, Brazil

Correspondence should be addressed to Eduards Skukis; edskukis@gmail.com

Received 28 August 2017; Accepted 5 November 2017; Published 29 November 2017

Academic Editor: Nerio Tullini

Copyright © 2017 Eduards Skukis et al. This is an open access article distributed under the Creative Commons Attribution License, which permits unrestricted use, distribution, and reproduction in any medium, provided the original work is properly cited.

Applicability of the vibration correlation technique (VCT) for nondestructive evaluation of the axial buckling load is considered. Thin-walled cylindrical shells with and without circular cutouts have been produced by adhesive overlap bonding from a sheet of aluminium alloy. Both mid-surface and bond-line imperfections of initial shell geometry have been characterized by a laser scanner. Vibration response of shells under axial compression has been monitored to experimentally determine the variation of the first eigenfrequency as a function of applied load. It is demonstrated that VCT provides reliable estimate of buckling load when structure has been loaded up to at least 60% of the critical load. This applies to uncut structures where global failure mode is governing collapse of the structure. By contrast, a local buckling in the vicinity of a cutout could not be predicted by VCT means. Nevertheless, it has been demonstrated that certain reinforcement around cutout may enable the global failure mode and corresponding reliability of VCT estimation.

1. Introduction

Thin-walled shell structures are extensively employed in applications where minimization of weight is of primary importance (e.g., in aerospace). Load-carrying capacity of such structures in compression is typically governed by buckling. The imperfection sensitivity exhibited by cylindrical shells renders particular emphasis on their design against instability in axial compression. Therefore, robust design approaches are being developed and validated, such as single perturbation load, single perturbation displacement, single boundary perturbation approaches, and their modifications (see, e.g., [1–7]) in order to replace the existing overconservative design guidelines.

Nevertheless, the possibility of a nondestructive evaluation of buckling load is indispensable for proof-testing of structures and also instrumental in validation of theoretical stability analyses. Vibration correlation technique (VCT) is

such a nondestructive vibration test method that allows estimating the buckling load based on experimentally obtained variation of a natural frequency with the applied load as detailed in [8, 9]. It should be noted that VCT can also be applied to determine the actual in situ boundary conditions of structures that can greatly enhance the accuracy of numerical prediction of buckling load [8]. VCTs have generally reached maturity for columns and plates [8], although further refinements are still being developed (e.g., for curved panels) [10]. Moreover, further work is still needed on the validation of the VCT in order to attain industrial applicability for shell structures [10, 11].

Application of VCT is usually based on a theoretically or experimentally determined functional form of the vibration frequency variation with the applied load that is fitted to the test data and extrapolated to estimate the critical buckling load. It has been demonstrated that, as for a variety of other structures possessing similar buckling and vibration modes,

the natural frequency squared is a linear function of the applied axial load also for perfect cylindrical shells [8, 9]. Although low-frequency vibration modes of closely stiffened shells are very similar to their buckling modes, the experimental dependence of frequency squared on axial load was found to exhibit a marked drop in the natural frequency at relatively high loads approaching buckling [8, 10]. The leading role of initial geometrical imperfections in causing such a vibration response has been highlighted by shell models of various complexities [11–13]. Semiempirical relations have been proposed and verified for extraction of buckling load from the experimental natural frequency versus axial load data of closely stiffened shells as discussed in [8, 10, 12, 14, 15]. In particular, using a simplified model of shell, Souza et al. [12, 15] suggested that $(1 - p)^2$ should be a linear function of $1 - f^4$; it can be presented analytically as [10]

$$(1 - p)^2 + (1 - \xi^2)(1 - f^4) = 1, \quad (1)$$

where the nondimensional load parameter $p = P/P_{cr}$ is given by the applied axial load P normalized by the buckling load of a perfect shell P_{cr} , and the frequency parameter $f = f_m/f_0$ is the ratio of the vibration frequency f_m measured at load P and the natural frequency of the unloaded shell f_0 . By fitting (1) to the vibration test results at relatively low loads, the knock-down parameter ξ is evaluated and the buckling load is estimated as

$$P_{pred} = (1 - \xi)P_{cr}, \quad (2)$$

that is, as the load at $f = 0$ from (1).

Unlike closely stiffened shells, unstiffened (monocoque) cylindrical shells exhibit buckling modes that differ from the fundamental vibration modes. Therefore, the VCT methods developed for closely stiffened shells may not be directly transferable to the unstiffened ones. Applicability of VCT to unstiffened stainless steel cylinders was explored in [16] employing linear and quadratic fitting polynomials for vibration frequency squared as a function of axial load, with encouraging but inconclusive preliminary results. The VCT proposed by Souza et al. [12, 15] was applied to unstiffened cylindrical shells by Arbelo et al. [17] using extensive numerical simulations. Negative values of the parameter ξ^2 in (1) were obtained having no physical meaning, thus invalidating the approach [12, 15] for unstiffened cylindrical shells. However, it inspired a modification of VCT as follows [17]. It was proposed to approximate the $(1 - p)^2$ data as a second-order polynomial of $1 - f^2$. The minimum value of $(1 - p)^2$ determined using this approximation was associated with the parameter ξ^2 characterizing the reduction of load-carrying capacity of unstiffened cylindrical shells due to the initial imperfections. Having thus determined the value of ξ^2 , the buckling load is estimated by (2).

The modified VCT of Arbelo et al. [17] has been extensively validated for thin-walled unstiffened cylindrical shells produced from carbon/epoxy [18–20], stainless steel [19], and aluminium [21] demonstrating its capacity of determining the axial buckling load via nondestructive tests. However, common applications from aerospace to civil structures require

isotropic shell structures to be accommodated with local cutouts. The principal aim of the current study is evaluation of the applicability of the modified VCT for estimation of buckling load of isotropic unstiffened cylindrical shells weakened by cutouts in the form of an open circular hole. Furthermore, the accuracy of nonlinear FEM analysis of instability using experimentally determined geometrical imperfection data of the shells and the effect of boundary condition model are evaluated.

2. Test Specimens

2.1. Manufacturing of Cylinders. A total of twelve cylindrical shells having nominal diameter $D_{shell} = 500$ mm and free height $H_{shell} = 460$ mm were manufactured from 0.5 mm thick EN AW 6082 T6 aluminium alloy sheet. The shells designated as R29–R32, R34, and R40 had no cutouts. Shells R33, R35, and R36 featured circular cutouts of diameter $D = 50$ mm, 80 mm, and 30 mm, respectively. Shell R37, in addition to a cutout of 30 mm diameter, was strengthened by a reinforcement ply made from the same sheet in the shape of 20 mm wide ring, with outer diameter 50 mm, attached around the cutout. Shells R38 and R39 had 80 mm diameter cutouts with 20 and 10 mm wide reinforcement rings, respectively. A summary of the test specimen geometry is presented in Table 1.

When prototyping the shells at RTU premises, the aluminium sheets were cut and machined manually before bonding with Araldite® 2011 universal two-component epoxy structural adhesive via a 25 mm overlap longitudinal joint and cured at room temperature. Both the opposite edges of a sheet to be joined were unsymmetrically taper-machined to ensure a uniform thickness distribution across the 25 mm wide overlap joint. Abrasive treatment was applied to the joint surfaces before bonding. Adhesive bonding was carried out on a steel mandrel of 500 mm diameter using vacuum bag to press the aluminium sheet to the mandrel. The joint area was pressed with clamps against the mandrel surface to facilitate uniform bonding. The average bond thickness amounted to 0.85 mm for shells R29 and R30, which were manufactured earlier during EC FP7 project DESICOS employing the same manufacturing technique [21], and 0.75 mm for the rest of shells. The subsequent stages of joining the sheet edges described above are illustrated in Figure 1.

The cutouts were machined upon production of the shells. All the cutouts were located in the shell mid-height and shifted by about 90° circumferentially with respect to the bonding line. The reinforced cutouts were manufactured by bonding the reinforcement ring to the assembled shell, while it was on the steel mandrel. The rings were made of the same aluminium sheet and adhesively bonded by Araldite 2011 adhesive used for shell bonding. The shell cutout was machined the same way as for unreinforced cutouts, matching the internal diameter of reinforcement ring. Cutout milling was performed employing hand-held tungsten carbide burr. The cutouts thus produced, both lacking reinforcement and reinforced by rings of different width, are shown in Figure 2.

Machining of cutouts in the already assembled shells allowed performing initial geometry scans of the shells before

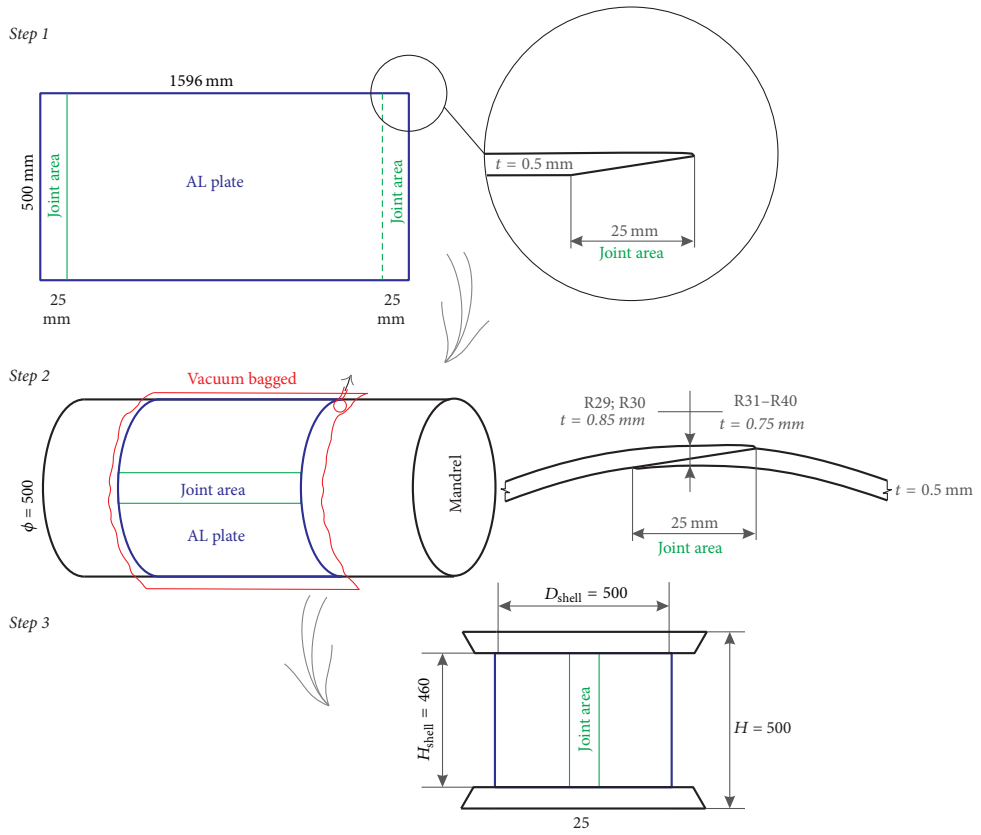


FIGURE 1: Subsequent stages for producing of an adhesively bonded overlap joint: tapering of both edges at the bonding line (Step 1); aluminium sheet wrapped around a cylindrical steel mandrel, vacuum-bagged with clamped joint area (Step 2); final assembly, cylindrical shell with edge casting blocks (Step 3).

TABLE 1: Test specimens.

Cylinder ID	Nominal diameter D_{shell}	Free height H_{shell}	Thickness	Total thickness at bonded area	Cutout diameter D	Reinforcement	Shimming
R29	500 mm	460 mm	0.5 mm	0.85 mm	No cutout	No	Lower loading plate
R30				0.85 mm	No cutout	No	Lower loading plate
R31				0.75 mm	No cutout	No	No
R32				0.75 mm	No cutout	No	No
R33				0.75 mm	50 mm	No	No
R34				0.75 mm	No cutout	No	No
R35				0.75 mm	80 mm	No	No
R36				0.75 mm	30 mm	No	No
R37				0.75 mm	30 mm	20 mm wide ring	No
R38				0.75 mm	80 mm	20 mm wide ring	No
R39	0.75 mm	80 mm	10 mm wide ring	No			
R40	0.75 mm	No cutout	No	No			

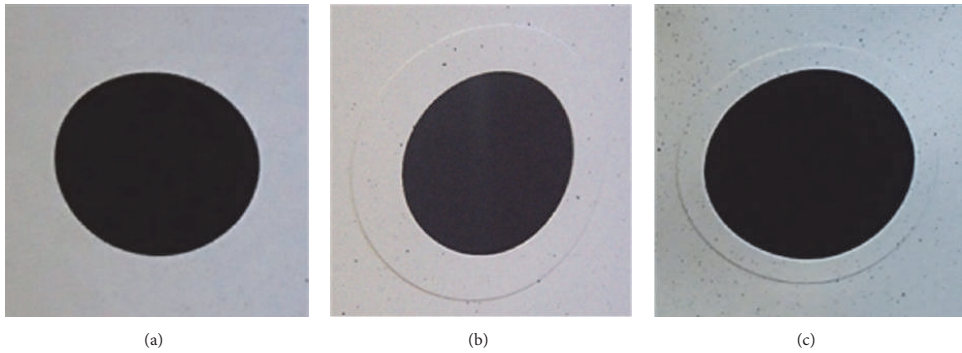


FIGURE 2: Different cutout edge conditions: unreinforced cutout (a) and cutouts with reinforcing rings of 20 (b) and 10 (c) mm width.

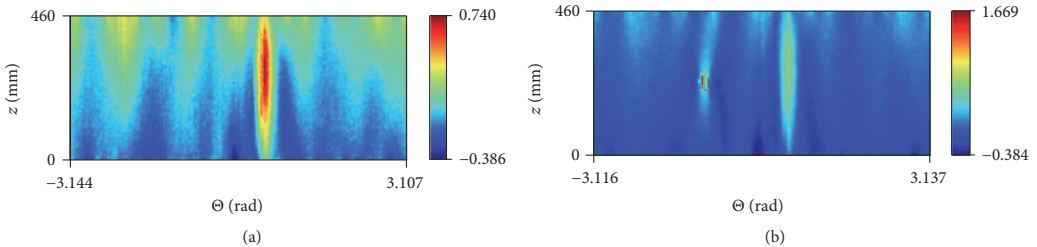


FIGURE 3: Imperfection scans by an internal laser scanner for R36 shell before (a) and after (b) introduction of cutout.

actual cutouts were made to gather imperfection data related to manufacturing imperfection signatures.

2.2. Characterization of Geometrical Imperfections of Shells. A laser scanner (Panasonic HL-G1 sensor) was used to measure the geometric imperfections of the inner surface of all the cylinders. The laser scan was controlled using an in-house software and the data acquired were exported in real time to a text file for postprocessing.

Upon scanning, the best-fit-cylinder algorithm was applied to the raw data in order to eliminate the rigid body motion modes from the measurements. The results presented in Figure 3 show unfiltered imperfection pattern for R36 shell, captured before and after introduction of the cutout. It should be noted that the cutout area was externally covered to avoid out-of-range readings of the laser; nevertheless, one may see that both the cutout and adhesive joint areas are exhibiting the most severe imperfections.

3. Mechanical Tests

3.1. Characterization of the Shell Wall Material. The procedure for material characterization according to ASTM E-8M-04 standard was carried out for 0.5 mm thick sheet of EN AW 6082 T6 aluminium alloy used for manufacturing of the cylindrical shells. The aim of material characterization was to determine the yield stress and ultimate stress, as well as the

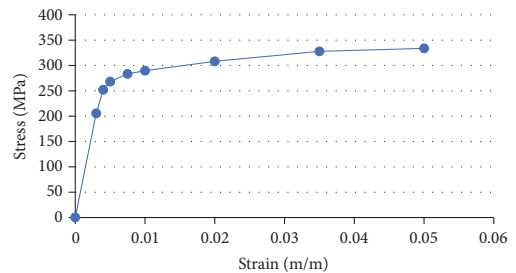


FIGURE 4: MISO curve of the aluminium sheet material with indicated experimental stress-strain data points used for its construction.

nonlinear plasticity diagram of the material to be employed in finite element analyses of buckling. Multilinear isotropic hardening (MISO) material model, exemplified in Figure 4, was established based on the experimentally obtained stress-strain curves. Typical Young's modulus value of aluminium alloys of 70 GPa was used in the material model.

3.2. Shell Buckling Tests. Experimental buckling test set-up for shells, shown in Figure 5, comprised three LVDTs (placed around the shell at 120° angular intervals) for shortening measurements, one of them aligned with the bonding line



FIGURE 5: Experimental test set-up.

of the shell. Both the top and bottom edges of shells, resting on the respective machine plates, were joined to the plates by means of potting with a resin/powder filler to eliminate loading imperfections and contact surface misalignments.

For most of the cylinder tests, the bottom plate was bolted to the respective crosshead as shown in Figure 6(a). By contrast, for shells R29 and R30 the test set-up contained a shimmed interface at the lower machine plate (Figure 6(b)). Shimming was performed by placing very thin sheets of metal between the lower loading plate and the load distributing washer attached to the load frame in order to eliminate the small gaps between both surfaces, so that an even distribution of load along the cylinder's circumference was ensured. When testing the rest of cylinders, this interface was eliminated by bolting both load distributing structures directly to the load frame (Figure 6(a)).

Universal quasi-static testing machine Zwick 100 was used for the tests. Loading was introduced by incremental upper edge displacement at a rate of 0.5 mm/min. Load measurement was carried out by a single load cell located between the upper loading plate and the upper crosshead of the loading frame.

A photogrammetry based technique was used to capture the 3D buckling mode shape deformation pattern and to build open plots.

3.3. Characterization of Vibration Response. The universal quasi-static testing machine Zwick 100 was used to apply axial compressive load on the cylinders. Starting from zero load (i.e., unloaded shell), the compressive load was gradually increased in 2 kN steps up to ca. 85% of the estimated buckling load. Upon each load increment, the natural frequencies and vibration modes were scanned by Polytec laser vibrometer on a grid of points distributed along a small area of the cylinder (Figure 7).

For structural excitation, a loudspeaker, placed 180° opposite to the scanned area, was used and measurements were conducted in the frequency range from 200 to 400 Hz. The scanned sector of cylinder was approximately 72° wide

that corresponds to 1/5 of cylinder surface. The scanned area consisted of 300 grid points that presented a good trade-off between the scanning time and the level of detail of modal response. The vibration mode shapes captured by the laser vibrometer and corresponding to the first natural frequency are shown in Figure 8 overlaid onto the respective shells tested.

4. Numerical Analyses

Numerical simulations were performed by means of ANSYS [22] finite element code as nonlinear buckling analyses with multilinear isotropic hardening material model to allow for plasticity. Newton-Raphson large deformation solver was used to solve the shell finite element model composed of shell (SHELL281), solid (SOLID186), and multipurpose constraint (MPC184) finite elements. Two approaches of implementation of the boundary conditions were covered in the current study, namely, simplified clamped boundary conditions (CBC), which consider clamped shell edges with uniform loading by edge translation, and real case boundary conditions (RBC), consisting of modeling of the actual load introducing parts of the test set-up, connected to the shell edges by multipoint constraint element rigid beams. The basic concern of the utilization of the more complicated FE analysis model versus the simplified one was related to the particular test set-up containing a circular adapter (25 mm long steel adapter stud of 63 mm diameter, connecting upper load transfer plate to the load cell, attached to the test frame crosshead) (see Figure 5), taking into account bending of the top and bottom load distribution plates resulting in rotation of the shell boundary region.

In the case of CBC, bottom edge of the shell was considered as clamped (i.e., the condition of all edge displacement and rotation components being equal to zero was imposed). The upper edge was considered clamped for all the rotations and displacements except that in the loading direction. Loading by displacement was applied to all the upper edge nodes.

In the case of RBC, all the set-up parts up to connection to the load cell were modeled by shell and solid finite elements representing physical interaction of the actual parts, allowing for loading edge rotation and bending of the loading plate. Clamped boundary conditions were applied on the central part of the bottom steel plate, while the shell edge was clamped to the plate, allowing for rotation. The upper loading unit was constrained in lateral directions, with displacement in the loading direction applied to all the nodes of the upper part of connector stud, thus allowing load redistribution through all the components to the shell. The respective FEM models are shown in Figure 9.

The critical buckling load of a perfect shell, needed for application of the VCT, was obtained by a linear FEM analysis of a shell lacking any imperfections and subjected to CBC.

5. Results and Discussion

5.1. Experimental Buckling Loads and Modes. The buckling loads and mode shapes determined for each of the specimens

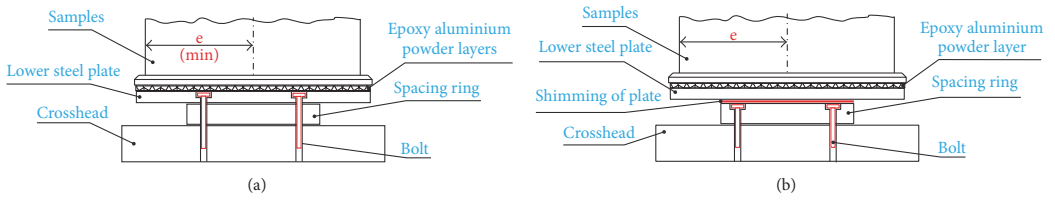


FIGURE 6: Schematic of the lower shell support for most of the specimens (a) and for shells R29 and R30 (b).



FIGURE 7: Experimental set-up for vibration tests.

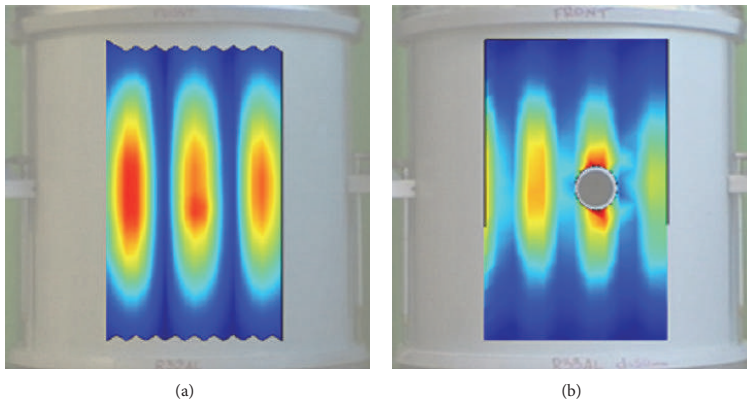


FIGURE 8: First vibration mode used in VCT of an intact cylinder (a) and a cylinder with cutout (b).

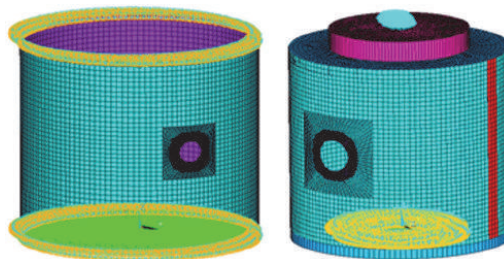
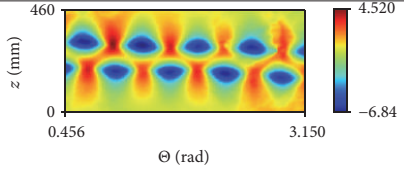
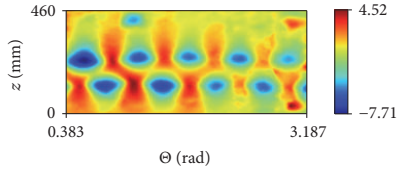
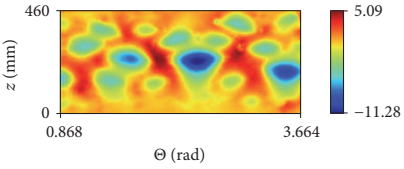
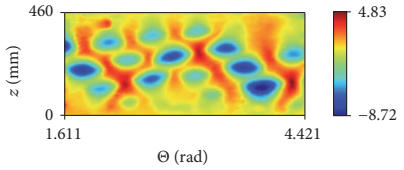
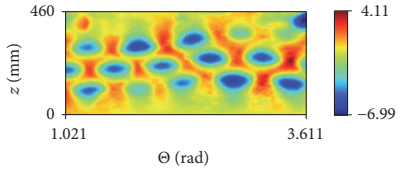
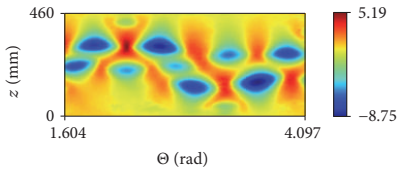


FIGURE 9: FEM models for CBC and RBC of a cylindrical shell with cutout.

TABLE 2: Experimental buckling loads and mode shapes of intact shells.

Cylinder	Experimental buckling load [kN]	Experimental buckling mode	
R29	36.3		
R30	38.3		
R31	51.98		
R32	51.96		
R34	51.57		
R40	52.52		

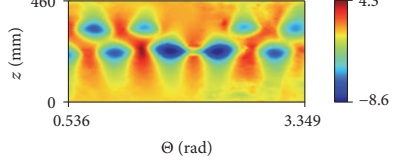
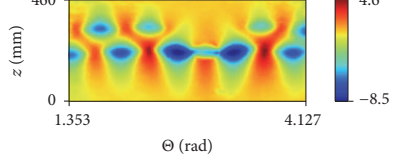
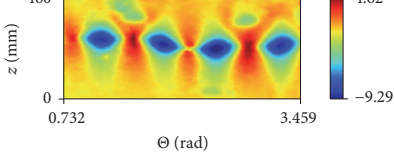
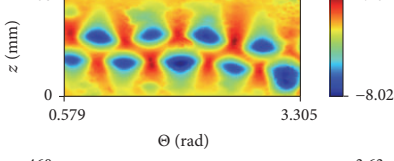
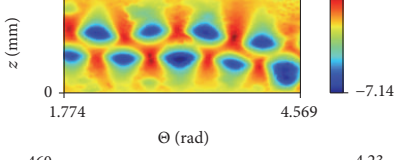
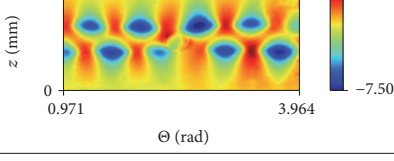
tested are summarized in Table 2 for intact shells and in Table 3 for shells with cutouts. If a local buckling at the cutout was observed preceding the global one, the local buckling load is given in brackets in Table 3.

The buckling mode shape patterns shown in Tables 2 and 3 were obtained by a photogrammetry technique. The method is based on reconstructing of the 3D shape of an object using a number of digital camera shots at different angles around the circumference. In this particular case, due to the tight space between test frame columns and the specimen, only a sector of about 1/3 of the shell could be

represented in the open plot, usually front and back sectors. The accuracy of determining the out-of-plane displacement magnitude is highly dependent on the number of shots taken and quality of the optical system used. Since there was no straightforward method of calibration available for this technique, the measured magnitudes should be used only for purposes of comparative analysis.

The intact shells R31, R32, R34, and R40, tested with the lower plate supported as shown in Figure 6(a), exhibited very close buckling loads at $52.0 \pm .4$ kN. Shells R29 and R30 possessed larger geometrical imperfections than the rest,

TABLE 3: Experimental buckling loads and mode shapes of shells with cutouts.

Cylinder	Experimental buckling load [kN]	Experimental buckling mode	
R33 $D = 50$ mm	25.85 (21.2)*		
R35 $D = 80$ mm	25.05 (21.5)*		
R36 $D = 30$ mm	25.39		
R37 $D = 30$ mm 20 mm wide ring	43.79		
R38 $D = 80$ mm 20 mm wide ring	30.9 (29.1)*		
R39 $D = 80$ mm 10 mm wide ring	28.12 (27.7)*		

* Load at the onset of local buckling.

which was likely the cause of their lower buckling load of ca. 37 kN reported in Table 2.

It is seen in Table 3 that shells with cutouts lacking reinforcement exhibited very close buckling loads of ca. 25 kN for cutout diameters ranging from 30 to 80 mm. Adding a 10 mm wide reinforcement layer to a shell with 80 mm cutout increased the critical load by about 10%, while a 20 mm wide reinforcement patch applied to a 30 mm cutout elevated buckling load by more than 70%.

It should be noted that the experimental results of the effect cutout on buckling load reported above are in close agreement with those of other authors that have studied this phenomenon. For instance, following the work presented by Toda [23], the authors evaluated the reinforcement ratio of the shells γ :

$$\gamma = \frac{W}{W_0}, \quad (3)$$

TABLE 4: Numerical buckling load prediction and VCT results for shells without cutouts.

Cylinder	Experimental buckling load [kN]	Numerical predicted buckling load [kN] RBC/CBC	Deviation from experimental results [%] RBC/CBC	KDF EXP/RBC/CBC	Predicted buckling load by VCT [kN]	Deviation from experimental results [%]
R29	36.33	36.45*	0.31*	0.54/-/0.55	38.16	-5.04
R30	38.32	44.96*	14.8*	0.57/-/0.67	38.36	-0.13
R31	51.98	49.76/51.08	-4.5/-1.8	0.78/0.75/0.77	46.08	11.35
R32	51.96	49.07/49.51	-5.9/-5.0	0.78/0.74/0.74	52.71	-1.44
R34	51.57	51.70/52.39	0.3/1.6	0.77/0.77/0.78	53.36	-3.47
R40	52.52	46.42/48.45	-13.1/-7.5	0.79/0.7/0.73	40.21	23.44

*CBC boundary conditions.

where W is the volume of stiffening and W_0 is the volume of the shell wall removed by the cutout. The unstiffened cylinders R33, R35, and R36 had $\gamma = 0$ due to lack of reinforcement. On the other hand, γ values for cylinders R37, R38, and R39 amounted to 0.44, 0.062, and 0.015, respectively. Toda [23] observed that, in general, the buckling load of an unstiffened cylindrical shell with a reinforced cutout would increase as γ increases, which agrees with the results presented herein.

Moreover, Toda also demonstrated that the effect of circular cutouts on buckling loads of cylindrical shells can be determined by the α parameter calculated as

$$\alpha = \frac{a}{\sqrt{R \cdot t}}, \quad (4)$$

where $a = D/2$, $R = D_{\text{shell}}/2$, and t is the wall thickness of the unstiffened cylinder. For $\alpha < 1$, cutouts exhibit no appreciable effect on the buckling strength of the cylinder. Buckling load is greatly reduced in the range of $1 < \alpha < 2$ and continues to decrease slightly as α increases. Furthermore, increasing the value of γ parameter at a fixed α leads to the growth of buckling load (up to that of intact shell for sufficiently large γ) [23]. For our study cases, the α parameter is equal to 1.34 for the cylinder R37 and takes the value of 3.57 for both R38 and R39 cylinders. This, together with the γ values of these shells discussed above indicates that the buckling load of R37 should be higher than that of R38 and R39 and also that the buckling load of R38 should exceed that of R39. Such a predicted ranking of buckling loads is confirmed by the experimental results presented in Table 3.

Furthermore, Yilmaz et al. [24] calculated the knock-down factor for the buckling load of unstiffened cylindrical shells with cutouts as a function of the α parameter. Their results agree with Toda's findings [23] and the experimental results presented in Table 3.

5.2. FEM Modeling of Buckling. As the numerical model of cylindrical shells, finite element model composed of SHELL281 shell elements, comprising 130 elements around the circumference and maintaining about 12×12 mm mesh aspect ratio, was selected based on mesh sensitivity analyses. The experimentally determined mid-surface imperfections, as well as bonding line thickness imperfections, were implemented into the finite element model for each shell.

A nonlinear analysis of buckling was performed, as described in Section 4, considering both RBC and CBC cases of boundary conditions for shells. The resulting buckling loads are presented in Table 4 for intact shells and in Table 5 for shells with cutouts. The knock-down factor (KDF), presented in the Tables, is calculated with respect to the buckling eigenload of a perfect intact cylinder, estimated by linear FEM analysis at 66.74 kN.

Comparison of the FEM results of buckling loads with their experimental values revealed that applicability of the simplified CBC was limited to shells which contained only mid-surface and bond-line imperfections. It is seen in Table 4 that in this case both CBC and RBC yield very close results which, moreover, are also in good agreement with the test results.

For shells containing cutouts, the local reduced stiffness in the cutout region is not adequately allowed for in FEM model with CBC due to the uniform edge translation imposed (i.e., displacement control). By contrast, the RBC model properly reflects such a reduced stiffness via the structural response through bending of the rigid elastic adapter and bending of the loading plates that can actually be considered as cantilever plates. Implementation of the RBC into the FEM model markedly improved prediction accuracy of the buckling load, as seen in Table 5.

As an example, experimental and predicted load-shortening curves for shells with and without cutouts are presented in Figure 10. Virtually no difference in the predicted shell response under CBC and RBC is seen for the intact shell R34 up to buckling. By contrast, for the shell R35 weakened by a cutout, the theoretical load-shortening diagrams diverge markedly upon local buckling of the shell at the cutout, with CBC producing a stiffer response and greater global buckling load. FEM analysis with RBC captures reasonably accurately both the local buckling, manifesting by a slight drop in load with subsequent lower slope of load-shortening diagrams seen in Figure 10(b), and the global buckling.

5.3. Application of VCT. The standard VCT is being applied to structural elements for which the shape of the vibration mode, where the frequency of which is monitored during compressive loading, matches or is close to their buckling mode shape [8]. This is clearly not the case for the first

TABLE 5: Numerical buckling load prediction and VCT results for shells with cutouts.

Cylinder	Experimental buckling load [kN]	Numerical predicted buckling load [kN] RBC/CBC	Deviation from experimental results [%] RBC/CBC	KDF EXP/RBC/CBC	Predicted buckling load by VCT [kN]	Deviation from experimental results [%]
R36	25.39	31.22/36.92	18.69/31.25	0.38/0.47/0.55	29.81	-17.4
R33	25.85 (21.2)*	28.80/36.88	10.22/29.90	0.39/0.43/0.55	—	—
R35	25.05 (21.5)*	28.51/36.66	12.14/31.66	0.38/0.43/0.55	—	—
R37	43.79	47.42/49.41	7.64/11.37	0.66/0.71/0.74	41.59	5.0
R38	27.93(26.76)*	31.48/35.10	11.26/20.43	0.42/0.47/0.53	—	—
R39	28.12 (27.2)*	31.33/38.29	10.24/26.58	0.42/0.47/0.57	24.94	11.3

*Load at the onset of local buckling.

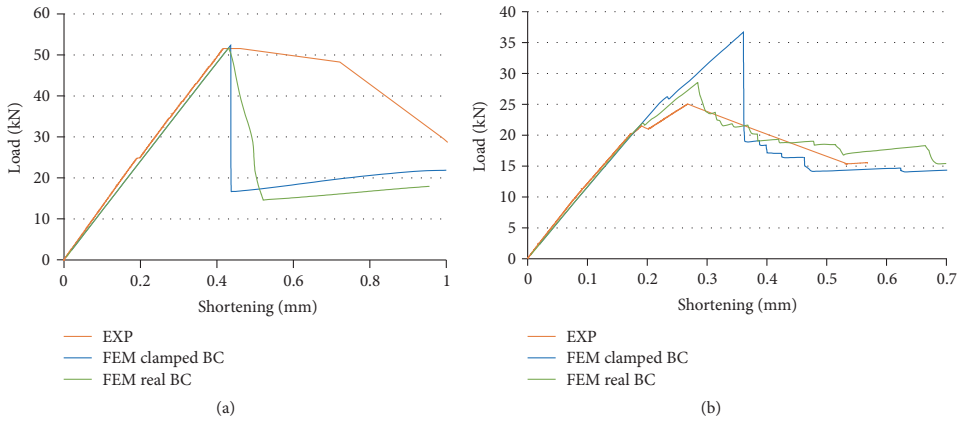


FIGURE 10: Experimental and predicted load-shortening curves for the shell R34 without cutout (a) and shell R35 with a cutout (b).

vibration mode monitored during axial compression for either the intact cylinders (cf. Figure 8(a) and Table 2) or the cylinders with cutouts (cf. Figure 8(b) and Table 3).

However, the modified VCT developed in [17] allows correlating reduction of the first natural frequency of an unstiffened cylindrical shell under axial compression to the buckling load when the buckling mode differs from the vibration one. In the following, we check the applicability of the modified VCT [17] to the unstiffened aluminium shells.

Natural frequency response of the intact shells, free from loading, is shown in Figure 11(a). Vibration characteristics of the different shells are seen to be rather similar as would be expected for cylinders of the same dimensions and material.

The limited variability present is thought to be stemming mostly from the differences in geometrical mid-surface and bond-line imperfections among shells. The first vibration mode was identified from natural frequency response of each cylinder (Figure 11(a)), and its variation was monitored during axial compressive loading of the shell. The experimentally determined reduction of the vibration frequencies of intact shells with incrementally growing load is presented in Figure 11(b). It is seen that the scatter in the first natural

frequency among specimens also decreases with increasing load.

Using the frequency variation data presented in Figure 11(b) and the critical load of a perfect intact cylinder estimated by FEM, the plots of $(1 - p)^2$ versus $1 - f^2$ were constructed for the pooled data of shells R31, R32, R34, and R40 characterized by relatively small imperfections and for pooled data of shells R29 and R30 having larger imperfections. (Each of the two sets of shells mentioned was produced under the same conditions resulting in close imperfection signatures within a set, which allowed considering the shells as nominally identical within each set.) The respective plots are shown in Figure 12 together with a second-order fitting curve as stipulated by the modified VCT [17]. From the minimum of the approximating second-order polynomial, the numerical value of the factor ξ^2 characterizing the reduction of buckling load caused by shell imperfections was determined as $\xi^2 = 0.0609$ for the set of Figure 12(a) and $\xi^2 = 0.1824$ for the set of Figure 12(b). Buckling load predicted by the modified VCT using (2) for the shells R31–R40 amounted to 50.27 kN, which is very close to the average experimental buckling load 52.0 kN of

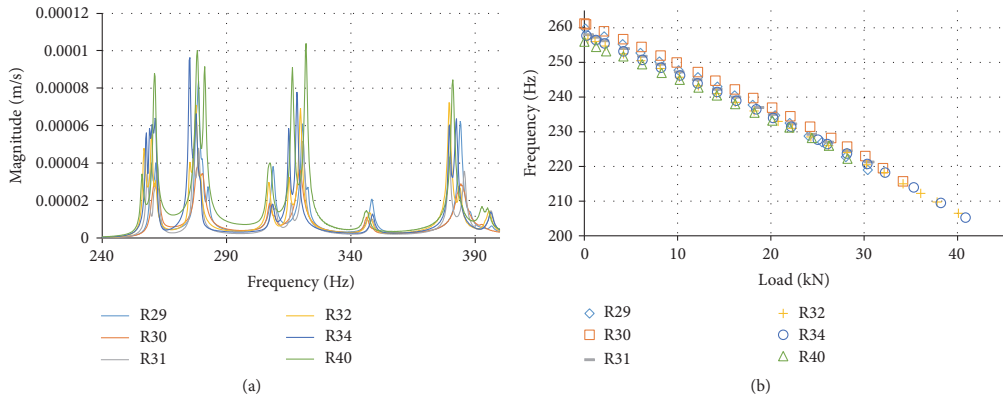


FIGURE 11: Natural frequency response of intact unloaded cylinders (a) and reduction of the first natural frequency with increasing axial load (b).

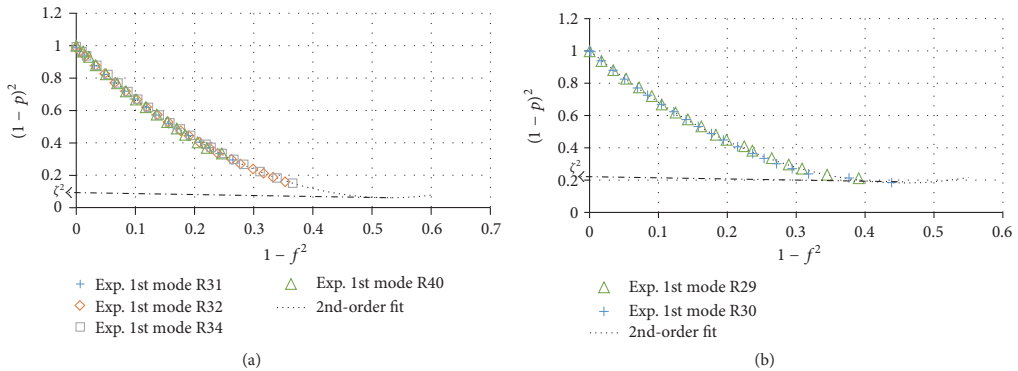


FIGURE 12: Plot of $(1 - p)^2$ as a function of $1 - f^2$ and the second-order fit for the sets of cylinders with comparatively small (a) and larger (b) imperfections.

these shells. Similarly, a good agreement of the predicted, 38.2 kN, and average experimental, 37.3 kN, buckling load was obtained for the shells R29 and R30 with larger imperfections. Notably, comparable accuracy of the VCT approach has also been reported in [18] for unstiffened cylindrical composite shells.

Such a good predictive capacity lends credence to the semiempirical VCT considered, but it should also be noted that capturing the vibration response of a set of nominally identical specimens up to a relatively high level of applied force P may not always be feasible in practice. In order to evaluate the effect of maximum load used in VCT on the prediction accuracy of buckling load, the latter was evaluated by the modified VCT for each specimen and load increment separately. The results are presented in Figure 13 in terms of the relative accuracy of prediction, characterized by the ratio of predicted and experimental buckling loads $P_{\text{pred}}/P_{\text{exp}}$, as

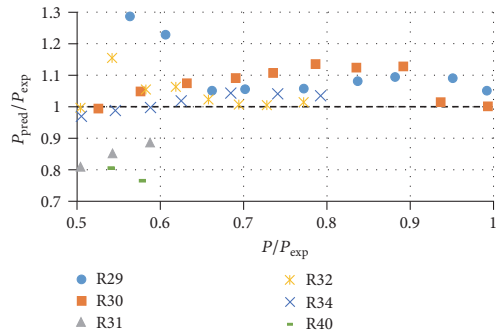


FIGURE 13: Predicted buckling load P_{pred} of an intact shell versus the maximum applied load P used in VCT, normalized by experimental buckling load of the shell P_{exp} .

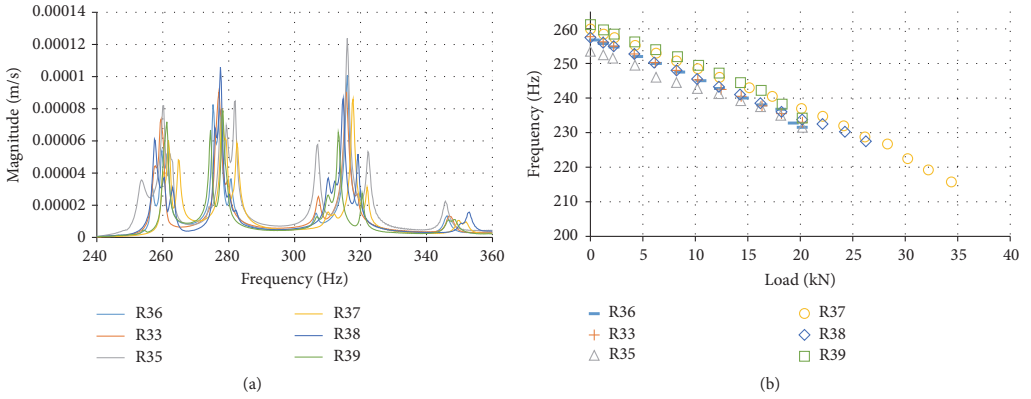


FIGURE 14: Natural frequency response of unloaded cylinders with cutouts (a) and reduction of the first natural frequency with increasing axial load (b).

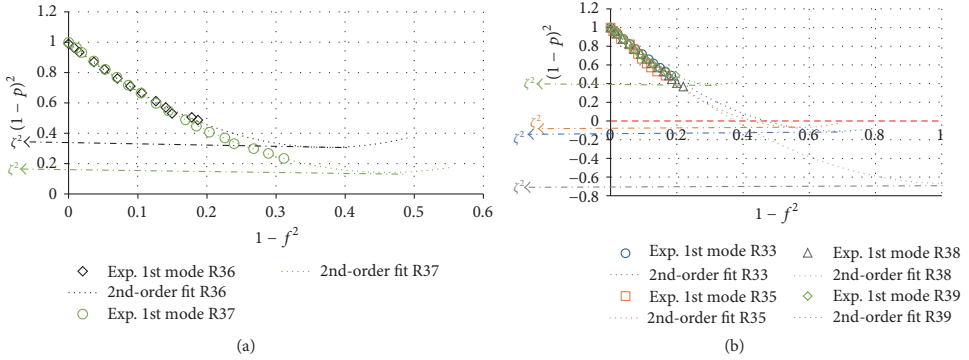


FIGURE 15: Plot of $(1 - p)^2$ as a function of $1 - f^2$ and the second-order fit for cylinders with cutouts that failed without (a) and with local buckling preceding global instability (b).

a function of the maximum load used in VCT expressed as a fraction of the buckling load, P/P_{exp} . Data for $P/P_{\text{exp}} > 0.5$ only are plotted since the VCT approach considered has been shown to yield insufficiently accurate results for smaller values of the maximum normalized load [18]. The numerical values of P_{pred} estimated using data up to the maximum applied load P for each shell are also given in Table 4.

It is seen in Figure 13 that the relative error of prediction can reach up to 30% if P is limited by 60% of P_{exp} . However, the accuracy of VCT can be markedly improved by extending the loading range: when $P/P_{\text{exp}} \geq 0.62$, the predicted buckling load differs by less than 10% from the experimental one for five of the six cylinders tested; even for the outlier R30, the error does not exceed 15%.

In order to further increase the accuracy of prediction, simultaneous monitoring of evolution of several vibration modes under axial load could be considered in the modified VCT. The results reported in [19] revealed that that using the second vibration mode for estimation of the buckling

load provided closer conservative prediction in some cases. Combining the data for several vibration modes of the same specimen may facilitate both accuracy and robustness of VCT, and validation of such an approach is the subject of further research.

Natural frequency response of free shells with cutouts shown in Figure 14(a) exhibited considerable variability among shells, presumably caused by differing diameters of the open holes and the reinforcement rings. The variability also persisted when the shells were subjected to axial loading, as seen in Figure 14(b) presenting experimentally determined reduction of the first natural frequency of each shell as a function of the axial compressive load.

Experimental results of the variation of frequency with axial load were normalized as above, obtaining $(1 - p)^2$ versus $1 - f^2$ data for each shell which were approximated by a second-order polynomial. The data and the best-fit polynomials, extrapolated in order to graphically reveal their minima, are plotted in Figure 15. It is seen that, for part of the cylinders

with cutouts, the modified VCT produced negative values of ξ^2 which is physically inadmissible. The reason the modified VCT failed for specimens with open holes is apparently related to a more complicated evolution of instability in the presence of a cutout. Specifically, for majority of the cylinders tested, a local buckling at the cutout was observed to precede the global one. VCT plots for these specimens are presented in Figure 15(b).

Appearance of the local buckling was associated with larger cutouts as follows from Table 3. Even for the shells R36, R37, and R39 for which the modified VCT could formally be applied since positive values of ξ^2 were obtained, the accuracy of prediction was not uniform; see Table 5.

Apparently, further work is needed to develop a nondestructive test method applicable to weakened shells exhibiting stable local buckling modes preceding the global buckling. A potentially fruitful alternative to monitoring the vibration response of the whole shell under load could be exploring the variation of local characteristics of the shell at the spots likely to undergo instability [25]. Additional tests are currently under development to further validate this proposed approach.

6. Conclusions

In general, the presence of a circular open-hole cutout was found to reduce the buckling load in axial compression of thin-wall unstiffened cylindrical shells produced from aluminium sheet by up to 50% with respect to intact shells. Reinforcement by a ring of the same material, adhesively bonded around cutout, alleviated its detrimental effect, and wider reinforcement rings lead to smaller reduction in buckling load due to cutout.

The modified VCT has been demonstrated to be an efficient tool for nondestructive prediction of the load-carrying capacity of intact shells. The discrepancy of the predicted and experimental critical load of less than about 10% was attained when the reduction of fundamental frequency of a shell was monitored under axial loads in excess of 60% of the buckling load. By contrast, appearance of a local buckling at the cutout, preceding the global buckling of a shell, was found to invalidate the considered VCT for shells with holes. Notably, a good agreement between the experimental and predicted buckling load from VCT was observed for the R37 cylinder possessing a relatively high stiffening ratio γ and low α parameter value. Further testing should be conducted in order to seek a correlation between these two parameters and the range of applicability of VCT for cylindrical shells with reinforced cutouts.

Implementing the experimentally determined geometrical imperfections of shells in a nonlinear analysis of instability by FEM enabled accurate prediction of buckling load of the intact shells, with the maximum error less than 15%. For shells with cutouts, the importance of applying the actual boundary conditions, allowing for deformations of the loading set-up during tests, was revealed. Specifically, the buckling load was overestimated by up to 31% under simplified clamped boundary conditions, while including the appropriate elements of the loading rig in the FEM analysis markedly increased the accuracy of prediction.

Disclosure

The information in this paper reflects only the authors' views and the European Community is not liable for any use that may be made of the information contained therein.

Conflicts of Interest

The authors have no conflicts of interest as the software and hardware are developed by authors of this manuscript.

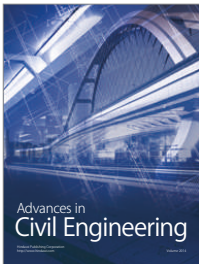
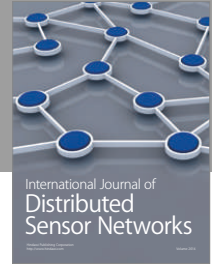
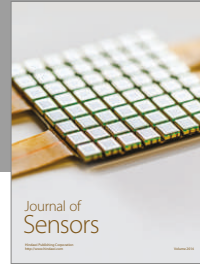
Acknowledgments

The research leading to these results has received partial funding from the European Community's Seventh Framework Programme (FP7/2007–2013), Grant Agreement no. 282522 (<http://www.desicos.eu>). The authors also acknowledge the National Council for Scientific and Technological Development (CNPq) for the financial support (Grant no. 300893/2015-9).

References

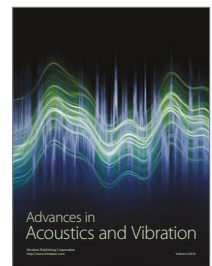
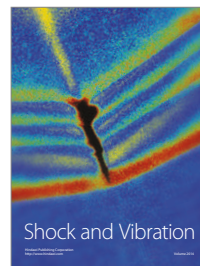
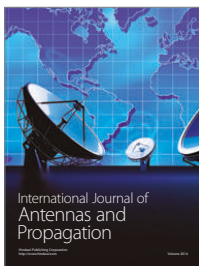
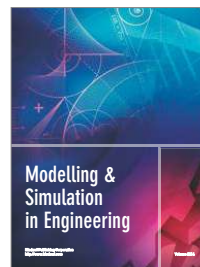
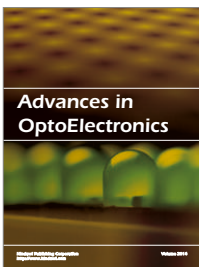
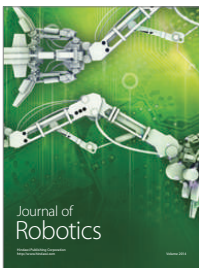
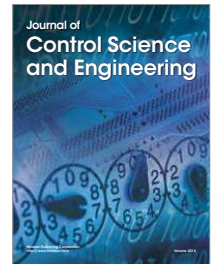
- [1] R. Degenhardt, S. G. P. Castro, M. A. Arbelo, R. Zimmerman, R. Khakimova, and A. Kling, "Future structural stability design for composite space and airframe structures," *Thin-Walled Structures*, vol. 81, pp. 29–38, 2014.
- [2] B. Kriegesmann, E. L. Jansen, and R. Rolfes, "Design of cylindrical shells using the Single Perturbation Load Approach – Potentials and application limits," *Thin-Walled Structures*, vol. 108, pp. 369–380, 2016.
- [3] H. N. R. Wagner, C. Hühne, S. Niemann, and R. Khakimova, "Robust design criterion for axially loaded cylindrical shells – Simulation and Validation," *Thin-Walled Structures*, vol. 115, pp. 154–162, 2017.
- [4] H. Wagner, C. Hühne, and S. Niemann, "Robust knockdown factors for the design of axially loaded cylindrical and conical composite shells – Development and Validation," *Composite Structures*, vol. 173, pp. 281–303, 2017.
- [5] S. G. P. Castro, R. Zimmermann, M. A. Arbelo, and R. Degenhardt, "Exploring the constancy of the global buckling load after a critical geometric imperfection level in thin-walled cylindrical shells for less conservative knock-down factors," *Thin-Walled Structures*, vol. 72, pp. 76–87, 2013.
- [6] S. G. P. Castro, R. Zimmermann, M. A. Arbelo, R. Khakimova, M. W. Hilburger, and R. Degenhardt, "Geometric imperfections and lower-bound methods used to calculate knock-down factors for axially compressed composite cylindrical shells," *Thin-Walled Structures*, vol. 74, pp. 118–132, 2014.
- [7] M. A. Arbelo, R. Degenhardt, S. G. P. Castro, and R. Zimmermann, "Numerical characterization of imperfection sensitive composite structures," *Composite Structures*, vol. 108, no. 1, pp. 295–303, 2014.
- [8] "Vibration Correlation Techniques," in *Buckling Experiments, Experimental Methods in Buckling of Thin-Walled Structures*, vol. 2, Chapter 15, pp. 1244–1284, John Wiley Sons, New York, NY, USA, 2002.
- [9] L. N. Virgin, *Vibration of Axially-Loaded Structures*, Cambridge University Press, North Carolina, NC, USA, 2007.

- [10] H. Abramovich, D. Govich, and A. Grunwald, "Buckling prediction of panels using the vibration correlation technique," *Progress in Aerospace Sciences*, vol. 78, pp. 62–73, 2015.
- [11] E. L. Jansen, H. Abramovich, and R. Rolfes, "The direct prediction of buckling loads of shells under axial compression using VCT - Towards an upgraded approach," in *Proceedings of the 29th Congress of the International Council of the Aeronautical Sciences (ICAS '14)*, September 2014.
- [12] M. A. Souza, W. C. Fok, and A. C. Walker, "Review of experimental techniques for thin-walled structures liable to buckling, part I—neutral and unstable buckling," *Experimental Techniques*, vol. 7, no. 9, pp. 21–25, 1983.
- [13] M. A. Souza, "The effects of initial imperfection and changing support conditions on the vibration of structural elements liable to buckling," *Thin-Walled Structures*, vol. 5, no. 6, pp. 411–423, 1987.
- [14] M. A. Souza and L. M. B. Assaid, "A new technique for the prediction of buckling loads from nondestructive vibration tests," *Experimental Mechanics*, vol. 31, no. 2, pp. 93–97, 1991.
- [15] M. A. Souza, "Coupled dynamic instability of thin-walled structural systems," *Thin-Walled Structures*, vol. 20, no. 1-4, pp. 139–149, 1994.
- [16] E. Skukis, K. Kalnins, and A. Chate, "Preliminary assessment of correlation between vibrations and buckling load of stainless steel cylinders," in *Proceedings of the 10th Jubilee Conference on "Shell Structures: Theory and Applications" (SSTA '13)*, pp. 325–328, October 2013.
- [17] M. A. Arbelo, S. F. M. de Almeida, M. V. Donadon et al., "Vibration correlation technique for the estimation of real boundary conditions and buckling load of unstiffened plates and cylindrical shells," *Thin-Walled Structures*, vol. 79, pp. 119–128, 2014.
- [18] M. A. Arbelo, K. Kalnins, O. Ozolins, E. Skukis, S. G. P. Castro, and R. Degenhardt, "Experimental and numerical estimation of buckling load on unstiffened cylindrical shells using a vibration correlation technique," *Thin-Walled Structures*, vol. 94, pp. 273–279, 2015.
- [19] K. Kalnins, M. A. Arbelo, O. Ozolins, E. Skukis, S. G. P. Castro, and R. Degenhardt, "Experimental nondestructive test for estimation of buckling load on unstiffened cylindrical shells using vibration correlation technique," *Shock and Vibration*, vol. 2015, Article ID 729684, 8 pages, 2015.
- [20] E. Skukis, O. Ozolins, K. Kalnins, and M. A. Arbelo, "Experimental Test for Estimation of Buckling Load on Unstiffened Cylindrical shells by Vibration Correlation Technique," in *Proceedings of the 12th International Conference Modern Building Materials, Structures and Techniques (MBMST '16)*, vol. 172, pp. 1023–1030, 2017.
- [21] H. Abramovich, K. Kalnins, and A. Wieder, "Test results on the stability and vibrations of composite shells," in *Stability and Vibrations of Thin Walled Composite Structures*, pp. 619–691, 2017.
- [22] ANSYS® Academic Research, Release 16.2.
- [23] S. Toda, "Buckling of cylinders with cutouts under axial compression - Experimental results are presented for circular cylindrical shells with both reinforced and unreinforced holes under axial compression," *Experimental Mechanics*, vol. 23, no. 4, pp. 414–417, 1983.
- [24] H. Yılmaz, İ. Kocabaş, and E. Özyurt, "Empirical equations to estimate non-linear collapse of medium-length cylindrical shells with circular cutouts," *Thin-Walled Structures*, vol. 119, pp. 868–878, 2017.
- [25] W. H. Horton, E. M. Nassar, and M. K. Singhal, "Determination of the critical loads of shells by nondestructive methods - The critical axial loads for conventional cylindrical-shell bodies are experimentally determined by measuring the static and dynamic properties of the shell wall at low levels of the applied loading," *Experimental Mechanics*, vol. 17, no. 4, pp. 154–160, 1977.



Hindawi

Submit your manuscripts at
<https://www.hindawi.com>



VI

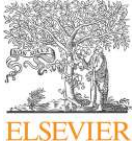
Franzoni F., Odermann F., Wilckens D., **Skuķis E.**, Kalniņš K., Arbelo M.A., Degenhardt, R.

“Assessing the axial buckling load of a pressurized orthotropic cylindrical shell through vibration correlation technique”

Thin-Walled Structures, Volume 137, April 2019, Pages 353-366

Parameters (2022/09/01)

DOI	10.1016/j.tws.2019.01.009
Citations in Scopus	19
FWCI	1.55
IF	4.0



Full length article

Assessing the axial buckling load of a pressurized orthotropic cylindrical shell through vibration correlation technique

Felipe Franzoni^{a,b,*}, Falk Odermann^a, Dirk Wilckens^a, Eduards Skuķis^c, Kaspars Kalniņš^c, Mariano Andrés Arbelo^d, Richard Degenhardt^{a,b,e}

^a DLR, Institute of Composite Structures and Adaptive Systems, Braunschweig, Germany

^b University of Bremen, Faserinstitut Bremen e.V., Bremen, Germany

^c RTU, Riga Technical University, Institute of Materials and Structures, Riga, Latvia

^d ITA, Technological Institute of Aeronautics, Department of Aeronautics, São José dos Campos, Brazil

^e PFH, Private University of Applied Sciences Göttingen, Composite Engineering, Campus Stade, Stade, Germany



ARTICLE INFO

Keywords:

Nondestructive experiments
Vibration correlation technique
Pressurized orthotropic cylindrical shells
Buckling
Imperfection-sensitive structures

ABSTRACT

Traditional buckling experiments of imperfection-sensitive structures like cylindrical shells can cause the permanent failure of the specimen. Nevertheless, an experimental campaign is crucial for validation of the design and numerical models. There is, therefore, interest in nondestructive methods to estimate the buckling load of such structures from the prebuckling stage. The vibration correlation technique allows determining the buckling load without reaching the instability point. Recently, a novel empirical vibration correlation technique based on the effects of initial imperfections on the first vibration mode demonstrated interesting results when applied to composite and metallic unstiffened cylindrical shells. In this context, this paper explores this novel approach for determining the axial buckling load of a metallic orthotropic skin-dominated cylindrical shell under internal pressure, which represents a simplified downscaled model of a launcher propellant tank. An experimental campaign consisting of buckling tests and noncontact vibration measurements for different axial load levels is conducted considering the specimen without and with three different internal pressure levels. The experimental results validate the above-mentioned vibration correlation technique for determining the axial buckling load of pressurized cylindrical shells. Moreover, finite element models are calibrated in order to evaluate the frequency variation within a broader and dense range of the axial loading leading to an assessment of the considered maximum load level and number of load steps as related to the deviation of the estimation. The results corroborate the applicability of the vibration correlation technique as a nondestructive experimental procedure to assess the axial buckling load of imperfection-sensitive orthotropic skin-dominated cylindrical shells under internal pressure.

1. Introduction

The vibration correlation technique (VCT) applied to thin-walled structures combines an initial numerical or analytical model with measured data prior to buckling to estimate the actual buckling load of the structure. In practice, the initial model concerns analytical or finite element (FE) analyses of the perfect structure to calculate the linear buckling load and the measurements consist of a sequence of vibration tests for different axial compression load levels in order to quantify the variation of the natural frequencies of vibration with the applied load. The VCT can be classified into indirect and direct methods [1]. Indirect methods determine the actual boundary conditions to update the initial model improving the estimation of the buckling load [2]. On the other

hand, direct methods consist of a curve fitting procedure relating the natural frequencies at different load levels prior to buckling to the applied axial compression load and, from this relationship, the buckling load is extrapolated [1]. General steps for applying a VCT for direct estimation of the buckling load can be established as:

1. Use the initial model to calculate the natural frequencies at zero load level and the buckling load of the perfect structure, which can be global or local buckling depending on the structure.
2. Perform a vibration test considering the unloaded structure.
3. Compare the experimental results of the natural frequencies to the calculated ones for validation of the initial boundary conditions of the numerical model.

* Corresponding author at: DLR, Institute of Composite Structures and Adaptive Systems, Braunschweig, Germany.
E-mail address: Felipe.Franzoni@dlr.de (F. Franzoni).

4. Apply the axial load stepwise and observe the reduction in the natural frequencies (up to the maximum vibration mode of interest) as the axial compression load is increased up to a specific load level, which must be below the predicted buckling load.
5. Plot the applicable VCT chart for the appropriate vibration mode.
6. Estimate the buckling load of the structure based on the VCT results.

The VCT is a straightforward nondestructive experimental procedure for beam structures. The differential equation governing the free vibration of an axially loaded simply supported column, in which the vibration and buckling modes exactly match, results in a linear relationship between the natural frequency squared and the applied load [1]:

$$f^2 + p = 1 \tag{1}$$

where f is the ratio between the loaded natural frequency $\bar{\omega}$ and the unloaded natural frequency ω , both associated with the same vibration mode, p is the ratio between the applied axial load P and the critical buckling load P_{CR} . The buckling load is associated with the applied load where the natural frequency of vibration is equal to zero; therefore, once measured frequency data is available for different compression load levels a best-fit linear relationship in the classic characteristic chart f^2 versus p can be found and extrapolated to the buckling load.

To the best of the authors' knowledge, the concept of relating applied axial load to natural frequency for estimating the buckling load is accredited to Sommerfeld at the beginning of the 20th century [3]. The author verified that the natural frequency of a clamped-free column with a variable mass at the free end decreases approaching zero as the mass was increased approaching the amount required to buckle the structure. Nevertheless, additional experimental investigations considering the VCT dated only from the 1950s, see for instance [4,5] among others. Even though the relationship between applied load and natural frequency squared deviates slightly from the linearity when other than simply supported boundary conditions are considered, the linear best-fit technique still presents good accuracy as verified in [4,6,7].

The use of VCT to directly estimate the buckling load of imperfection-sensitive structures like plates and cylindrical shells continues as an open and important research topic [8]. Although the linear relationship between applied load and frequency squared can be demonstrated for simply supported plates and cylindrical shells [9], its applicability is restricted to imperfection-insensitive structures. Lurie [4] was not able to validate the mentioned linear relationship for simply supported flat plates in the 1950s. In the 1970s, Chailleux et al. [7] succeeded in applying the linear best-fit technique considering simply supported flat plate specimens with small imperfections. More recently, Chaves-Vargas et al. [10] explored the best-fit linear relationship between the natural frequency squared and the applied load to assess the buckling load of flat carbon fiber-reinforced polymer (CFRP) stiffened plates.

Considering more imperfection-sensitive structures, as curved panels and cylindrical shells, modified VCT approaches were proposed to account for the more complex relationship between natural frequency and applied load [1]. Radhakrishnan [11] suggested tracking the vibration mode similar to the buckling mode and extrapolating the final linear path of the classic characteristic chart to the applied load axis. The author obtained exact results for tubes made of Hostaphan.

Assuming that the VCT applied to direct predictions of the buckling load of cylindrical shell structures is essentially a curve fitting procedure to the experimental results, a method based on an optimal parameter q and a linear best-fit approximation was proposed by Segal [12], as referenced in [1]. The author investigated the methodology for 35 experiments and achieved a considerable reduction in the scatter of the knock-down factors (KDF) when compared to the indirect VCT method based on Eq. (1) [1]. In addition, Plaut and Virgin [13] investigated the mentioned method through an analytical study for upper and lower

Table 1
Geometric characteristics of the Z38 structure.

Description	Symbol	Magnitude
Total height [mm]	L	1000.00
Outer best-fit radius [mm]	R	400.38
Skin's thickness [mm]	t	0.55
Stiffeners' height [mm]	H_{ST}	5.20
Stiffeners' thickness [mm]	t_{ST}	0.55
Distance between stiffeners [mm]	b	19.97

bounds characterization of the buckling load.

Souza et al. [14] and Souza and Assaid [15] proposed VCT approaches for structures presenting unstable postbuckling behavior. In Souza et al. [14] a modified characteristic chart is proposed in the form $(1 - p)^2$ versus $1 - f^4$; besides, the critical buckling load is evaluated as:

$$P_{CR} = \frac{\omega^2 P_1}{\omega^2 - \bar{\omega}_1^2} \tag{2}$$

where $(P_1, \bar{\omega}_1)$ is a measured point of the experiment. The value of $(1 - p)^2$ for $1 - f^4 = 1$ is denominated ξ^2 and it represents the square of the drop of the load-carrying capacity due to initial imperfections. The VCT estimation of the buckling load is defined in terms of ξ as:

$$P_{VCT} = P_{CR}(1 - \xi) \tag{3}$$

In Souza and Assaid [15], the authors suggested representing the classic characteristic chart by a cubic parametric curve; furthermore, the Hermite form was considered to define the parametric equations. Both methods proposed by Souza and his colleagues [14,15] were validated based on experimental results of stiffened cylindrical shells tested at Technion, which are available in [16].

Abramovich et al. [8] investigated the applicability of a VCT based on a second-order best-fit relationship of the classic characteristic chart for stringer stiffened curved panels. The VCT predictions accounting for load levels up to 50% of the buckling load of the perfect structure were reasonable; however, the authors suggested load levels near the typical sharp bend of the frequency squared versus applied load relation for improving the accuracy.

Arbelo et al. [17] proposed a novel empirical VCT modifying the work done by Souza et al. [14]. The authors suggested evaluating the second-order best-fit relationship of the results in the modified characteristic chart $(1 - p)^2$ versus $1 - f^2$. The second-order relationship is evaluated for the minimum value of the $(1 - p)^2$ axis, which is defined as ξ^2 . The actual buckling load is calculated by Eq. (3) as suggested in Souza et al. [14]. Moreover, this method relies on the effects of the initial imperfections in the vibration response of the structure and, typically, the first two or three natural frequencies can be investigated. Four experimental campaigns were performed to validate the proposed VCT in [18–21].

Arbelo et al. [18] performed tests considering three identical CFRP unstiffened cylindrical shells and the variation of the first natural frequency was tracked through the load steps. The VCT results were in good agreement with the buckling load – within 2.3% and 7.8% of deviation. Kalnins et al. [19] tested two CFRP and two metallic unstiffened cylindrical shells and good correlations were found for the first and second vibration modes, within 0–10% deviation from the buckling load. Skukis et al. [20] tested two identical CFRP unstiffened cylindrical shells. The VCT estimations based on the first vibration mode presented good correlation with the buckling load, within 4.8% and 8.4% of deviation. Furthermore, the authors performed a statistical evaluation of the VCT estimations and concluded that using load steps up to 65% of the buckling load gives a reliability close to 90%. Skukis et al. [21] tested thin-walled cylindrical shells with and without a cutout. The authors demonstrated that the method applied to first vibration mode measurements leads to good results when the failure of the specimen is governed by a global failure mode, which was observed for uncut and

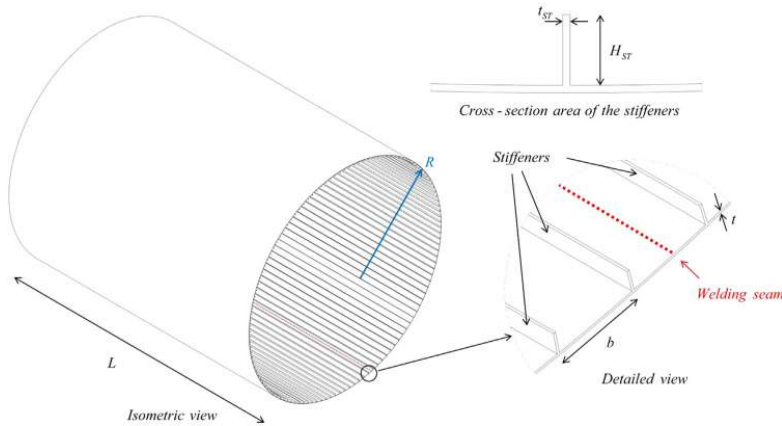


Fig. 1. Isometric view of the cylinder and detailed schematic views of the stiffeners and welding seam.

Table 2
Mechanical material properties of the aluminum alloy AL7075-T7351 [24].

Description	Symbol	Magnitude
Compressive elastic modulus [MPa]	E_C	73,084
Poisson's ratio	ν	0.33
Mass density [kg/m ³]	ρ	2796

condition, which increases the axial buckling load and reduces the destabilizing effect of initial imperfections [22]. Nevertheless, the skin-dominated orthotropic cylinder can still experience unstable buckling phenomenon; thus, the above-mentioned structures are sized as an imperfection-sensitive cylindrical shell [22]. Hence, there is interest in investigating nondestructive experimental procedures for the buckling load of such structures considering operational conditions.

Therefore, the present work explores the empirical VCT method proposed in [17] considering a metallic skin-dominated orthotropic cylindrical shell with and without internal pressure, in which the specimen and the loading condition are both representative of a real launcher vehicle's structure. Throughout the present study, an experimental campaign is proposed validating the above-mentioned method for the estimation of the axial buckling load of pressurized skin-dominated cylindrical shells. Additionally, an FE model is adjusted and considered for a thorough evaluation of the tendency of the VCT estimated buckling load, which provides an insight on the suitable number of load steps and the maximum axial load level to be considered in the experiment. In addition, the development of non-destructive experimental procedures for imperfection-sensitive structures consists of an important step in the implementation of robust design guidelines like in the just finished European Union project "New Robust Design Guideline for Imperfection-Sensitive Composite Launcher Structures" (DESCICOS) [23].

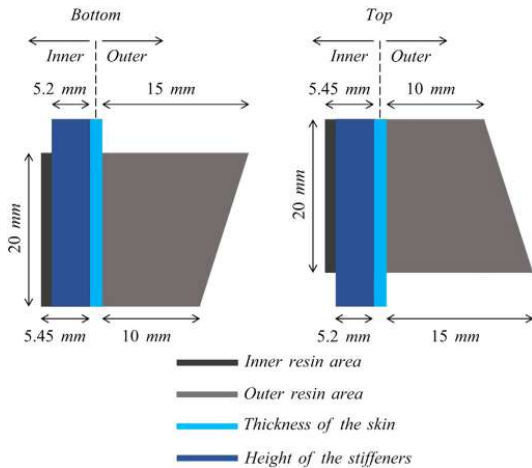


Fig. 2. Cross-section of the resin areas.

cut structures considering a reinforcement in the cut region, loaded up to at least 60% of the buckling load. On the other hand, the authors concluded that the VCT method proposed in [17] is not applicable when a local failure mode governs the failure behavior of the structure.

In this context, the above-mentioned VCT is a promising method for assessing the buckling load of imperfection-sensitive cylindrical shell structures, like thin-walled skin-dominated orthotropic shells for aerospace applications, through a nondestructive experiment. In particular, for launch vehicles applications, the operational load envelope imposes high compressive loads, which causes buckling to be one of the main sizing criteria in the development phase of the structural design. In addition to the compressive load, there is usually the pressurized

2. Test structure

The research concerns a metallic orthotropic skin-dominated cylindrical shell designed for elastic buckling named Z38 made of aluminum alloy AL7075-T7351. The specimen consists of a milled panel with 126 closely spaced integral blade stiffeners and, as usual for metallic cylindrical shells manufactured for space applications, the joint edge of the cylinder was welded using an electron beam based process. Table 1 describes and presents the magnitudes of the main nominal geometric characteristics of the cylinder Z38 while Fig. 1 shows an isometric view of the structure and detailed schematic views of the stringers and the welding seam.

Table 2 presents the mechanical material properties of the aluminum alloy AL7075-T7351, obtained from Metallic Materials Properties Development and Standardization (MMPDS) [24].

Considering the boundary conditions, the cylindrical shell was potted into circular steel rings with 20 mm in height using an epoxy resin. The inner and outer rings provide rectangular and trapezoidal cross-sections for the resin areas, respectively; Fig. 2 presents views of



(a) Overview of the potted cylindrical shell. (b) Detail of the upper steel ring.

Fig. 3. Cylinder Z38 potted into the steel rings.

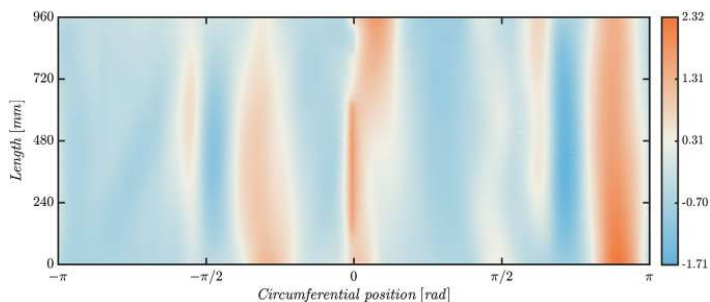


Fig. 4. Measured initial imperfection signature.



Fig. 5. Cylinder Z38 positioned in the test facility.

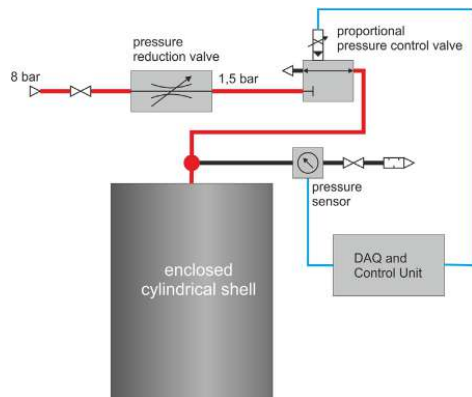


Fig. 6. Scheme representation of the pressure control system.

the bottom and top cross-sections of the resin areas and their main dimensions and Fig. 3 shows an overview of the cylinder potted into the steel rings (a) and a detailed view of the upper steel ring (b).

Prior to the experimental campaign, a digital image correlation (DIC) system based on photogrammetry, named ATOS, was used for measuring the initial geometric imperfections of the potted cylindrical shell. Through this procedure, the outer surface of the shell was

measured and its deviation based on the ideal best-fit geometry stored, as presented in Fig. 4 (in mm). These measurements were used to update the initial position of the nodes in the nonlinear FE models.

3. Experimental campaign

This section provides a description of the procedures executed

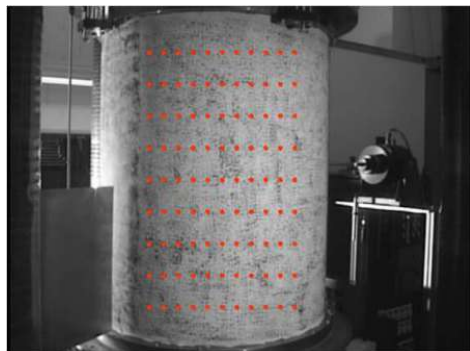


Fig. 7. Grid of measured vibration points.

during the test campaign, as well, it presents the experimental results for the buckling and vibration tests.

3.1. Test procedure

The experimental campaign was performed in a buckling test facility at DLR Institute of Composite Structures and Adaptive Systems. The test rig consists of an axially supported top plate and a lower drive plate activated by a servo controller hydraulic cylinder. Between the top plate and the test specimen, a load distributor was placed to ensure an equal force distribution within three load cells, which were used for measuring the applied load. Moreover, a thin layer of epoxy concrete, consisting of epoxy reinforced with a mixture of sand and quartz powder, was added to the interface between the lower drive plate and the specimen in order to overcome any further misalignment and to enclose the cylindrical shell volume for applying the internal pressure. More details of the mentioned test facility and its established procedures for buckling tests are published in [25,26]. Fig. 5 presents an overview of the cylinder Z38 positioned in the test facility.

Considering the loading procedure during the vibration tests, first, the specimen was loaded with internal pressure, which was applied at a constant rate of 0.03 bar/min from zero to the desired magnitude. A closed-loop control was used within the pressure system to preserve the applied pressure constant during the axial loading, see the scheme represented in Fig. 6. In sequence, the specimen was loaded in compression using displacement control at a constant velocity of 0.12 mm/min. Once the desired load level was reached, the movable lower drive of the test facility is held in place so the vibration test can be started. For the buckling tests, the displacement control was applied until buckling takes place and the movable lower drive was held on the initial postbuckling load so the surface displacements were measured.

Additionally, during the axial loading of the cylindrical shell, a

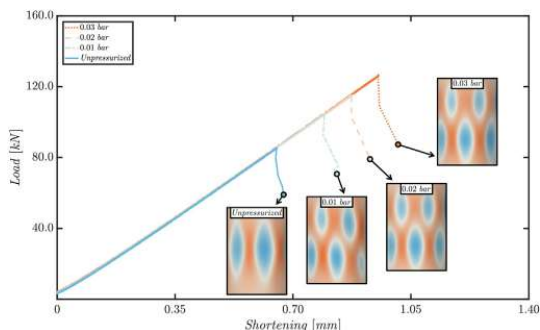


Fig. 8. Experimental load-shortening curves and initial postbuckling displacements.

second DIC system, named ARAMIS, was used for recording the in-plane deformations and out-of-plane displacements. Prior to the test, the surface of the cylindrical shell was painted with a dotted pattern. Two pairs of cameras were available during the test campaign, the first pair was positioned around the welding seam and the second was positioned where the buckling was expected to initiate. The DIC results were postprocessed and qualitatively compared with the FE model.

Concerning the vibration tests for VCT purposes, the cylindrical shell was excited with a random signal using a mechanical shaker while a laser scanning vibrometer was used for assessing the modal parameters for the entire signal spectrum. The laser scanning vibrometer was positioned covering a segment of the cylindrical shell surface defined by an arc length of 459 mm and a height of 768 mm considering a mesh of 9 per 11 measured points, as shown in Fig. 7. For each measured point at least three measurements were taken for averaging the signal; moreover, it was assumed a frequency band from 80 Hz to 200 Hz considering 480 spectral lines resulting in a frequency resolution of 0.25 Hz.

3.2. Experimental results

Four compression tests were performed, one unpressurized and three pressurized with different internal pressure levels. The internal pressure levels were chosen based on FE analyses aiming to achieve a substantial increase in the buckling load within the elastic range. Although the specimen was sized for elastic buckling, the test campaign considered all the VCT measurements performed prior to the buckling tests; moreover, before and after each buckling test, measurements of the surface displacements were taken and compared to ensure no plastic deformations. At least one buckling test per internal pressure level was conducted.

Table 3 shows the buckling load $P_{EXP,(m,n)}$ and the first natural

Table 3
Experimental results of the buckling and vibration tests.

Unpressurized		$P_{INT}: 0.01$ [bar]		$P_{INT}: 0.02$ [bar]		$P_{INT}: 0.03$ [bar]	
$P_{EXP,(1,8)}: 86.53$ [kN]		$P_{EXP,(2,10)}: 104.36$ [kN]		$P_{EXP,(2,10)}: 116.80$ [kN]		$P_{EXP,(2,10)}: 127.86$ [kN]	
P_i [kN]	$F_{1,(1,9)}$ [Hz]	P_i [kN]	$F_{1,(1,9)}$ [Hz]	P_i [kN]	$F_{1,(1,9)}$ [Hz]	P_i [kN]	$F_{1,(1,9)}$ [Hz]
14.59	93.50	16.30	105.50	19.24	116.00	20.42	124.25
36.27	86.00	42.84	98.00	46.96	108.50	50.86	117.00
44.29	83.00	65.05	90.50	65.30	103.25	70.54	111.75
62.05	75.50	70.11	88.75	77.38	99.25	85.01	108.00
66.36	73.50	74.18	87.25	82.59	97.25	88.45	106.75
68.04	72.25	76.46	86.50	85.45	96.75	93.43	105.75
70.33	71.25	83.37	83.25	88.47	95.75	96.83	104.25
72.73	69.00	87.30	81.50	92.60	94.50	100.80	103.50

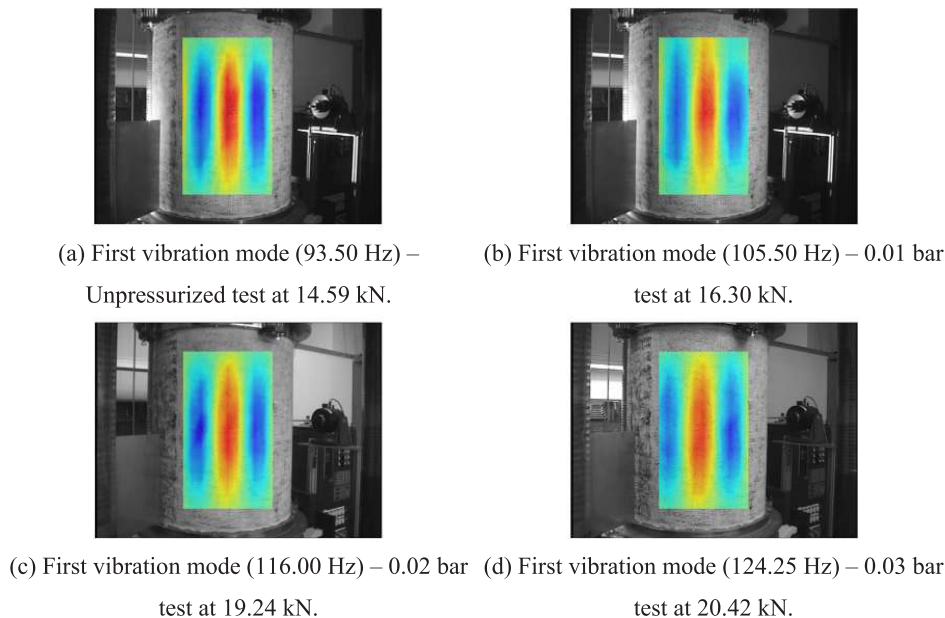


Fig. 9. First vibration modes measured at the first compressive load step from Table 3.

Table 4
Comparison between DLR and RTU vibration tests.

Unpressurized			P_{INT} : 0.03 [bar]		
P_i [kN]	$\bar{F}_{1,(1,9),DLR}$ [Hz]	$\bar{F}_{1,(1,9),RTU}$ [Hz]	P_i [kN]	$\bar{F}_{1,(1,9),DLR}$ [Hz]	$\bar{F}_{1,(1,9),RTU}$ [Hz]
4.62	96.75	96.75	6.10	128.00	128.00
32.13	87.50	87.50	77.38	110.25	110.00
57.99	77.25	77.25	85.01	108.00	108.00
62.05	75.50	75.25	88.45	106.75	106.75
66.36	73.50	73.50	93.43	105.75	105.75
70.33	71.25	72.75	96.83	104.25	104.25

frequency $\bar{F}_{1,(m,n)}$ for each compressive load step P_i considering all the internal pressure levels P_{INT} , where m is the number of axial half-waves and n the number of circumferential waves associated with the corresponded buckling or vibration mode; these results were extrapolated from the measured data.

Fig. 8 presents the load-shortening curves and the shape of the postbuckling displacements for each internal pressure level.

From Fig. 8, one may notice that there is a shift between the origin of the chart and the initial load level, this effect is inherent to the experimental procedure once for low load levels there is clearance between the edge of the cylinder and the surface of the steel rings.

Fig. 9 presents the first vibration mode shape measured at the first compressive load step: 14.59, 16.30, 19.24, and 20.42 kN for unpressurized, 0.01, 0.02, and 0.03 bar, respectively.

3.3. Additional measurements

Riga Technical University (RTU) performed a set of independent measurements of the vibrations of the cylindrical shell for 12 load steps within the unpressurized and 0.03 bar tests. This procedure considered a second laser scanning vibrometer positioned in a different location of the cylindrical shell, which was closer to the mechanical shaker. A different approach based on a denser mesh consisted of 214 measured

points and one vibration measurement per point was employed. The measurements considered a frequency band from 20 Hz to 200 Hz and 720 spectral lines resulting in a frequency resolution of 0.25 Hz. Table 4 compares the DLR and RTU measurements for the first natural frequency $\bar{F}_{1,(m,n)}$ considering chosen compressive load levels P_i for the unpressurized and 0.03 bar of P_{INT} tests.

From Table 4, it can be noticed that both measurements have an excellent correlation, once only three pairs of measurements are slightly different, as highlighted. This procedure corroborated both strategies as equivalent and hereafter the results from DLR are considered for the VCT assessment.

4. Finite element analyses

Finite element analyses were performed using the commercial FE solver Abaqus Standard 6.16[®]. Based on previous investigations [27–29], the Newton-Raphson iterative procedure with artificial damping stabilization was used as the nonlinear solver for the axial loading step. When considered, the nonlinear preload step for applying internal pressure was based on the Newton-Raphson solver without artificial damping. For the eigenvalues problems, i.e. linear buckling and free vibration analysis, the default Lanczos solver was employed.

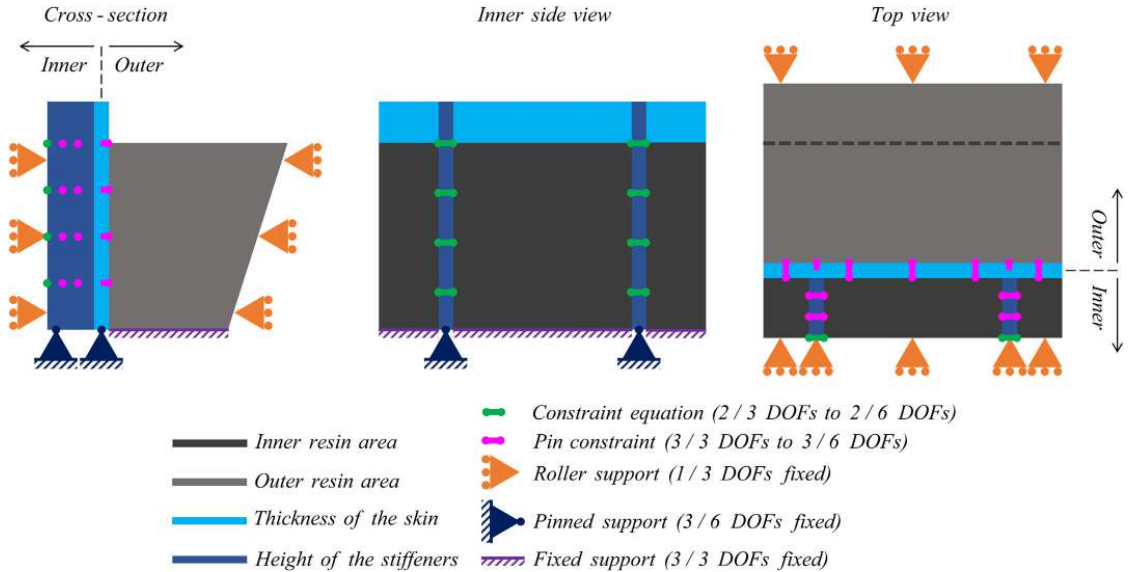


Fig. 10. Schematic views of the boundary conditions of the bottom resin areas as defined in the FE models.

Table 5
Summary of the parameters of the FE models.

Solver	Standard
Shell element type	S4R
Solid element type	C3D8R
Number of nodes	53,396
Elements around the cylinder's circumference	256
Elements through the stiffeners' height	2
Elements through the resin areas' height	3

4.1. Detailed boundary conditions and definition of the finite element mesh

The skin and stiffeners of the cylindrical shell were meshed considering linear quadrilateral thin-shell elements with 4 nodes, 6 degrees of freedom per node and reduced integration; labeled S4R elements in Abaqus® library. Detailed boundary conditions were considered, thus,

Table 6
Linear buckling load and unloaded first natural frequency as related to the internal pressure level.

P_{INT} [bar]	$P_{CR}(m, n)$ [kN]	$F_{1,(1,9)}$ [Hz]
Unpressurized	109.10 (2,12)	97.75
0.01	120.70 (3,14)	111.76
0.02	130.35 (3,13)	122.72
0.03	139.35 (3,13)	131.57

the FE models are based on the total length of the cylinder and the resin potting regions are represented by 3D elements. The solid and shell meshes are coincident within the coordinate perpendicular to the regarded interface and the connections between them were modeled by constraint equations. This approach has been validated for CFRP unstiffened cylindrical shells [28,29] and, it was here extended for the



(a) Isometric view of the FE model.

(b) Schematic detailed view of the cross-section area of the shell elements.

Fig. 11. Isometric view of the FE mesh and schematic detailed view of the geometry representing the cross-section area of the shell elements.

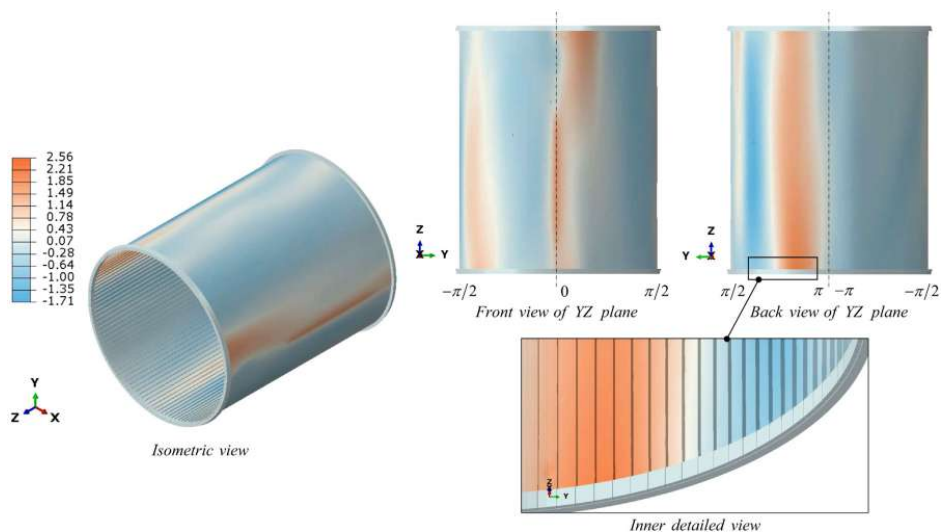


Fig. 12. Applied stress-free initial geometric imperfections.

Table 7
Nonlinear solver parameters.

Damping factor	10^{-7}
Initial increment	0.001
Minimum increment	10^{-6}
Maximum increment	0.001
Maximum number of increments	10,000

case of a stiffened skin-dominated structure. Moreover, the FE models consider an open cylinder, therefore, only circumferential prestresses were considered and there was no relaxation of the axially applied load in the model, which is slightly different from the experimental condition – about 1.5 kN for the worst case (0.03 bar).

Fig. 10 presents schematic views of the boundary conditions of the bottom resin areas as considered in the FE analyses, which were as well employed in the top resin areas. It is important to mention that the 0.25 mm difference between the thickness of the inner resin rings and the height of the stiffeners, as can be seen in Fig. 1, was not considered.

Based on convergence studies, the FE models consider 256 elements over the circumference (two elements between stiffeners for most of the bays), two elements within the stiffeners’ height and three elements through the region of the detailed boundary conditions. A finer mesh (4 elements between stiffeners) was considered in the bay that contains the welding seam aiming a better representation of the locally scattered initial imperfections and in the welding seam opposite bay for keeping the model’s symmetry. Elements in other directions were chosen automatically considering a global size of 13.2 mm. Thus, the FE models consider 39,624 shell elements (S4R) associated with 40,132 nodes and 4608 linear hexahedral elements (C3D8R) associated with 13,264 nodes. In addition, the FE mesh considers the inner surface of the cylinder as a reference, hence, the elements associated with the skin consider offset avoiding a superposition of the skin and stiffeners cross-section areas.

Table 5 presents a summary of the parameters of the FE models while Fig. 11 shows an isometric view of the FE mesh and a schematic detailed view of the geometry representing the shell elements cross-section area in the skin and stiffeners region.

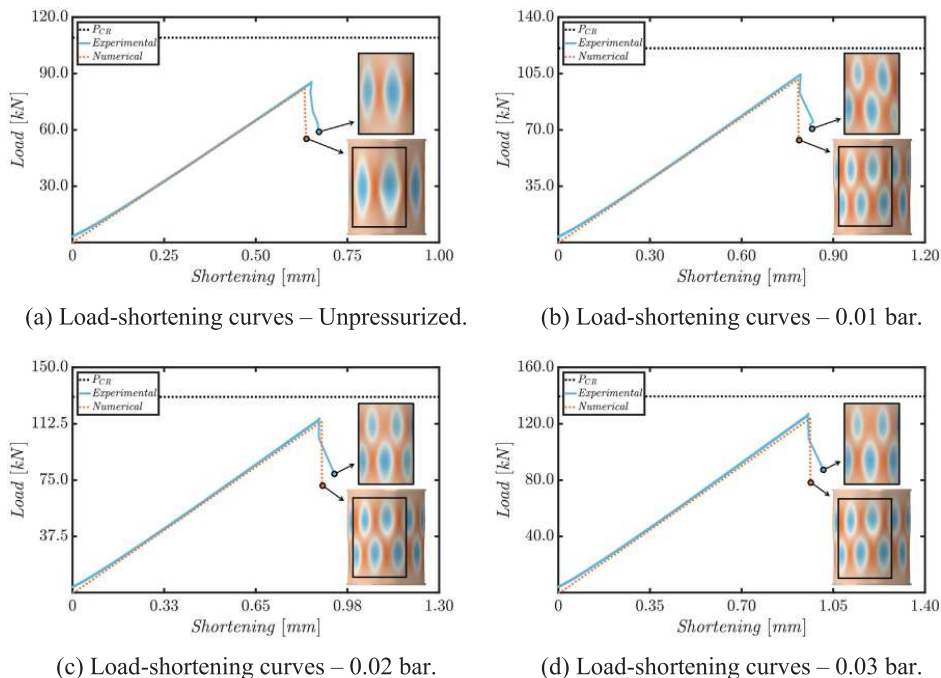
4.2. Definition of the finite element models and numerical results

In order to assess the VCT proposed by Arbelo [17], two FE models were defined. First, a reference model based on the nominal geometry of the cylindrical shell with or without internal pressure applied to the inner surface of the skin of the cylinder was considered for two eigenvalue problems: linear buckling and free vibrations analyses. These results are used as the reference for the numerical and the experimental evaluation of the VCT. Table 6 summarizes the linear buckling load P_{CR} and the unloaded first natural frequency $F_{1,(m,n)}$ as related to the internal pressure level P_{INT} . Furthermore, the numerical results for the pair (m, n) are given in front of the respective magnitude of the linear buckling mode.

As the measured initial imperfection signature was available only for the outer surface of the cylinder, a linear static step for estimating consistent stress-free initial geometric imperfections for the stiffeners of the specimen was defined. Through this step, a python script calculates new positions for each node associated with the elements of the skin of the cylinder based on the measured signature. The interpolated initial positions were applied as radial enforced displacement in the skin of the cylinder in the linear static step generating consistent deformations for the stiffeners. The results were used to update the initial position of the FE mesh considered in the nonlinear static analyses. The described procedure uses the same inverse-weighted interpolation rule presented in [27] for the 5 closest measured points. Fig. 12 depicts detailed views of the deformed cylindrical shell considering the applied stress-free initial geometric imperfections – the scale is defined in terms of the radial displacements (in mm).

The second FE model was defined based on a nonlinear static step considering initial geometric imperfections with or without internal pressure applied to the inner surface of the skin of the cylinder. Uniform distributed displacement was applied in the axial direction on the top edge of the cylindrical shell and, for selected load levels, additional free vibration analyses were defined. Thus, the main purpose of this model is to assess the static response and the variation of the natural frequencies of vibration during axial loading of the cylindrical shell. These results are employed in the numerical evaluation of the VCT method. Table 7 shows the main parameters considered during the nonlinear static analyses for axial loading.

Fig. 13 presents a comparison between the numerical and



(a) Load-shortening curves – Unpressurized.

(b) Load-shortening curves – 0.01 bar.

(c) Load-shortening curves – 0.02 bar.

(d) Load-shortening curves – 0.03 bar.

Fig. 13. Comparison between the numerical and experimental load-shortening curves and initial postbuckling displacements.

Table 8
Comparison between the numerical and experimental buckling loads.

P_{INT} [bar]	P_{EXP} (m, n) [kN]	γ_{EXP}	P_{NUM} (m, n) [kN]	γ_{NUM}	δ [%]
Unpressurized	86.53 (1,8)	0.79	81.86 (1,8)	0.75	- 5.40
0.01	104.36 (2,10)	0.86	101.27 (2,10)	0.84	- 2.96
0.02	116.80 (2,10)	0.90	113.77 (2,10)	0.87	- 2.59
0.03	127.86 (2,10)	0.92	123.56 (2,10)	0.89	- 3.36

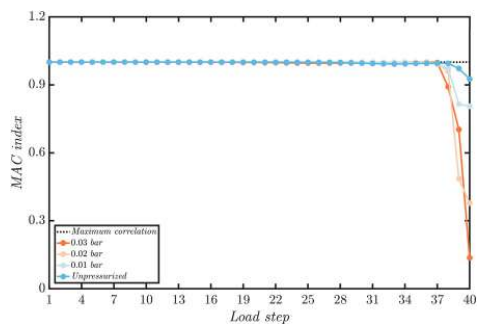


Fig. 14. MAC index variation for the first vibration mode.

experimental load-shortening curves and initial postbuckling displacements while Table 8 summarizes the deviations δ between the experimental P_{EXP} and numerical P_{NUM} results of the buckling loads (related to P_{EXP} from Table 3) with the respective pair (m, n) in front of the magnitude. Moreover, the KDF are defined based on the linear buckling loads from Table 6 for the corresponding experimental and nonlinear buckling loads, named as γ_{EXP} and γ_{NUM} , respectively.

Analyzing Fig. 13, one may notice that the apparent stiffness of the cylinder is being correctly represented in the FE models. Moreover, as shown in Table 8, the deviations associated with the results considering the internal pressure condition are smaller when compared to the unpressurized condition; this can be related to a smaller influence of the initial imperfection on pressurized cylindrical shells [22]. Given these points, the numerical results can be considered in good agreement with the experimental ones as the FE models consider an estimation of initial imperfections for the stiffeners' nodes, do not address loading misalignments and, consider typical material properties.

Concerning the numerical frequency variation during axial loading, 40 evenly spaced load steps up to 98% of the nonlinear buckling load P_{NUM} were selected for assessing the first 10 natural frequencies up to the vicinity of buckling. The free vibration results were analyzed in Matlab® through an algorithm based on the modal assurance criterion (MAC) to identify the variation of each vibration mode during axial loading; the MAC index performs a comparison between two vectors of the same length and the index returns a value close to one if a linear relationship between the two vectors exists and near zero if they are linearly independent [30].

In this script, the MAC index is calculated between each vibration mode in the current load step and all the vibration modes of the next load step, the greater MAC index is assumed to be associated with the same vibration mode in the next load step so the process starts again until the final load step is analyzed. Furthermore, a figure is generated containing top views of the tracked vibration mode associated with each load step consistent with the MAC-based sequence. Fig. 14 presents the MAC index variation for the first vibration mode considering the internal pressure levels.

From Fig. 14, it is possible to conclude that the first vibration mode for the unpressurized cylindrical shell presents a smooth transition from one load step to the other until the vicinity of buckling. On the other hand, for the pressurized cylinders, the first vibration mode presents a

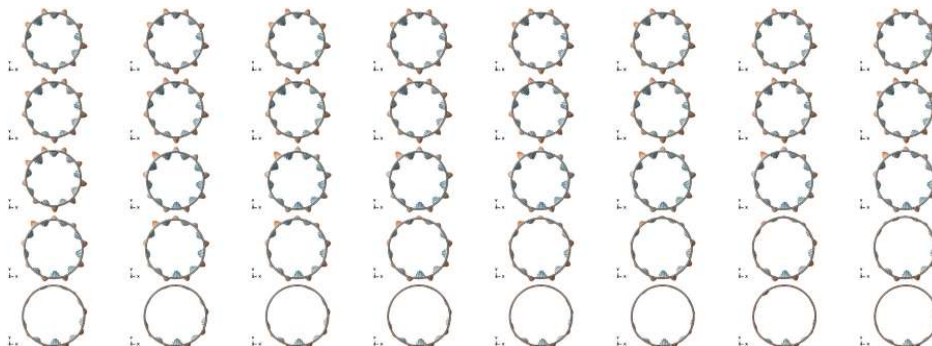


Fig. 15. First vibration mode variation during axial loading – Unpressurized.

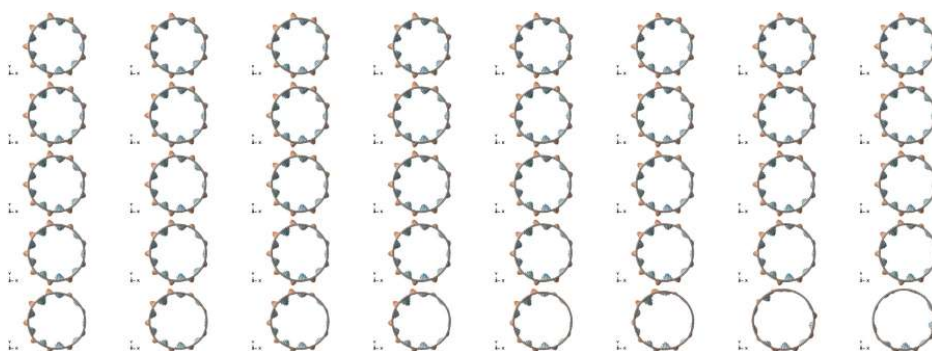


Fig. 16. First vibration mode variation during axial loading – 0.01 bar.

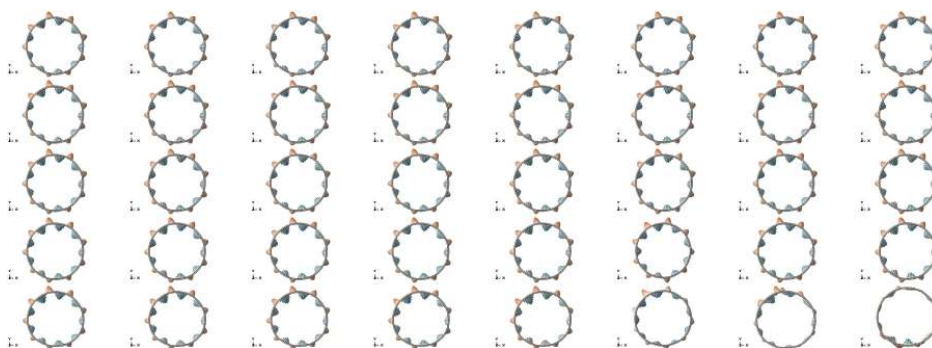


Fig. 17. First vibration mode variation during axial loading – 0.02 bar.

suddenly lost of correlation with relation to the vibration modes from the previous load step. For all pressure levels, this occurred between the load steps 38 and 39, which are corresponding to a compressive load between 92.6% and 95.1% of the nonlinear buckling load P_{NUM} , respectively, indicating that a significant change in the vibration modes has happened in between these increments. Figs. 15–18 show top views of the first vibration modes during axial loading consistent with the MAC index variation ascending from left to right and top to bottom.

From Figs. 15–18, one may visualize the effects of the initial imperfections in the first vibration mode of the cylindrical shell as the compressive load is increased for all internal pressure levels. Furthermore, the results corroborate the applicability of the MAC index for the

proper identification of the vibration mode variation with axially loading up to the vicinity of buckling.

5. Validation of the vibration correlation technique

Although the method proposed in [17] can be considered for the first natural frequencies of the cylindrical shell, as presented in [19], for the specimen herein studied, the numerical and experimental estimations based on the first natural frequency are in better agreement with the respective numerical and experimental buckling loads. Thus, the following steps are considered for applying the VCT:

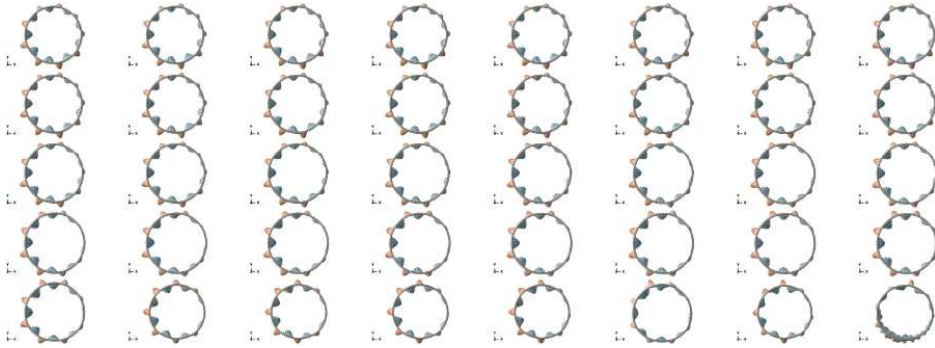


Fig. 18. First vibration mode variation during axial loading – 0.03 bar.

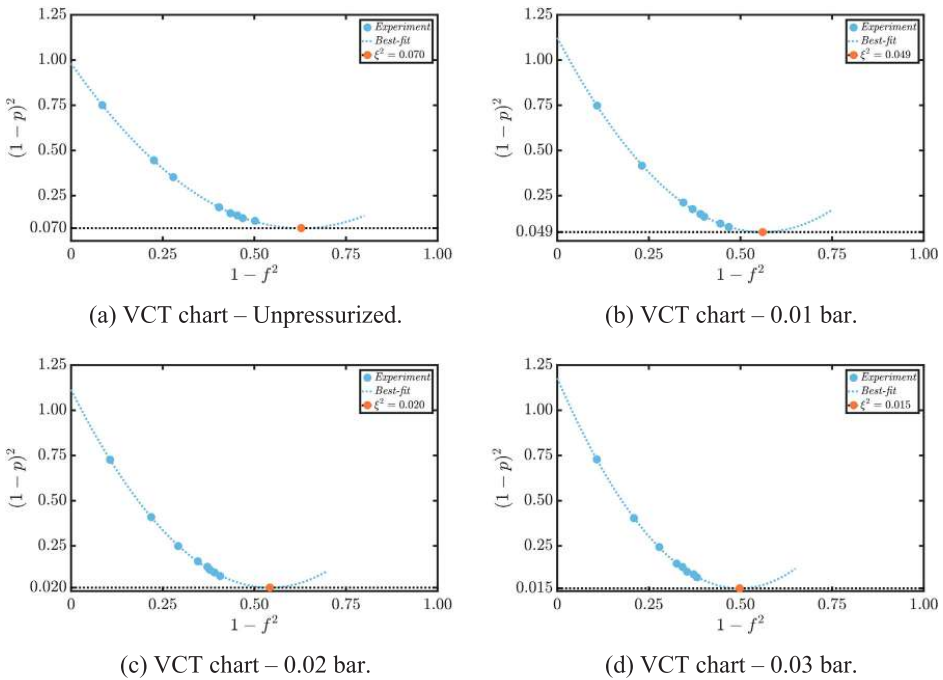


Fig. 19. Arbelo's VCT applied to the experimental results.

Table 9
VCT applied to the buckling load estimation.

P_{INT} [bar]	P_{MAX} [%]	P_{EXP} [kN]	$P_{VCT-EXP}$ [kN]	δ [%]
Unpressurized	66.66	86.53	80.14	- 7.39
0.01	72.33	104.36	93.95	- 9.98
0.02	71.04	116.80	112.09	- 4.03
0.03	72.34	127.86	122.00	- 4.61

1. Calculate the critical buckling load and the first natural frequency of the perfect structure. These are reference values for the experimental and numerical evaluations.
2. Track the first natural frequency during axial loading. This step was completed via FE models and noncontact vibration tests for the numerical and experimental evaluations, respectively.

3. Plot the charts $(1 - p)^2$ versus $1 - f^2$, where p is the ratio of applied axial load P and the critical buckling load P_{CR} and f is the ratio of the first natural frequency at P_1 load level F_1 and the first natural frequency of the unloaded structure F_1 .
4. Find the second-order best-fit relationship between $(1 - p)^2$ and $1 - f^2$ and minimize the quadratic equation for evaluating the square of the drop of the load-carrying capacity ξ^2 .
5. Estimate the buckling load of the structure using ξ as proposed by Souza [14] and herein presented in Eq. (3).

5.1. Vibration correlation technique applied to the experimental results

The evaluation of the VCT proposed in [17] is carried out taking into account the experimental results presented in Table 3. Fig. 19 depicts the modified characteristic chart $(1 - p)^2$ versus $1 - f^2$ for each

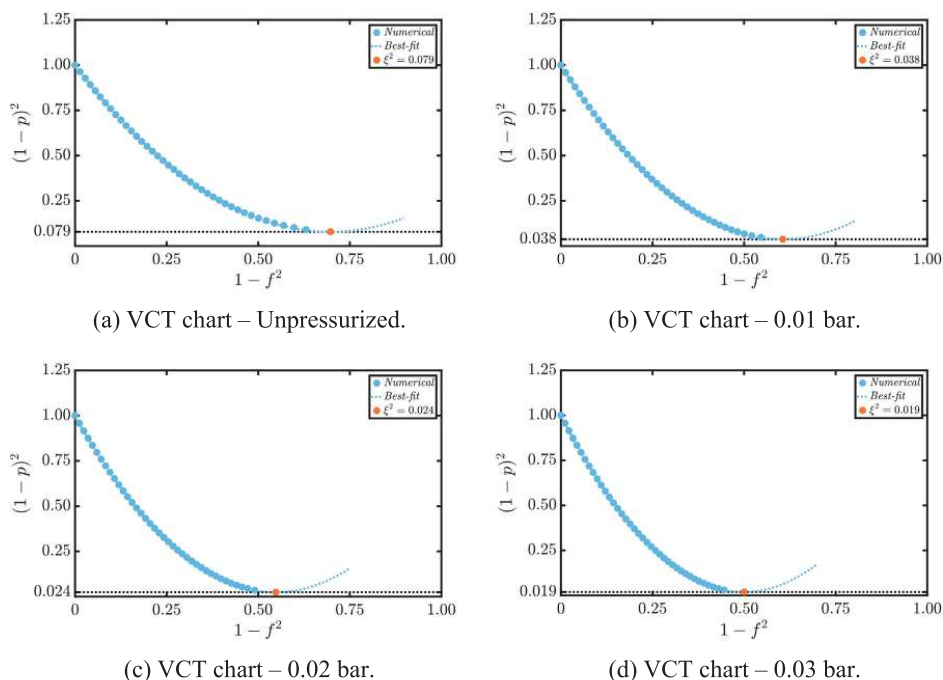


Fig. 20. Arbelo's VCT applied to the numerical results.

Table 10
VCT applied to the nonlinear buckling load estimation.

P_{INT} [bar]	P_{MAX} [%]	P_{NUM} [kN]	$P_{VCT-NUM}$ [kN]	δ [%]
Unpressurized	73.53	81.86	78.43	- 4.19
0.01	82.22	101.27	97.30	- 3.92
0.02	85.53	113.77	110.00	- 3.32
0.03	86.90	123.56	119.97	- 2.91

internal pressure level; moreover, the second-order best-fit adjusted curves and the respective minimum value of the $(1 - p)^2$ axis, regarded as ξ^2 , are highlighted in the chart.

From Fig. 19, one may notice that the second-order relationship holds for the variation of the natural frequency associated with the first vibration mode. Moreover, the ξ^2 estimations are decreasing as the internal pressure level is increased, which is an expected result once greater values of the KDF are expected for greater internal pressure levels. Summarizing the results, Table 9 presents a comparison between the buckling load P_{EXP} and the VCT estimations $P_{VCT-EXP}$ with the respective deviations δ (presented in percentage of the correspondent magnitude of P_{EXP}) and maximum applied load level P_{MAX} (presented in percentage of the linear buckling load P_{CR}).

As shown in Table 9, the predictions of the VCT method are in good agreement with the respective experimental results, within 4.61% and 9.98% in deviation magnitude; moreover, the results are conservative, once the estimations are smaller than the correspondent experimental buckling load. Additionally, one may notice that the smaller deviations are associated with the pressurized tests, which present greater values of the KDF - 0.02 and 0.03 bar of internal pressure. Furthermore, the maximum applied load level is 72.34% of the linear buckling load for 0.03 bar of internal pressure, therefore, the method has demonstrated to be truly nondestructive.

5.2. Vibration correlation technique applied to the numerical results

The FE models results are considered for a numerical assessment of the VCT as proposed in [17] for a greater number of load steps up to 98% of the nonlinear buckling load. Fig. 20 presents the modified characteristic chart $(1 - p)^2$ versus $1 - f^2$ for each internal pressure level, in which the second-order best-fit adjusted curves and the respective ξ^2 are highlighted. For all internal pressure levels, the minimum deviation is achieved considering all the load steps up to 98% of the nonlinear buckling load P_{NUM} .

From Fig. 20, the second-order relationship holds for all 40 load steps until the vicinity of the buckling phenomenon. Similar to the experimental results, the estimations of ξ^2 are decreasing as the internal pressure level is increased. In addition, Table 10 presents a comparison between the nonlinear buckling load P_{NUM} and the VCT estimations $P_{VCT-NUM}$ with the respective deviations δ (related to the correspondent P_{NUM}) and maximum applied load level P_{MAX} (presented in percentage of the linear buckling load P_{CR}).

Analyzing the results from Table 10 and comparing them with the predictions from Table 9, there is a smaller deviation between the VCT predicted buckling load and the respective nonlinear buckling load for all the internal pressure levels, this can be associated with the greater number of load steps as well with the greater maximum load levels. Once more, all the VCT predictions are conservative and present a good correlation to the respective nonlinear buckling load and, similar to the experimental predictions, the deviations are smaller for greater values of the KDF.

A priori, the number of load steps and the maximum load level needed to achieve a good approximation of the buckling load using VCT are unknown; therefore, one can evaluate the convergence of the method to support the planning of the test. In this paper, a numerical study is proposed increasing simultaneously the number of load steps and the maximum load level to assess the convergence of the VCT

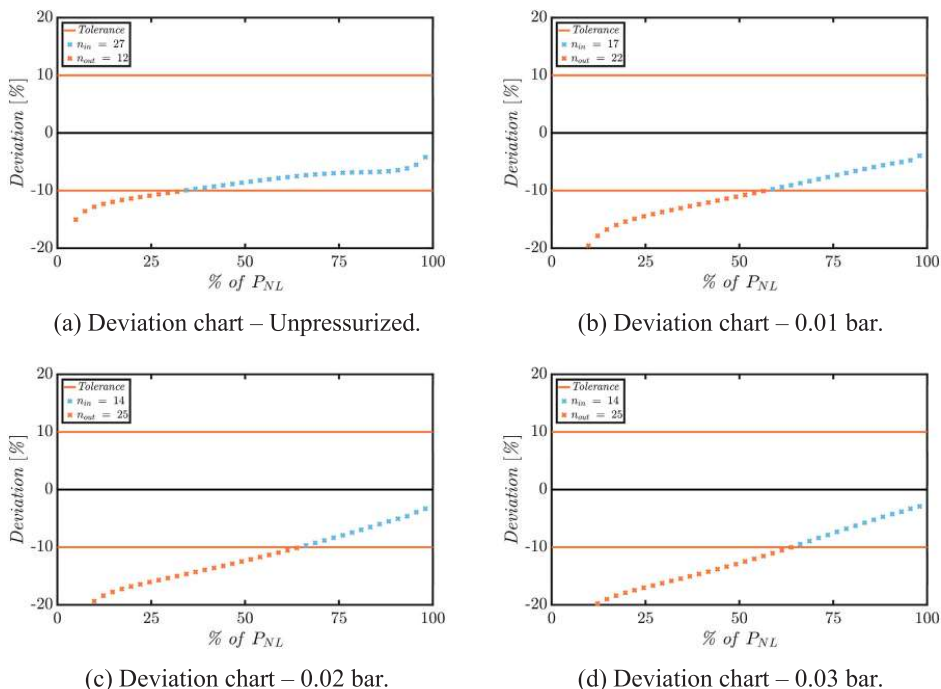


Fig. 21. Variation of the deviation of the VCT estimation related to the maximum load step.

method. Thus, Fig. 21 depicts the deviation of the VCT estimation as a function of the maximum load level considered; besides, a tolerance of 10% in magnitude of the deviation is kept as a reference and the number of estimations within the tolerance is highlighted.

Analyzing Fig. 21, one may conclude that the deviation is decreasing as the maximum load level and the number of load steps considered are increased simultaneously. Additionally, it is noteworthy that the predictions are conservative as the estimations are always associated with negative values of the deviation. Furthermore, greater internal pressure levels, which are associated with greater values of the KDF, increase the load level required for an estimation within the defined tolerance. To conclude, such results, if available before the VCT test campaign, could help determining the maximum load level and the number of load steps considered during the experimental campaign.

6. Final remarks

Throughout this paper, the empirical VCT method proposed in [17] is verified as a nondestructive experimental procedure for the estimation of the axial buckling load considering a pressurized orthotropic skin-dominated cylindrical shell. The specimen, a simplified down-scaled model of a launcher propellant tank, was manufactured considering standard procedures for aerospace applications. An experimental campaign was proposed for the corroboration of the methodology, in which buckling and noncontact vibration tests were performed. As well, a numerical investigation based on FE models is proposed for evaluating the variation of the natural frequency up to the vicinity of buckling allowing a study of the convergence of the VCT method as the number of load steps and the considered maximum load level are increased simultaneously.

During the experimental campaign, the first vibration mode was measured for 8 axial load steps considering three internal pressure

levels and the unpressurized condition. The VCT estimations presented a good correlation when compared to their respective experimental result for the buckling load, once the deviations are within 4.03% and 9.98%. Moreover, the method provided better estimations of the buckling load for the tests associated with greater values of the KDF. To conclude, the VCT herein applied is a nondestructive experimental procedure once the maximum axial load level considered during the vibration tests is 72.34% of the linear buckling load for the test considering 0.03 bar of internal pressure.

Considering the numerical assessment, techniques for including measured initial geometric imperfections and detailed boundary conditions in the FE model previously validated for unstiffened cylindrical shells were extended for the case of stiffened cylindrical shells. The nonlinear buckling load is within 2.96% and 5.40% deviation of the experimental results of the buckling load. Moreover, the numerical vibration modes and natural frequencies results were analyzed through an algorithm based on the MAC index. This procedure allows a high density of load steps to be considered resulting in a good understanding of the variation of the natural frequencies and vibration modes as related to the axial loading. The VCT method is employed for a numerical assessment achieving a good correlation and a conservative convergence when compared to the nonlinear buckling load. Moreover, the internal pressure level increases the load level required for an estimation within the defined tolerance.

The numerical study concludes that the VCT method applied to the test specimen herein evaluated provides conservative results and show a decreasing deviation from the nonlinear buckling load when the number of load steps and the maximum load level are both simultaneously increased. These results could be reproduced prior to the planning of a VCT test helping to define the maximum applied axial load level and the number of load steps needed for a good estimation of the buckling load.

Currently, the authors are addressing another experimental campaign to extend the VCT methodology for composite unstiffened cylindrical shells made of thin-ply laminates and considering in-plane imperfections.

Acknowledgments

The research leading to these results has received funding from the European Space Agency (ESA), Contract number 4000119184/17/NL/MH/GM. All support is gratefully acknowledged. The information in this paper reflects only the authors' views and the European Space Agency is not liable for any use that may be made of the information contained therein.

References

- [1] J. Singer, J. Arbocz, T. Weller, *Buckling Experiments: Experimental Methods in Buckling of Thin-Walled Structures, Shells, Built-up Structures, Composites and Additional Topics Vols. 2* John Wiley & Sons, New York, 2002.
- [2] J. Singer, H. Abramovich, *Vibration correlation techniques for definition of practical boundary conditions in stiffened shells*, *AIAA J.* 17 (7) (1979) 762–769.
- [3] A. Sommerfeld, *Eine einfache Vorrichtung zur Veranschaulichung des Knick-ungsvorganges*, *Z. Des. Ver. Dtsch. Ing.* 49 (1905) 1320–1323.
- [4] H. Lurie, *Lateral vibrations as related to structural stability*, *ASME J. Appl. Mech.* 19 (2) (1952) 195–204.
- [5] E.E. Johnson, B.F. Goldhammer, *The determination of the critical load of a column or stiffened panel in compression by the vibration method*, *Proc. Soc. Exp. Stress Anal.* 11 (1) (1953) 221–232.
- [6] D. Burgreen, *End-fixity effect on vibration and instability*, *Trans. Am. Soc. Civil. Eng.* 126 (1) (1961) 1058–1073.
- [7] A. Chailleux, Y. Hans, G. Verchery, *Experimental study of the buckling of laminated composite columns and plates*, *Int. J. Mech. Sci.* 17 (1975) 489–498.
- [8] H. Abramovich, D. Govich, A. Grunwald, *Buckling prediction of panels using the vibration correlation technique*, *Prog. Aerosp. Sci.* 78 (2015) 62–73.
- [9] L. Virgin, *Vibration of Axially Loaded Structures*, Cambridge University Press, Cambridge, 2007.
- [10] M. Chaves-Vargas, A. Dafnis, H.-G. Reimerdes, K.-U. Schröder, *Modal parameter identification of a compression-loaded CFRP stiffened plate and correlation with its buckling behaviour*, *Prog. Aerosp. Sci.* 78 (2015) 39–49.
- [11] R. Radhakrishnan, *Prediction of buckling strengths of cylindrical shells from their natural frequencies*, *Earthq. Eng. Struct. Dyn.* 2 (1973) 107–115.
- [12] Y. Segal, *Prediction of Buckling Load and Loading Conditions of Stiffened Shells from Vibration Tests*, M.Sc. Thesis Israel Institute of Technology, Haifa, Israel, 1980.
- [13] R.H. Plaut, L.N. Virgin, *Use of frequency data to predict buckling*, *J. Eng. Mech.* 116 (10) (1990) 2330–2335.
- [14] M.A. Souza, W.C. Fok, A.C. Walker, *Review of experimental techniques for thin-walled structures liable to buckling: neutral and unstable buckling*, *Exp. Tech.* 7 (9) (1983) 21–25.
- [15] M.A. Souza, L.M.B. Assaid, *A new technique for the prediction of buckling loads from nondestructive vibration tests*, *Exp. Mech.* 31 (2) (1991) 93–97.
- [16] J. Singer, *Buckling Experiments on Shells – A Review of Recent Developments* (Eng. Report TAE No 403), Technion Israel Institute of Technology, 1980.
- [17] M.A. Arbelo, S.F.M. de Almeida, M.V. Donadon, S.R. Rett, R. Degenhardt, S.G.P. Castro, K. Kalnins, O. Ozolins, *Vibration correlation technique for the estimation of real boundary conditions and buckling load of unstiffened plates and cylindrical shells*, *Thin-Walled Struct.* 79 (2014) 119–128.
- [18] M.A. Arbelo, K. Kalnins, O. Ozolins, E. Skukis, S.G.P. Castro, R. Degenhardt, *Experimental nondestructive test for estimation of buckling load on unstiffened cylindrical shells using a vibration correlation technique*, *Thin-Walled Struct.* 94 (2015) 273–279.
- [19] K. Kalnins, M.A. Arbelo, O. Ozolins, E. Skukis, S.G.P. Castro, R. Degenhardt, *Experimental nondestructive test for estimation of buckling load on unstiffened cylindrical shells using vibration correlation technique* (2015), *Shock Vib.* (2015) 1–8.
- [20] E. Skukis, O. Ozolins, K. Kalnins, M.A. Arbelo, *Experimental test for estimation of buckling load on unstiffened cylindrical shells by vibration correlation technique*, *Procedia Eng.* 172 (2017) 1023–1030.
- [21] E. Skukis, O. Ozolins, J. Andersons, K. Kalnins, M.A. Arbelo, *Applicability of the vibration correlation technique for estimation of the buckling load in axial compression of cylindrical isotropic shells with and without circular cutouts* (2017), *Shock Vib.* (2017) 1–14.
- [22] V.I. Weingarten, P. Seide, J.P. Peterson, *Buckling of Thin-walled Circular Cylinders* (NASA SP-8007), NASA Space Vehicle Design Criteria - Structures (Revised 1968), 1965.
- [23] DESICOS, [Online]. Available: <<http://www.desicos.eu>>.
- [24] MMPDS-07, *Metallic Materials Properties Development and Standardization* (MMPDS), 2012.
- [25] R. Degenhardt, A. Kling, H. Klein, W. Hillger, C. Goetting, R. Zimmermann, R. Rohwer, A. Gleiter, *Experiments on buckling and postbuckling of thin-walled CFRP structures using advanced measurement systems*, *Int. J. Struct. Stab. Dyn.* 7 (2) (2007) 337–358.
- [26] R. Zimmermann, H. Klein, A. Kling, *Buckling and postbuckling of stringer stiffened fibre composite curved panels – Tests and computations*, *Compos. Struct.* 73 (2006) 150–161.
- [27] S.G.P. Castro, R. Zimmermann, M.A. Arbelo, R. Khakimova, M.W. Hilburger, R. Degenhardt, *Geometric imperfections and lower-bound methods used to calculate knock-down factors for axially compressed composite cylindrical shells*, *Thin-Walled Struct.* 74 (2014) 118–132.
- [28] R. Degenhardt, A. Kling, A. Bethge, J. Orf, L. Kärger, R. Zimmermann, K. Rohwer, A. Calvi, *Investigations on imperfection sensitivity and deduction of improved knock-down factors for unstiffened CFRP cylindrical shells*, *Compos. Struct.* 92 (2010) 1939–1946.
- [29] R. Khakimova, S.G.P. Castro, D. Wilckens, K. Rohwer, R. Degenhardt, *Buckling of axially compressed CFRP cylinders with and without additional lateral load: experimental and numerical investigation*, *Thin-Walled Struct.* 119 (2017) 178–189.
- [30] LMS International, *The LMS Theory and Background Book*, Leuven, Belgium, 2000.

VII

Skukis E., Jekabsons G., Andersons J., Ozolins O., Labans E., Kalnins, K.

“Robustness of empirical vibration correlation techniques for predicting the instability of unstiffened cylindrical composite shells in axial compression”

Polymers, Open access, Volume 12, Issue 12, Pages 1 – 18, December 2020, Article ID 3069

Parameters (2022/09/01)

DOI	10.3390/polym12123069
Citations in Scopus	1
FWCI	-
IF	3.13

Article

Robustness of Empirical Vibration Correlation Techniques for Predicting the Instability of Unstiffened Cylindrical Composite Shells in Axial Compression

Eduards Skukis ¹, Gints Jekabsons ¹, Jānis Andersons ^{2,*}, Olgerts Ozolins ¹, Edgars Labans ³ and Kaspars Kalnins ^{1,4,*}

¹ Institute of Materials and Structures, Riga Technical University, 6A Kipsalas str., LV-1048 Riga, Latvia; edskukis@gmail.com (E.S.); gints.jekabsons@rtu.lv (G.J.); olgerts.ozolins@rtu.lv (O.O.)

² Institute for Mechanics of Materials, University of Latvia, 3 Jelgavas str., LV-1004 Riga, Latvia

³ Faculty of Aerospace Engineering, Delft University of Technology, 2629HS Delft, The Netherlands; edgars.labans@gmail.com

⁴ Ikšķile Centre of Composite Competence Ltd., LV-5015 Ikšķile, Latvia

* Correspondence: janis.andersons@pmi.lv (J.A.); kaspars.kalnins@rtu.lv (K.K.)

Received: 7 December 2020; Accepted: 17 December 2020; Published: 21 December 2020



Abstract: Thin-walled carbon fiber reinforced plastic (CFRP) shells are increasingly used in aerospace industry. Such shells are prone to the loss of stability under compressive loads. Furthermore, the instability onset of monocoque shells exhibits a pronounced imperfection sensitivity. The vibration correlation technique (VCT) is being developed as a nondestructive test method for evaluation of the buckling load of the shells. In this study, accuracy and robustness of an existing and a modified VCT method are evaluated. With this aim, more than 20 thin-walled unstiffened CFRP shells have been produced and tested. The results obtained suggest that the vibration response under loads exceeding 0.25 of the linear buckling load needs to be characterized for a successful application of the VCT. Then the largest unconservative discrepancy of prediction by the modified VCT method amounted to ca. 22% of the critical load. Applying loads exceeding 0.9 of the buckling load reduced the average relative discrepancy to 6.4%.

Keywords: polymer composite; buckling; imperfection; vibration correlation technique; natural frequencies

1. Introduction

Carbon fiber-reinforced polymer (CFRP) composites possess highly competitive specific strength and stiffness properties. Moreover, the properties of CFRP laminates can be tailored to the expected loading conditions by optimizing their lay-up. The excellent strength-to-weight and stiffness-to-weight ratios, combined with controlled anisotropy of mechanical properties, has ensured a widening application of CFRPs. These characteristics of CFRPs are particularly beneficial in weight-conscious sectors of industry, such as aerospace (see, e.g., [1,2]).

For thin-walled CFRP structures subjected to compressive service loads, the failure mode limiting their load-bearing capacity is, typically, the loss of stability. Estimates of the buckling load based on an idealized shell geometry and loading are known to be unconservative due to imperfection sensitivity of the onset of instability, especially pronounced for monocoque (unstiffened) shells. In the design phase, the effect of imperfections on the buckling load can be allowed for via a knock-down factor (KDF), i.e., the ratio of the actual critical load of imperfect shell, P_b , and the predicted buckling load of a perfect shell, P_{cr} , estimated according to the linear bifurcation theory. Such empirical lower-bound KDFs for

cylindrical shells have been established in 1960s based on accumulated experimental data [3], and later specified for anisotropic, laminated composite cylinders in axial compression [4]. An alternative approach of determining KDF for conservative design is based on the nonlinear numerical modelling of buckling in the presence of an assumed worst-case imperfection in the composite cylinder. Such a worst-case situation can be presented by, e.g., an appropriately scaled linear buckling mode-shaped imperfection, a geometric dimple-shaped imperfection, a single boundary perturbation, a single perturbation load, axisymmetric imperfections, scaled mid-surface imperfections, or the membrane stiffness reduction, as described in [5–9]. Since the characteristics of imperfections can be considered as random variables [10], probabilistic methods are also applied in the shell buckling analysis, leading to probabilistic design approaches [8–11]. Deterministic and probabilistic methods providing lower-bound estimate of KDF ensure safe, but not necessarily efficient, design of shells.

The accuracy of buckling load prediction for an already produced shell can be further increased using additional information on its specific individual characteristics obtainable by nondestructive means of inspection. Imperfections in composite shells can be of geometrical, structural, material nature, or related to loading of the shell. When an imperfection signature of a shell can be determined in sufficient detail, a nonlinear numerical buckling analysis allowing for imperfections provides a close estimate of the buckling load [12–15]. Notably, shells sensitive to geometrical imperfections also exhibit sensitivity to load imperfections [16]. It precludes neglecting either group of imperfections, although the relative contribution of different types of imperfections to facilitating the onset of instability may vary [12,15,17]. The incorporation of measured initial geometric and thickness imperfections, thickness-adjusted material property variations, measured loading imperfections, elastic radial support conditions, and allowing for selected specimen parameter uncertainties (e.g., uncertainty in the imperfection measurement accuracy, fiber and matrix properties, fiber volume fraction, etc.) in shell models enabled an accurate prediction of the compression response of unstiffened thin-walled graphite-epoxy cylindrical shells [13]. However, such a detailed characterization of a shell may appear impractical in most industrial applications.

A viable alternative to measuring imperfections, with a subsequent numerical analysis of their effect on stability, is the nondestructive testing of a shell. In this way, the integral effect of imperfections on its eigenfrequencies is established and the buckling load is evaluated by the vibration correlation technique (VCT). The VCT approach implies experimentally determining the reduction in the natural frequency of a structural element with increasing compressive applied load and estimating the buckling load based on such data. Simply-supported imperfection-insensitive structural elements, for which the vibration and buckling modes coincide, exhibit a linear relation between the applied load P and the first natural frequency f_m squared (see., e.g., [18,19])

$$\frac{P}{P_b} + \left(\frac{f_m}{f_0}\right)^2 = 1 \quad (1)$$

where P_b is the buckling load and f_0 denotes the respective natural frequency at $P = 0$. Having measured the variation of the natural frequency with load in the range of relatively low loads, Equation (1) can be applied to estimating the buckling load as $P_b = P$ at $f_m = 0$. However, imperfection-sensitive plates and shells exhibit a much steeper reduction in the natural frequency when the applied load approaches the actual P_b than that implied by Equation (1), which leads to an unconservative prediction for the buckling load.

A number of empirical and semi-empirical modified VCTs have been proposed to reflect the effect of imperfections on the load–natural frequency relation of shells, as recently reviewed in, e.g., [20–22]. The most accurate and extensively studied VCT method for unstiffened cylindrical shells, proposed in [23], departs from the common approach of relating the onset of buckling to fading of the natural frequency of the shell. Instead, it is suggested that buckling takes place when $(1 - P/P_{cr})^2$, assumed to be a second-order polynomial function of $1 - (f_m/f_0)^2$, reaches its minimum. A graphical interpretation of the procedure is as follows [23]: the experimental load–natural frequency data are

presented as a plot of $(1 - P/P_{cr})^2$ versus $1 - (f_m/f_0)^2$, the data points are approximated by fitting a second-order polynomial, the minimum value of this polynomial, ξ^2 , is found, and the VCT estimate of the buckling load P_{VCT} is obtained from the equality $1 - P_{VCT}/P_{cr} = \xi$. The described approach has also been validated numerically [24], although only considering one specific imperfection group, namely, geometrical imperfections.

This VCT method has been applied for estimation of the buckling load in axial compression of CFRP shells of various lay-ups [21,23,25–28], including a variable-angle tow CFRP shell [28], as well as grid-stiffened glass/epoxy [29], composite lattice sandwich [22], stainless steel [26] and aluminum alloy [30,31] shells. Apart from a pure axial loading, the critical load for pressurized aluminum alloy shells [31] has also been studied. Notably, a numerical simulation of the experimental VCT procedure of shells, implementing either real measured imperfections or appropriate assumed imperfections in the shell model, has also produced encouraging results [32].

Each of the methods for estimating the critical load discussed above has its specific advantages and conditions of application. In the design stage, the buckling load of a shell can be evaluated only by the KDF approach, either based on accumulated data [3,4] or a worst-case imperfection analysis [5–11]. Since a lower-bound estimate of KDF is determined in this way, the critical load is underestimated, leading, possibly, to overdesigning of the shell. When an actual shell is produced, its imperfection signature can be determined, or vibration tests conducted, in order to characterize the specific shell. The advantage of imperfection characterization with a subsequent numerical modelling of instability onset [12–15] is that no mechanical tests of the shell are needed. However, a sufficiently detailed characterization of shell imperfections may be overly complicated in industrial applications. The advantage of VCT is that only a relatively uncomplicated nondestructive mechanical test of a shell is required [20–31] instead of a detailed inspection of different imperfections of the shell. However, the boundary conditions of the structural element have to be accurately recreated in the shell test. Another limiting factor of applying the VCT is disappearing of the monitored mode shapes, sometimes observed at increasing load levels [28].

Evaluation of the applicability of VCT [23] has not been conclusive yet, partially due to rather limited testing programs—only a few monocoque CFRP shells were tested in each of the studies [21,23,25–28]. Although most works report close conservative estimates of the buckling load by the VCT, overestimations are also revealed in some studies, e.g., in [27], where buckling loads nonconservative by about 5 and 8% were found by the VCT for the two cylinders tested. Therefore, a more extensive testing appears necessary to elucidate the accuracy and robustness of the VCT.

With such an aim, a wider test program has been initiated; in the current study, 21 cylindrical CFRP shells of the same lay-up, but four different diameter and height combinations, have been produced and tested. Their response has been analyzed by means of the VCT technique [23] and by an empirical modification of the latter. The contribution of the present study to the experimental and analytical development of VCT comprises:

- presenting results of one of the largest test programs to-date concerning the application of VCT for evaluating the axial buckling load of unstiffened cylindrical CFRP shells;
- proposing an empirical modification of the existing VCT analysis that increases the accuracy of estimates of the buckling load;
- evaluating the robustness of VCT with respect to variations in shell geometry, mounting and loading methods, and the preload.

The results obtained suggest that the vibration response from the unloaded state of the shell up to loads exceeding 0.25 of the linear buckling load needs to be characterized to enable a reliable VCT prediction. The largest discrepancy in overestimation of the critical load by VCT was limited to about 22% when the modified VCT method was applied using the load range mentioned. The accuracy of the VCT was found to be virtually insensitive to shell geometry, the method of load introduction, and the absence of natural frequency data for the unloaded shell.

2. Empirical VCT Techniques

The VCT method for unstiffened cylindrical shells proposed in [23] assumes the relation between the natural frequency f_m of the shell and the applied compressive load P in the form (see also [21,28])

$$(1 - p)^2 = C_2 (1 - f^2)^2 + C_1 (1 - f^2) + C_0 \tag{2}$$

where p denotes the applied load normalized by the linear buckling load, $p = P/P_{cr}$, and $f = f_m/f_0$ is the ratio of natural frequencies of the shell under an axial load and in the load-free condition. The onset of instability is related to $(1 - p)^2$ reaching its minimum, i.e., the first derivative of the function Equation (2) with respect to its argument $1 - f^2$ being zero,

$$\frac{d(1 - p)^2}{d(1 - f^2)} = 0 \tag{3}$$

and the second derivative being positive. It follows from Equations (2) and (3) that

$$Min[(1 - p)^2] = \xi^2 = C_0 - \frac{C_1^2}{4C_2} \tag{4}$$

and $C_2 > 0$. In Equation (4), ξ is interpreted as the reduction in the load-carrying capacity of a shell due to the presence of imperfections. Finally, the VCT-predicted critical load is

$$P_{VCT} = P_{cr} (1 - \xi) \tag{5}$$

The functional form of Equation (2), with $C_2 = C_0 = 1$ and $C_1 = -2$, has been noted to comply with that of a perfect simply supported shell given by Equation (1), and Equation (3) shown to provide a correct buckling condition of $f_m = 0$ in such a case [24]. A similar derivation for a clamped shell has been performed in [32].

A comparison of applications of this VCT based on monitoring the reduction of each of the first four natural frequencies revealed that using the lowest natural frequency in Equation (2) produced the most accurate prediction for the buckling load [28]. The prediction accuracy was also found to generally improve when experimental data of f_m vs. P for greater P/P_b ratios were used, as expected. The VCT-predicted and experimental KDFs for the highest load levels used in each of the studies [21,25–31] are presented in a parity plot in Figure 1a. Specifically, for CFRP shells, the maximum loads in these VCT studies amounted to $P/P_b = 0.81 \dots 0.98$ [21,25–28], whereas for metal shells, they were $P/P_b = 0.54 \dots 0.99$ [26,30,31].

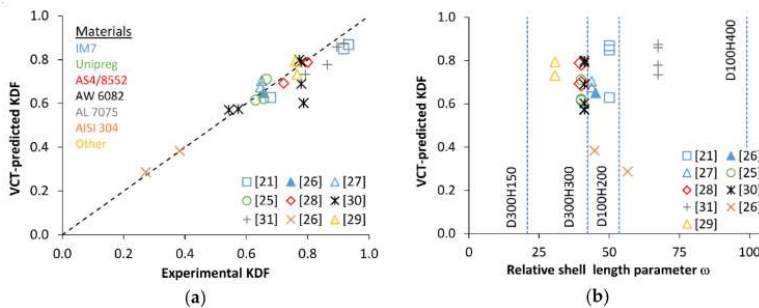


Figure 1. Application of vibration correlation technique (VCT) [23] to monocoque shells: (a) Parity plot of VCT-predicted vs. experimental knock-down factors (KDFs); (b) VCT-predicted KDF as a function of the relative length parameter of shell (the dashed lines indicate the composite shell geometries considered in the present study).

Further, a wide range of cylinder geometries, as characterized by the relative shell length parameter $\omega = H/\sqrt{R}\cdot t$ [33], expressed via cylinder height H , radius R , and wall thickness t , has been covered in the tests, Figure 1b. A very close correlation between the KDFs determined by buckling tests and by the VCT is seen in Figure 1a, with the most conservative VCT-predicted buckling load P_{VCT} amounting to about 76% of the experimental critical load and the most unconservative P_{VCT} exceeding P_b by ca. 8%.

Such a good predictive capacity is likely to stem from correctly capturing the phenomenology of the underlying physical mechanism of instability by this VCT method. Experimental studies (see, e.g., [20,23]) have indicated that shell buckling is preceded by a swift transition from the gradual reduction in the natural frequency with increasing load to a rapid drop of frequency. This has also been demonstrated by a theoretical modelling of vibrations of imperfect shells, which allowed constructing load–eigenfrequency diagrams up to the critical load [34]. Notably, instability criterion Equation (3) can also be interpreted as marking the onset of a rapid change in the natural frequency, $df/dp \rightarrow \infty$ or, equivalently, $dp/df \rightarrow 0$. Indeed, elementary transformations of the left-hand side of Equation (3) yield

$$\frac{d(1-p)^2}{d(1-f^2)} = \frac{\frac{d(1-p)^2}{dp} dp}{\frac{d(1-f^2)}{df} df} = \frac{1-p}{f} \frac{dp}{df}, \quad (6)$$

demonstrating that meeting the instability condition Equation (3) also implies that $dp/df = 0$.

Since the form of the right-hand side of Equation (2) has been arrived at empirically [23], it appears plausible that similar functions with this property can be used to locate the instability onset. We consider an empirical modification of Equation (2) employing a second-order polynomial of $1-f$:

$$(1-p)^2 = c_2(1-f)^2 + c_1(1-f) + c_0 \quad (7)$$

Then, the minimum value of $(1-p)^2$ as a function of $1-f$ is given by

$$\xi^2 = c_0 - \frac{c_1^2}{4c_2} \quad (8)$$

at $c_2 > 0$, and the predicted buckling load is determined by Equation (5) using the value of ξ from Equation (8). It can be easily checked that

$$\frac{d(1-p)^2}{d(1-f)} = 2(1-p) \frac{dp}{df} \quad (9)$$

i.e., the condition $dp/df = 0$ holds at the critical load.

3. Materials and Methods

In the following subsections, the material and the manufacturing method of shells are described, the methods for mounting of shells in the test rig are defined, and procedures for determining the shell thickness, buckling load, and vibration response are presented.

3.1. Material

A unidirectional carbon fiber/epoxy prepreg Unipreg® (UNICARBON®, produced in Kaunas, Lithuania), with a 100 g/m² nominal areal density, was used for manufacturing of cylindrical composite shells. Two batches of nominally identical prepreps were obtained from the producer in consecutive separate shipments. For clarity and traceability, the letter N was included in identifiers of the shells made using prepreg of the latest batch.

The elastic properties of a unidirectionally reinforced (UD) composite produced from the prepreg are presented in Table 1.

Table 1. Elastic properties of a Unipreg® UD composite [25].

Longitudinal Young's Modulus E_{11} , GPa		Transverse Young's Modulus E_{22} , GPa		In-Plane Shear Modulus G_{12} , GPa	Poisson's Ratio ν_{12}
Tension	Compression	Tension	Compression		
116.4	91.7	6.7	6.4	3.6	0.34

3.2. Manufacture of Shells

Three-ply cylindrical shells of lay-up [0/45/−45] (angles were measured with respect to the cylinder axis, starting from the innermost ply) were produced by hand lay-up using steel mandrels. The shells were consolidated by means of vacuum bagging and cured at elevated temperatures. The cure cycle consisted of subjecting the shells to an 80 °C temperature for 1 h followed by 3 h at 130 °C. In this way, shells of nominal diameter $D = 100$ mm and two different heights, $H = 200$ and 400 mm, as well as shells with $D = 300$ mm and $H = 150$ and 300 mm, were manufactured.

3.3. Tests

3.3.1. Characterization of Shell Thickness

The variation of thickness for each shell was determined by an ultrasonic technique. To enable an efficient scanning of cylinders, a Hilgus USPC 3010 HF equipment (Hilgert NDT GMBH, Braunschweig, Germany) was modified to replace the y -coordinate drive by a rotational drive. A support frame for cylinders was made of an aluminum profile system with front and rear axles, a lathe chuck on the drive end, and a PLA6 cone passive end. During ultrasonic scanning, the cylindrical shells were supported on machined foam end plates.

3.3.2. Shell Buckling Tests

A universal Zwick 100 quasi-static testing machine (Zwick GMBH, Ulm, Germany) was used for axial compression tests of the composite cylinders.

Two methods of load introduction, shown schematically in Figure 2, were applied. The majority of the cylinders were tested employing horizontal parallel steel plates, with a compression plate rigidly bolted to the machine crosshead, Figure 2a. The loading was displacement-controlled, at a rate of 1 mm/min. The load was measured by a single load cell located between the loading plate and the respective crosshead of the loading frame, while the shortening was determined as the average of readings of three LVDTs placed around the shell at 120° angular intervals.

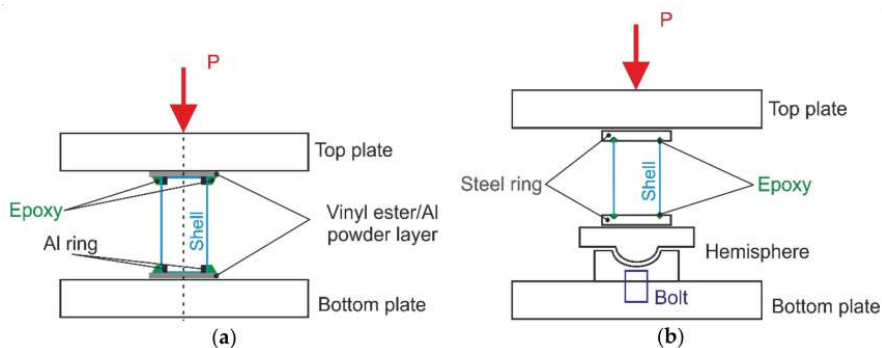


Figure 2. Schematic of the setup for compression tests of composite cylinders: (a) Testing by means of parallel loading plates; (b) Testing using a hemispherical joint.

The rest of specimens were tested as shown schematically in Figure 2b. Specifically, a hemispherical joint was installed on the bottom plate, enabling rotation of the supporting plate, thus eliminating bending moments and, hence, promoting self-alignment of the cylinder axis with the loading direction. For this loading set-up, the shortening of specimens was measured via the crosshead displacement.

Edges of the 100-mm-diameter shells were mounted between parallel steel rings, in 8 mm deep circular grooves with a V-shaped cross section, which were filled with a mixture of epoxy resin and fine sand, as schematically presented in Figure 3a. Specimens with such a mounting were tested either employing a hemispherical joint, Figure 2b, or placing them between the parallel steel plates of the test machine.

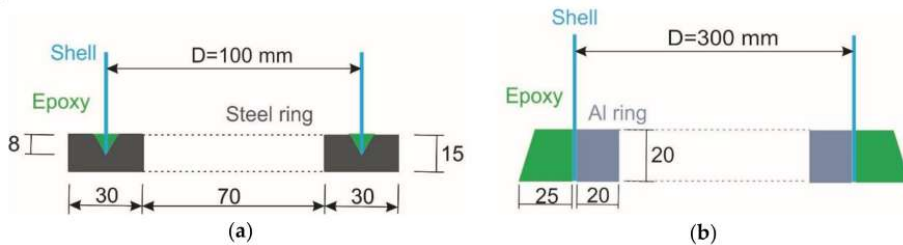


Figure 3. Schematic of the mounting of composite cylinders: (a) In the groove of a steel ring; (b) Potting onto plates of the test machine. Dimensions in the figure are in mm.

The top and bottom edges of the 300-mm-diameter shells were both clamped by aluminum rings from the inside and potted with an epoxy mortar containing fine sand and slag, Figure 3b. The shells were mounted directly unto the loading plates, as shown in schematic Figure 2a, filling the narrow gaps between the specimen and the plates by a fast-curing alumina powder-filled vinyl ester resin in order to mitigate the effects of contact surface unevenness, which would result in loading imperfections.

The buckling mode shapes of the cylinders were captured photographically.

3.3.3. Characterization of Vibration Response

The natural frequencies and vibration modes were determined using a Polytec laser vibrometer (Polytec GMBH, Waldbronn, Germany); the test setup is shown in Figure 4.

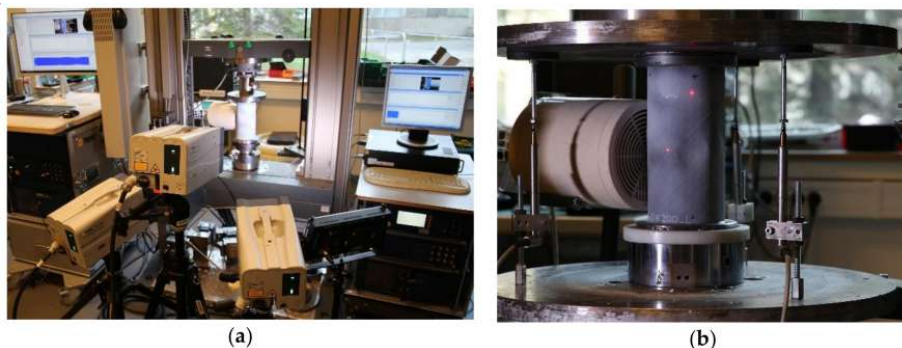


Figure 4. Test setup for characterization of the vibration response of a carbon fiber-reinforced polymer (CFRP) cylinder: (a) Overview of the experimental setup with a specimen installed between loading plates; (b) Placement of the loudspeaker for excitation of vibrations.

A grid of points distributed on a small area of the cylinder was scanned. The area with 600 grid points for scanning was found to yield a sufficiently detailed modal response. For excitation of

vibrations, a loudspeaker was used. It was placed perpendicularly to the measurement zone on the opposite side of the specimen, Figure 4b. The measurements were conducted within the frequency range from few hundreds of Hz, well below the lowest natural frequency, to ca. 1600 Hz to ensure that more than ten first natural vibration modes were covered. The vibration response was characterized at 9 to 18 load levels, ranging from the unloaded state to more than 90% of the buckling load.

4. Results and Discussion

4.1. Buckling Loads and Modes

Axial compression tests of CFRP cylinders were performed as described in Section 3.3.2, and the load–shortening diagrams obtained are presented in Figure 5.

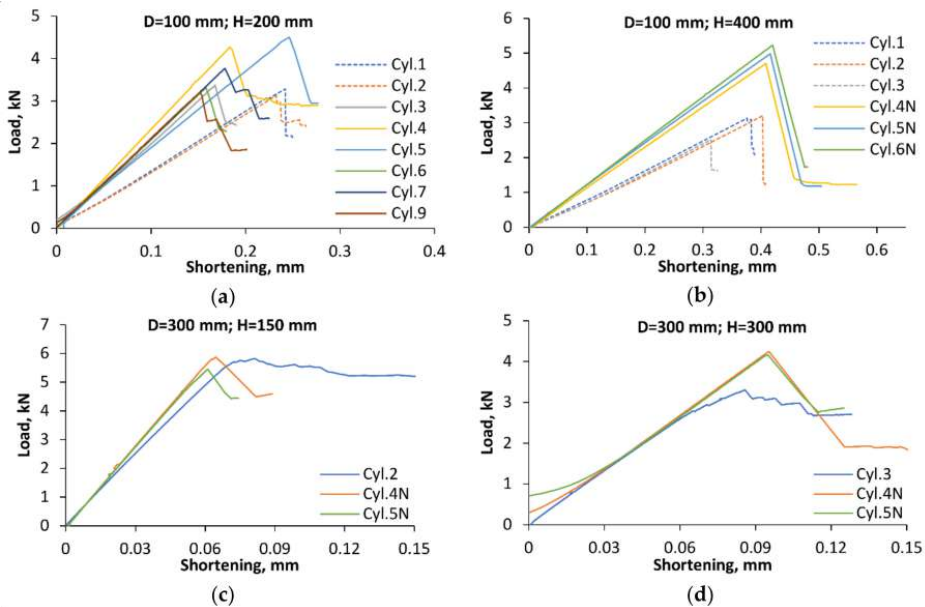


Figure 5. Load–shortening diagrams of cylinders with dimensions: (a) $D = 100$ mm and $H = 200$ mm; (b) $D = 100$ mm and $H = 400$ mm; (c) $D = 300$ mm and $H = 150$; (d) $D = 300$ mm and $H = 300$. Results of tests employing a hemispherical joint are plotted by dashed lines, for parallel plates—by solid lines.

The largest number of cylinders tested had a diameter of 100 mm and height of 200 mm; they were produced from the same prepreg batch and shared the same mounting technique. The specimens were tested either employing parallel loading plates, as shown schematically in Figure 2a, or a hemispherical joint (Figure 2b). It is seen in Figure 5a that the loading method markedly affected the apparent stiffness and the instability onset of shells. Specifically, the specimens tested using a hemispherical joint (Cyl. 1 and 2) exhibited lower apparent stiffness and buckled at lower loads than the nominally identical specimens (Cyl. 3 to 9) placed between parallel loading plates. The critical load data obtained are presented in Table 2. The variability of the apparent stiffness among the specimens sharing the same load introduction method is likely to be caused by fiber alignment and potting geometry variations, as well as by the scatter in shell thickness.

For shells of the same 100-mm diameter but a larger height of 400 mm, an additional factor of variability was manufacturing the specimens from two batches of a nominally identical prepreg material. The letter N in the cylinder number is used to identify the shells made from prepreg of the latest batch. In this case, the apparent stiffness and critical load of the cylinders tested using a

hemispherical bearing (Cyl. 1 to 3 in Figure 5b) also appeared to be consistently lower than that obtained via parallel-plate tests (Cyl. 4N to 6N). Since this trend held both for single-batch shells, Figure 5a, and for shells produced from different batches, Figure 5b, we tentatively conclude that variations in the prepreg properties between these batches, if any, can be neglected in the buckling analysis.

Table 2. Buckling loads of CFRP shells.

Shell Geometry			Load Introduction	Critical Load P_b , kN
Diameter D , mm	Height H , mm	Wall Thickness t , mm		
100	200	0.294 (0.001) ¹	Hemispherical joint	3.05 (0.21) ¹
		0.273 (0.010)	Parallel plates	3.65 (0.49)
	400	0.298 (0.005)	Hemispherical joint	2.97 (0.39)
		0.355 (0.019)	Parallel plates	4.96 (0.29)
300	150	0.359 (0.014)	Parallel plates	5.63 (0.21)
	300	0.336 (0.046)		3.88 (0.51)

¹ Standard deviation.

The shells of 300-mm diameter were produced from prepreps coming from either of the two batches, but mounted and tested in the same way. The load–shortening diagrams in Figure 5c,d suggest that the prepreg batch used for specimen production had no apparent systematic effect on either the buckling load or the apparent stiffness of shells.

The buckling modes of shells can be discerned in the photographs in Figure 6.

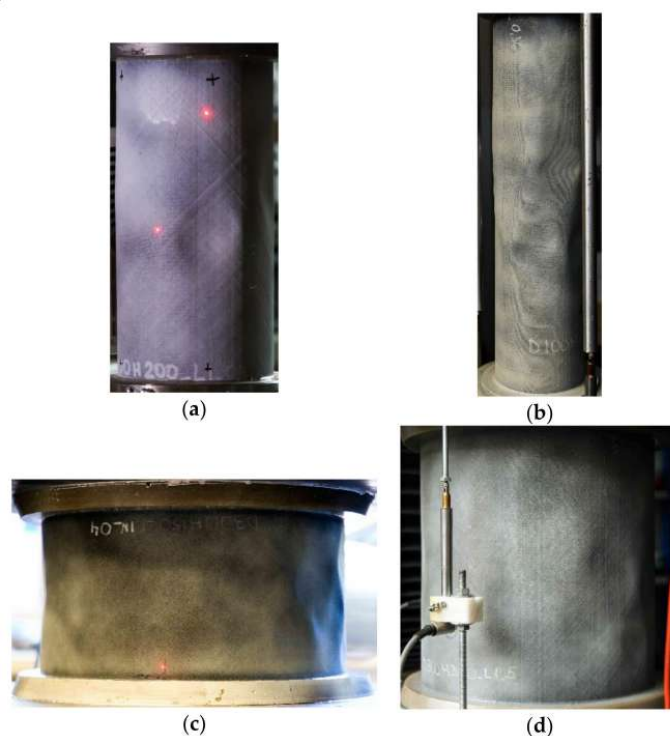


Figure 6. Buckling modes of cylinders with the following dimensions: (a) $D = 100$ mm and $H = 200$ mm; (b) $D = 100$ mm and $H = 400$ mm; (c) $D = 300$ mm and $H = 150$; (d) $D = 300$ mm and $H = 300$.

4.2. Vibration Spectra and Modes

The application of VCT implies identification of the first (or one of the lowest) natural frequency of a shell and experimentally determining the reduction in this frequency with increasing compressive load. With this aim, the natural frequency spectra of the shells were measured as described in Section 3.3.3, starting from load-free conditions. An exception was the cylinders tested using a hemispherical joint, see the schematic in Figure 2b. For these specimens, a small controlled compressive load P_{\min} (in the range of 0.14 to 0.25 kN) was applied instead of $P = 0$ to reliably fix the specimen in position when characterizing the initial natural frequency spectrum. Typical spectra for the shells of each geometry considered are shown in Figure 7. Vibration characteristics of the shells are seen to differ, as expected, reflecting differences in their geometry. The lowest eigenfrequency of each of the cylinders was determined from the relatively densely populated low-frequency part of the spectrum.

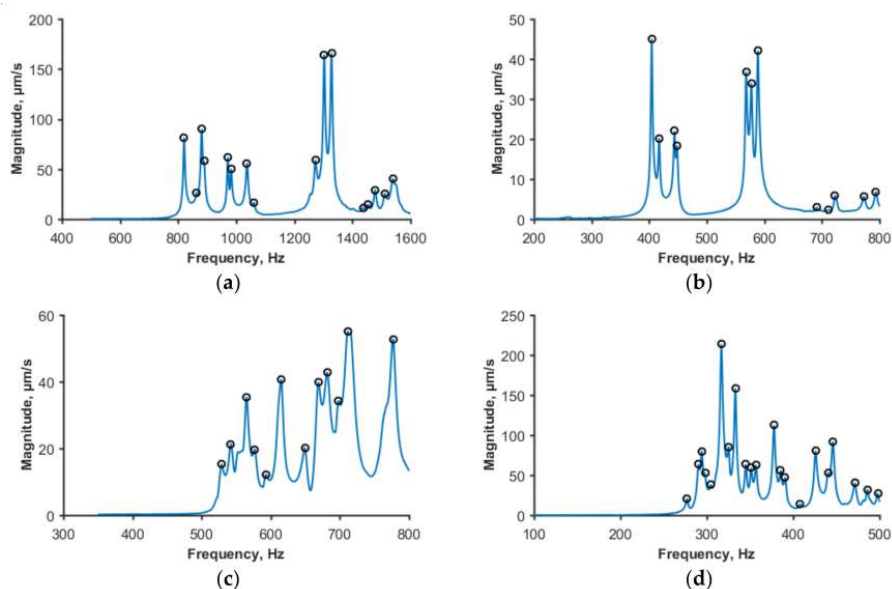


Figure 7. Typical natural frequency spectra of unloaded cylinders of dimensions: (a) $D = 100$ mm and $H = 200$ mm; (b) $D = 100$ mm and $H = 400$ mm; (c) $D = 300$ mm and $H = 150$; (d) $D = 300$ mm and $H = 300$.

Vibration mode shapes for the first natural frequency are presented in Figure 8. The vibration modes obviously differed from the shell buckling modes seen in Figure 6, as expected for thin-walled unstiffened cylinders. For all the shell geometries considered, the first vibration mode exhibited one longitudinal half-wave, $n = 1$, while the number of circumferential half-waves, m , depended on shell geometry. The circumferential half-wave number was estimated as in [28], by measuring the angular size φ of a single half-wave and evaluating the integer part of the ratio $360^\circ/\varphi$. The characteristics (m, n) obtained from mode shapes captured by vibrometer, Figure 8, were as follows: (12, 1) for 200-mm and (6, 1) for 400-mm height cylinders with a 100-mm diameter; (32, 1) for 150-mm; and (22, 1) for 300-mm height cylinders with 300-mm diameter. No change in the half-wave numbers (m, n) was observed with increasing load.

The experimentally determined variation of the natural frequency with compressive load is shown in Figure 9 (the data are plotted by markers, whereas the lines are only meant as a guide to the eye). Notably, for each shell geometry, the cylinders with higher buckling loads also tended to have higher natural frequencies. For example, specimens Cyl. 4 and 5, exhibiting the highest buckling loads for the

shells with $H = 200$ and $D = 100$ mm, also possessed the highest first natural frequencies (Figure 9a); Cyl. 3 with the lowest buckling load of cylinders with $H = 300$, $D = 300$ mm dimensions also had the lowest eigenfrequency among them (Figure 9d).

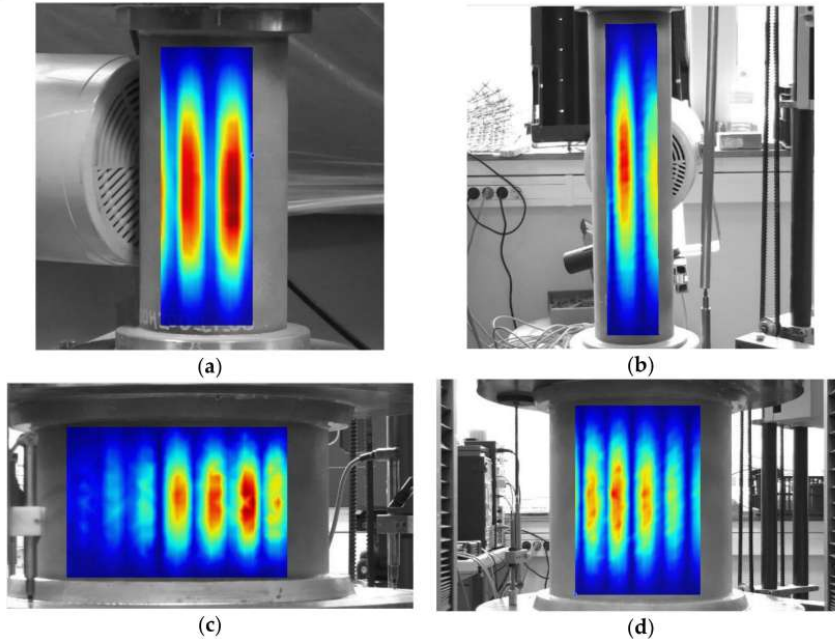


Figure 8. Mode shapes corresponding to the first natural frequency of unloaded cylinders of dimensions: (a) $D = 100$ mm and $H = 200$ mm; (b) $D = 100$ mm and $H = 400$ mm; (c) $D = 300$ mm and $H = 150$; (d) $D = 300$ mm and $H = 300$.

However, this is a tendency rather than an exact equivalence of specimen rankings in terms of the buckling load and eigenfrequency magnitude. So, among the shells with $H = 400$ and $D = 100$ mm, the specimens Cyl. 4N to 6N (loaded by parallel plates) had considerably higher buckling loads than Cyl. 1 to 3 (tested using a hemispherical joint), and this distinction also held for eigenfrequency magnitudes (Figure 9b). By contrast, the ranking of specimens in terms of the buckling load and natural frequency within each of these two subgroups did not coincide exactly.

The coefficient of correlation between the critical loads and the lowest eigenfrequencies for the unloaded shells with $D = 100$ mm amounted to 0.73 ($H = 200$ mm) and 0.67 ($H = 400$ mm), whereas for the shells with $D = 300$ mm, it was 0.97 ($H = 300$ mm) and 0.40 ($H = 150$ mm). Such a correlation apparently originates from the sensitivity of both the buckling load and the first natural frequency to imperfections and boundary conditions of thin-walled shells. It has been shown (see, e.g., [34]) that the presence of geometrical imperfections in shells reduce not only the critical load, but also the frequency of the lowest vibration mode. The sensitivity of the lowest eigenfrequency to actual boundary conditions has been used to evaluate the equivalent elastic restraints of shell edges in order to enable a more accurate prediction of the buckling load [18,23]. Stiffer restraints, naturally, also lead to greater critical load and natural frequency.

It is seen in Figure 9 that the reduction in the first natural frequency of cylinders under an increasing compressive load P is, in general, initially smooth under low loads, apart from a few cases. Namely, for Cyl. 6N (Figure 9b), the natural frequency in the unloaded state was actually lower than at low loads. Such an effect has also been reported before [28]. Conversely, for Cyl. 7 (Figure 9a)

and Cyl. 4N (Figure 9b), the drop in frequency at the first loading step was markedly larger than the subsequent, smoother reduction of f_m at further load steps. Such an irregularity in the frequency response of these shells in the nominally unloaded state is likely to be caused by an interaction of the actual boundary conditions at $P = 0$ [21] and the stress state in the shells introduced by potting. The magnitude of such stresses was not assessed in the present work, but, notably, prestresses in cylindrical shells due to a minor mismatch of the shell and mounting ring geometry have been evaluated [11] and found to be capable of affecting the numerically estimated instability onset. The measured load-free spectra of the shells mentioned were excluded from a further VCT analysis, and the values of f_0 were replaced by those obtained at the smallest non-zero axial load.

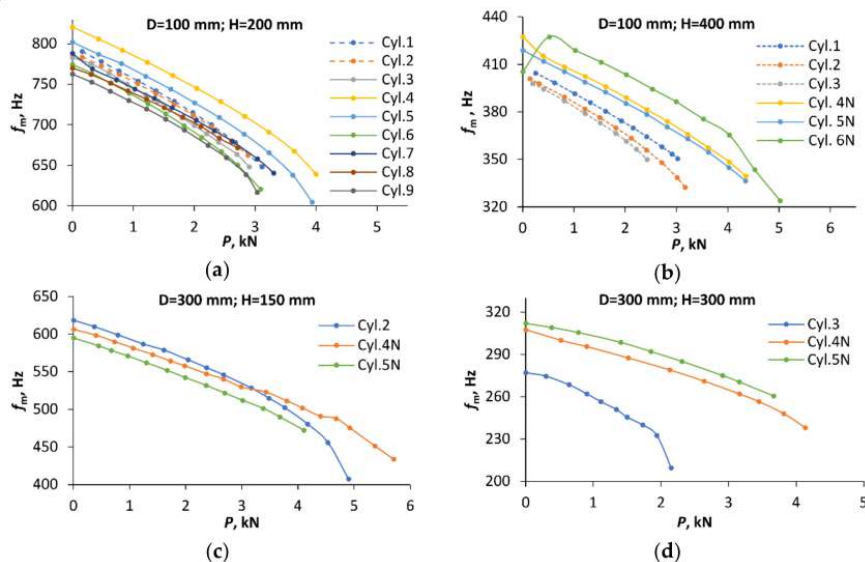


Figure 9. Reduction of the natural frequency due to the axial compression for cylinders of dimensions: (a) $D = 100$ mm and $H = 200$ mm; (b) $D = 100$ mm and $H = 400$ mm; (c) $D = 300$ mm and $H = 150$; (d) $D = 300$ mm and $H = 300$. The results of tests employing a hemispherical joint are plotted by the dashed lines, and for parallel plates—by the solid lines.

4.3. VCT-Based Prediction of the Critical Load

The linear buckling loads of shells needed for a VCT analysis were estimated by the respective finite-element models generated employing the ANSYS© Mechanical finite element analysis software. Linear elastic FEM analyses of cylindrical shells lacking any imperfections were performed using SHELL281 elements. The elasticity characteristics of UD plies reported in Table 1 were employed in calculations; the values of Young's moduli as determined in compression tests were used. For 300-mm-diameter cylinders, exhibiting relatively large scatter in wall thickness t among shells (the coefficient of variation being ca. 0.2), the experimentally determined t value for each shell was implemented in the FEM model. For 100-mm-diameter cylinders, possessing smaller thickness scatter, the average value of ply thickness of 0.104 mm was used. Clamped boundary conditions were applied as follows: on the bottom edge of the shell, the condition of all edge displacement and rotation components being equal to zero was imposed. The boundary conditions of the upper edge differed only in that the vertical displacement of the edge nodes, equal for all the nodes, was applied to model the displacement-controlled axial compressive loading.

The predicted buckling loads P_{VCT} , derived using the whole range of load–eigenfrequency data obtained and their relative deviations $\delta = |1 - P_{VCT}/P_b|$ from the experimental ones are presented in

Table 3. For the ease of reference, the VCT method [23] using Equation (2) for fitting the load–frequency data is further denoted by M1 and its empirical modification using Equation (7)—by M2. The largest deviation of VCT prediction by both the methods, ca. 35%, is seen for the specimen that was subjected to the lowest relative maximum load $P/P_b = 0.65$. For the rest of cylinders, vibration tests to higher relative maximum loads were performed, and the accuracy of the VCT-derived critical load estimates improved, as expected. Specifically, when eigenfrequency data up to $P/P_b \geq 0.87$ were used, the maximum deviation of P_{VCT} was 29% for M1 method and 16% for M2. The average relative error of prediction by the method M2, amounting to 6.4%, was also lower than that by M1, 9.7%. Thus, the maximum and mean deviations of the VCT-predicted buckling load were both smaller for the empirical method M2.

Table 3. Comparison of experimental and VCT-predicted buckling loads.

Cylinder Diameter and Height, mm	Loading	Cylinder Number	Buckling Load P_b , kN	Load Range in Vibration Tests		VCT-Predicted Buckling Load			
				Min. P/P_b	Max. P/P_b	M1		M2	
						P_{VCT} , kN	Relat. Error δ , %	P_{VCT} , kN	Relat. Error δ , %
D = 100 H = 200	Hemi-spherical joint	01	3.20	0.05	0.97	3.61	12.9	3.34	4.5
		02	2.90	0.05	0.99	3.40	17.4	3.17	9.3
		03	3.35	0	0.93	3.50	4.7	3.26	2.5
	Parallel plates	04	4.24	0	0.94	4.26	0.4	4.03	5.0
		05	4.42	0	0.89	3.95	10.5	3.85	12.8
		06	3.29	0	0.94	3.41	3.7	3.2	2.6
		07	3.55	0.09	0.93	3.87	9.1	3.59	1.2
		08	3.50	0	0.95	4.17	19.3	3.77	7.7
		09	3.19	0	0.95	3.19	0.2	3.07	3.5
D = 100 H = 400	Hemi-spherical joint	01	3.15	0.08	0.97	4.08	29.4	3.66	16.2
		02	3.23	0.04	0.99	3.43	6.3	3.27	1.2
		03	2.52	0.08	0.96	3.04	20.8	2.83	12.4
	Parallel plates	04N	4.67	0.08	0.93	4.77	1.9	4.48	4.2
		05N	4.96	0	0.88	4.91	0.9	4.51	9.0
		06N	5.26	0.10	0.95	4.9	6.8	4.92	6.4
D = 300 H = 150	Parallel plates	02	5.61	0	0.87	4.8	14.4	4.84	13.8
		04N	5.85	0	0.98	6.49	11.0	5.84	0.1
		05N	5.44	0	0.92	6.0	10.4	5.22	4.0
D = 300 H = 300	Parallel plates	03	3.29	0	0.65	2.14	34.9	2.15	34.6
		04N	4.24	0	0.97	4.57	8.0	4.27	0.7
		05N	4.11	0	0.89	3.84	6.5	3.71	9.8

The critical loads predicted by both methods appear to correlate rather closely, as seen in Figure 10 presenting the ratio of VCT-estimated and experimental buckling loads, P_{VCT}/P_b , for M2 as a function of that for M1. Such a correlation is likely to stem from the same implicit underlying criterion of instability, $dp/df = 0$, shared by both methods, as demonstrated in Section 2. However, M2 produced more conservative estimates of the critical load than M1, and that feature became particularly pronounced for $P_{VCT}/P_b > 1$, i.e., when the critical load was overestimated by the VCT. As can be inferred from Figure 10 and Table 3, P_{VCT} predicted by M1 deviates by no more than -14 to 29% from the experimental buckling load, while for prediction by M2, the deviation is within the range of -14 to 16% , when vibration data up to the maximum load $P/P_b \geq 0.87$ are used.

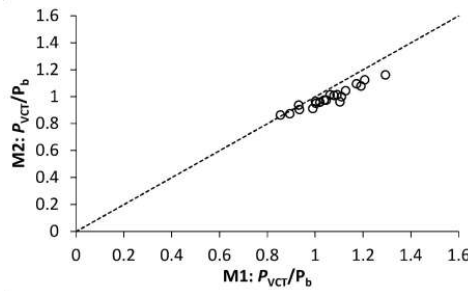


Figure 10. Ratio of VCT-estimated and experimental buckling loads, P_{VCT}/P_b , for method M2 as a function of that for method M1, using the maximum load $P/P_b \geq 0.87$ in vibration tests.

Notably, both VCT methods tend to slightly underestimate the critical load for shells with large experimental KDF values, as seen in Figure 11. It follows from the previous research, Figure 1a, and present results, Figure 11a, that M1 yields a conservative prediction for the experimental KDF exceeding about 0.65. For M2, the data in Figure 11b suggest that the transition to a conservative prediction takes place at a slightly lower KDF of ca. 0.55. Such a feature of the VCT-predicted critical loads appears beneficial for shells with a high fabrication quality leading to a high KDF, as would be expected in the aerospace sector. For such high-quality shells, the VCT provides not only close, but also conservative buckling load estimates.

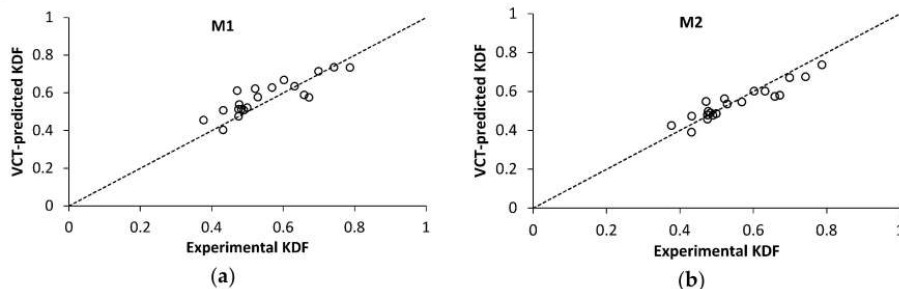


Figure 11. VCT-predicted knock-down factor, using maximum load in vibration tests $P/P_b \geq 0.87$, as a function of the experimental KDF for VCT method: (a) M1; (b) M2.

Both the VCT methods considered are robust to using either the natural frequency of an unloaded specimen or of a specimen loaded with a small axial force $P \leq 0.1P_b$ as the starting point f_0 for characterization of the natural frequency dependence on the axial load: the corresponding mean values of δ were 7.5 and 13.1% for M1, and 6.0 and 6.9% for M2 at $P/P_b \geq 0.87$. This is in agreement with a previous finding that the VCT prediction by M1 is not affected by the absence of data for the first natural frequency of an unloaded shell [21]. Similarly, the geometrical characteristics of the tested cylinders have little effect on the prediction accuracy, Table 4.

Table 4. Accuracy of VCT prediction (at maximum $P/P_b \geq 0.87$) as a function of cylinder geometry.

Relative Length Parameter of Shell $\omega=H/\sqrt{R \cdot t}$	Mean Relative Error of Prediction δ , %	
	M1	M2
21	11.9	6.0
42	7.3	5.3
54	8.7	5.5
99	11.0	8.2

Method M2 is also virtually robust with respect to variations in the mounting and loading methods of specimens, as demonstrated by the minor difference in the average accuracy of prediction among the three combinations of shell edge support and load introduction methods, Table 5.

Table 5. Accuracy of VCT prediction (at maximum $P/P_b \geq 0.87$) for different loading and boundary conditions of cylinders.

Loading and Boundary Conditions	Mean Relative Error of Prediction δ , %	
	M1	M2
Steel ring, hemispherical joint	17.4	8.7
Steel ring, parallel plates	5.8	5.5
Potted, parallel plates	10.1	5.7

For eventual practical applications of VCT, it is of interest to consider the maximum axial load to be used for evaluating the reduction of the natural frequency in terms of the linear buckling load P_{cr} . Analyzing the incremental evolution of the VCT-predicted critical load as a function of the axial load, natural frequency variation up to which is used in VCT analysis, $P_{VCT} = P_{VCT}(P)$, spurious results were obtained for some of specimens at relatively low numbers of loading steps and, hence, at low P values. The minimum number of load–frequency data points allowing the evaluation of the parameters of VCT relations Equations (2) and (7) is, naturally, equal to the number of equation parameters, namely, three. They correspond to the unloaded state of the shell and two subsequent loading steps. Using such a limited dataset in the analysis occasionally led to physically unreasonable results, such as a negative predicted buckling load, $P_{VCT} < 0$, or $\xi^2 < 0$ (as calculated by Equation (4) or (8)), which eventually disappeared when a greater number of load steps, corresponding to a higher load, were used. These findings apparently agree with the suggestions concerning load steps [28] and the maximum load level [21] in vibration tests. It is recommended to use a greater number of experimental points, at least 15 [28], to reach a reliable buckling prediction by the VCT. However, increasing the maximum load level was found to be even more effective for reducing the deviations δ than the number of load steps [21]. Based on the current dataset, we selected a cut-off load level at $P/P_{cr} = 0.25$, starting from which to consider the accuracy of VCT. This corresponded to at least four to seven load levels in vibration tests. The predicted buckling load P_{VCT}/P_b as a function of the highest axial load used in vibration tests, expressed as a fraction of the linear buckling load, P/P_{cr} , is shown in Figure 12 for all the specimens tested.

It is seen that, for both VCT methods considered, the lower bound of the normalized predicted buckling load P_{VCT}/P_b increased almost linearly with the maximum load used in vibration tests (the dotted lines in Figure 12), approaching unity at $P/P_{cr} = 0.65$ for method M1 and 0.9 for method M2. By contrast, the upper bound of the predicted buckling load data had no clear dependence on the axial load up to $P/P_{cr} \sim 0.6$ for M2, the greatest overestimation of the experimental buckling load being $P_{VCT}/P_b = 1.22$ (the dashed line in Figure 12b). Similarly, method M1 overestimated the experimental buckling load by, at most, the factor of $P_{VCT}/P_b = 1.33$ for $P/P_{cr} > 0.3$, as marked by the dashed line in Figure 12a. It can be inferred from these results that, for the VCT-predicted buckling load, a knock-down factor of about 0.81 has to be applied if M2 is used on load–eigenfrequency data up to loads $P \geq 0.25 P_{cr}$, whereas an even smaller knock-down factor or a larger load range is needed for M1.

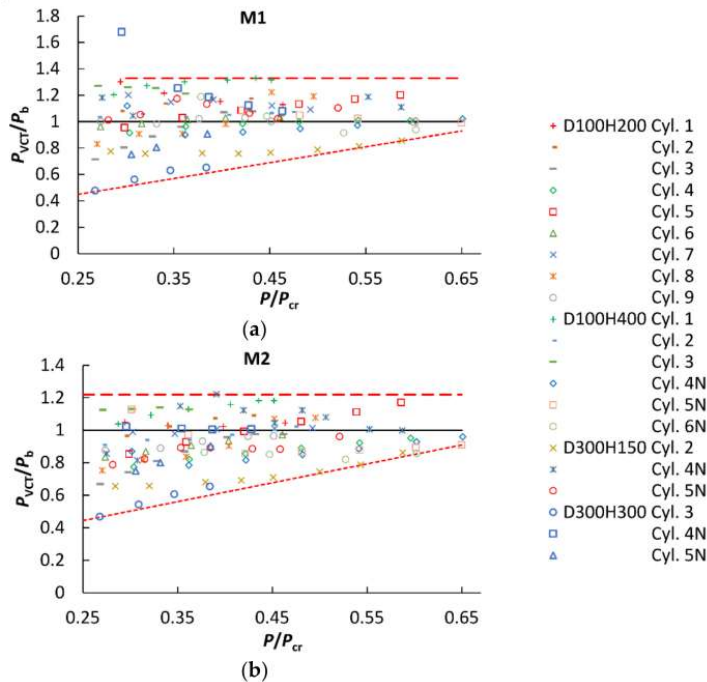


Figure 12. Predicted buckling load P_{VCT}/P_b as a function of the highest axial load used in vibration tests, P/P_{cr} , for $P/P_{cr} > 0.25$, using the VCT method: (a) M1; (b) M2.

5. Conclusions

The vibration correlation technique for nondestructive evaluation of the critical load of thin-walled imperfection-sensitive shells has been applied for prediction of the buckling load of CFRP cylinders. The buckling loads in axial compression have been determined experimentally for 21 unstiffened cylindrical CFRP shells with identical lay-ups, four different geometries, two shell mounting techniques, and two load introduction methods. The modal behavior of the CFRP cylindrical shells under axial compression was investigated by exciting the vibrations by a loudspeaker, thus determining the variation of the first natural frequency of vibrations with the applied load.

It was found that the prediction accuracy of the buckling load using either VCT approach proposed by Arbelo et al. [23] or its empirical modification was virtually insensitive to shell geometry and mounting and loading methods. Moreover, the VCT methods also appeared robust with respect to a lack of natural frequency data for an unloaded shell, caused, e.g., by the need for a preload to reliably fix the shell in the test rig. Both VCT methods tended to slightly underestimate the critical load for shells with relatively large experimental KDF values thus providing not only close, but also conservative estimates of the limit load for high-quality shells.

The modified VCT method yielded an average relative error of prediction of 6.4% when natural frequencies at loads exceeding ca. 0.9 of the buckling load were used. Upon reframing the VCT results in terms of the critical load of a perfect shell, it appeared that the vibration response under loads exceeding 0.25 of the linear buckling load enabled a successful application of VCT, but a knock-down factor of ca. 0.81 had to be applied. Further elaboration of the VCT approach is warranted to reduce the load range needed for eigenfrequency monitoring and to increase the prediction accuracy of the buckling load.

Author Contributions: Conceptualization, K.K. and J.A.; methodology, K.K. and G.J.; software, G.J.; validation, E.S. and O.O.; formal analysis, G.J. and J.A.; investigation, E.S., O.O., and E.L.; resources, K.K.; data curation, G.J.; writing—original draft preparation, J.A.; writing—review and editing, K.K., O.O., G.J., and E.L.; visualization, E.S.; supervision, K.K. All authors have read and agreed to the published version of the manuscript.

Funding: This research was funded by Latvian Council of Science, grant number LZP-2018/2-363.

Conflicts of Interest: The authors declare no conflict of interest. The funders had no role in the design of the study; in the collection, analyses, or interpretation of data; in the writing of the manuscript, or in the decision to publish the results.

References

1. Mouritz, A. Fibre–polymer composites for aerospace structures and engines. In *Introduction to Aerospace Materials*, 1st ed.; Woodhead Publishing Ltd.: Cambridge, UK, 2012; Chapter 15; pp. 338–393.
2. McCarville, D.A.; Guzman, J.C.; Dillon, A.K.; Jackson, J.R.; Birkland, J.O. Design, manufacture and test of cryotank components. In *Comprehensive Composite Materials II*; Beaumont, P.W.R., Zweben, C.H., Eds.; Elsevier Ltd.: Amsterdam, The Netherlands, 2018; Volume 3, pp. 153–179.
3. Peterson, J.P.; Seide, P.; Weingarten, V.I. *Buckling of Thin-Walled Circular Cylinders*; NASA SP-8007; NASA: Washington, DC, USA, 1965; revised 1968.
4. Takano, A. Statistical knockdown factors of buckling anisotropic cylinders under axial compression. *J. Appl. Mech.* **2012**, *79*, 051004. [[CrossRef](#)]
5. Castro, S.G.P.; Zimmermann, R.; Arbelo, M.A.; Khakimova, R.; Hilburger, M.W.; Degenhardt, R. Geometric imperfections and lower-bound methods used to calculate knock-down factors for axially compressed composite cylindrical shells. *Thin Walled Struct.* **2014**, *74*, 118–132. [[CrossRef](#)]
6. Wagner, H.N.R.; Hühne, C.; Niemann, S.; Khakimova, R. Robust design criterion for axially loaded cylindrical shells—Simulation and validation. *Thin Walled Struct.* **2017**, *115*, 154–162. [[CrossRef](#)]
7. Wagner, H.N.R.; Hühne, C.; Niemann, S. Robust knockdown factors for the design of axially loaded cylindrical and conical composite shells—Development and validation. *Compos. Struct.* **2017**, *173*, 281–303. [[CrossRef](#)]
8. Wagner, H.N.R.; Hühne, C.; Niemann, S.; Tian, K.; Wang, B.; Hao, P. Robust knockdown factors for the design of cylindrical shells under axial compression: Analysis and modeling of stiffened and unstiffened cylinders. *Thin Walled Struct.* **2018**, *127*, 629–645. [[CrossRef](#)]
9. Wagner, H.N.R.; Hühne, C.; Elishakoff, I. Probabilistic and deterministic lower-bound design benchmarks for cylindrical shells under axial compression. *Thin Walled Struct.* **2020**, *146*, 106451. [[CrossRef](#)]
10. Bolotin, V.V. Statistical aspects in the theory of structural stability. In *Dynamic Stability of Structures*; Herrmann, G., Ed.; Pergamon Press: Oxford, UK, 1967; pp. 67–81.
11. Schillo, C.; Kriegesmann, B.; Krause, D. Reliability based calibration of safety factors for unstiffened cylindrical composite shells. *Compos. Struct.* **2017**, *168*, 798–812. [[CrossRef](#)]
12. Starnes, J.H., Jr.; Hilburger, M.W.; Nemeth, M.P. The effects of initial imperfections on the buckling of composite cylindrical shells. In *Composite Structures: Theory and Practice*; Grant, P., Rousseau, Q.C., Eds.; ASTM STP 1383; American Society for Testing and Materials: West Conshohocken, PA, USA, 2000; pp. 529–550.
13. Hilburger, M.W.; Starnes, J.H., Jr. Effects of imperfections on the buckling response of compression-loaded composite shells. *Int. J. Non Linear Mech.* **2002**, *37*, 623–643. [[CrossRef](#)]
14. Hilburger, M.W.; Starnes, J.H., Jr. Effects of imperfections of the buckling response of composite shells. *Thin Walled Struct.* **2004**, *42*, 369–397. [[CrossRef](#)]
15. Schillo, C.; Röstermundt, D.; Krause, D. Experimental and numerical study on the influence of imperfections on the buckling load of unstiffened CFRP shells. *Compos. Struct.* **2015**, *131*, 128–138. [[CrossRef](#)]
16. Hühne, C.; Zimmermann, R.; Rolfes, R.; Geier, B. Sensitivities to geometrical and loading imperfections on buckling of composite cylindrical shells. In Proceedings of the European Conference on Spacecraft Structures, Materials and Mechanical Testing, Toulouse, France, 11–13 December 2002; pp. 1–12.
17. Kepple, J.; Prusty, B.G.; Pearce, G.; Kelly, D.; Thomson, R.; Degenhardt, R. Influence of imperfections on axial buckling load of composite cylindrical shells. In Proceedings of the 19th International Conference on Composite Materials, Montreal, QC, Canada, 28 July–2 August 2013; pp. 1–10.

18. Singer, J.; Arbocz, J.; Weller, T. Vibration correlation techniques (VCT). In *Buckling Experiments, Experimental Methods in Buckling of Thin-Walled Structures*; John Wiley & Sons, Inc.: New York, NY, USA, 2002; Volume 2, Chapter 15.2; pp. 1244–1284.
19. Virgin, L.N. *Vibration of Axially-Loaded Structures*; Cambridge University Press: Cambridge, UK, 2007.
20. Abramovich, H.; Govich, D.; Grunwald, A. Buckling prediction of panels using the vibration correlation technique. *Prog. Aerosp. Sci.* **2015**, *78*, 62–73. [[CrossRef](#)]
21. Franzoni, F.; Odermann, F.; Labans, E.; Bisagni, C.; Arbelo, M.A.; Degenhardt, R. Experimental validation of the vibration correlation technique robustness to predict buckling of unstiffened composite cylindrical shells. *Compos. Struct.* **2019**, *224*, 111107. [[CrossRef](#)]
22. Shahgholian-Ghahfarokhi, D.; Rahimi, G.; Liaghat, G.; Degenhardt, R.; Franzoni, F. Buckling prediction of composite lattice sandwich cylinders (CLSC) through the vibration correlation technique (VCT): Numerical assessment with experimental and analytical verification. *Compos. B* **2020**, *199*, 108252. [[CrossRef](#)]
23. Arbelo, M.A.; de Almeida, S.F.M.; Donadon, M.V.; Rett, S.R.; Degenhardt, R.; Castro, S.G.P.; Kalnins, K.; Ozoliņš, O. Vibration correlation technique for the estimation of real boundary conditions and buckling load of unstiffened plates and cylindrical shells. *Thin Walled Struct.* **2014**, *79*, 119–128. [[CrossRef](#)]
24. Franzoni, F.; Degenhardt, R.; Albus, J.; Arbelo, M.A. Vibration correlation technique for predicting the buckling load of imperfection-sensitive isotropic cylindrical shells: An analytical and numerical verification. *Thin Walled Struct.* **2019**, *140*, 236–247. [[CrossRef](#)]
25. Arbelo, M.A.; Kalnins, K.; Ozoliņš, O.; Skukis, E.; Castro, S.G.P.; Degenhardt, R. Experimental and numerical estimation of buckling load on unstiffened cylindrical shells using a vibration correlation technique. *Thin Walled Struct.* **2015**, *94*, 273–279. [[CrossRef](#)]
26. Kalnins, K.; Arbelo, M.A.; Ozoliņš, O.; Skukis, E.; Castro, S.G.P.; Degenhardt, R. Experimental nondestructive test for estimation of buckling load on unstiffened cylindrical shells using vibration correlation technique. *Shock Vib.* **2015**. [[CrossRef](#)]
27. Skukis, E.; Ozoliņš, O.; Kalnins, K.; Arbelo, M.A. Experimental test for estimation of buckling load on unstiffened cylindrical shells by vibration correlation technique. *Procedia Eng.* **2017**, *172*, 1023–1030. [[CrossRef](#)]
28. Labans, E.; Abramovich, H.; Bisagni, C. An experimental vibration-buckling investigation on classical and variable angle tow composite shells under axial compression. *J. Sound Vib.* **2019**, *449*, 315–329. [[CrossRef](#)]
29. Shahgholian-Ghahfarokhi, D.; Rahimi, G. Buckling load prediction of grid-stiffened composite cylindrical shells using the vibration correlation technique. *Compos. Sci. Technol.* **2018**, *167*, 470–481. [[CrossRef](#)]
30. Skukis, E.; Ozoliņš, O.; Andersons, J.; Kalnins, K.; Arbelo, M.A. Applicability of the vibration correlation technique for estimation of the buckling load in axial compression of cylindrical isotropic shells with and without circular cutouts. *Shock Vib.* **2017**. [[CrossRef](#)]
31. Franzoni, F.; Odermann, F.; Wilckens, D.; Skukis, E.; Kalnins, K.; Arbelo, M.A.; Degenhardt, R. Assessing the axial buckling load of a pressurized orthotropic cylindrical shell through vibration correlation technique. *Thin Walled Struct.* **2019**, *137*, 353–366. [[CrossRef](#)]
32. Tian, K.; Huang, L.; Sun, Y.; Du, K.; Hao, P.; Wang, B. Fast buckling load numerical prediction method for imperfect shells under axial compression based on POD and vibration correlation technique. *Compos. Struct.* **2020**, *252*, 112721. [[CrossRef](#)]
33. European Standard. *Eurocode: EN 1993-1-6 Eurocode 3—Design of Steel Structures—Part 1–6: Strength and Stability of Shell Structures*; European Committee for Standardization: Brussels, Belgium, 2007.
34. Jansen, E. The influence of initial geometric imperfections on composite shell stability and vibrations. In *Stability and Vibrations of Thin Walled Composite Structures*; Abramovich, H., Ed.; Woodhead Publishing Inc.: Cambridge, UK; Volume 2, Chapter 10; pp. 509–548.

Publisher's Note: MDPI stays neutral with regard to jurisdictional claims in published maps and institutional affiliations.



© 2020 by the authors. Licensee MDPI, Basel, Switzerland. This article is an open access article distributed under the terms and conditions of the Creative Commons Attribution (CC BY) license (<http://creativecommons.org/licenses/by/4.0/>).



Eduards Skuķis dzimis 1981. gadā Preiļos. Rīgas Tehniskajā universitātes (RTU) Būvniecības fakultātē ieguvis bakalaura (2002) un maģistra grādu (2004). Ir RTU Materiālu un konstrukciju institūta pētnieks ar 20 gadu pieredzi, specializējies mehānikā, skaitliskajos un eksperimentālajos svārstību pētījumos un modālajā analīzē. Veicis pētījumus dažādās programmās: Eiropas Kosmosa aģentūras, Eiropas Reģionālās attīstības fonda, Eiropas Sociālā fonda un Eiropas Komisijas 5.–7. ietvarprogrammas projektos.

Eduards Skuķis was born in 1981 in Preiļi. He received a Bachelor's degree in 2002 and Master's degree in 2004 from Riga Technical University (RTU). Eduards is a researcher at the Institute of Materials and Structures, RTU, and has 20 years of experience, specialising in mechanics, numerical and experimental vibration research and modal analysis. He has carried out research in various programs of European Space Agency, European Regional Development Fund, European Social Fund and European Commission Framework Projects